



## Review

# Transition metal-based nanozymes: Classification, catalytic mechanisms and emerging biomedical applications

Dandan Zhang<sup>b</sup>, Qing Chen<sup>a</sup>, Qunxiang Ren<sup>a</sup>, Wenbin Zhong<sup>c</sup>, Hongjin Zhang<sup>c</sup>, Guannan Wang<sup>a,\*</sup>, Yang Zhang<sup>a,\*</sup>

<sup>a</sup> Shenyang Key Laboratory of Medical Molecular Theranostic Probes in School of Pharmacy, Shenyang Medical College, 146 Huanghe North Avenue, Shenyang 110034, China

<sup>b</sup> School of Public Health, Shenyang Medical College, 146 Huanghe North Avenue, Shenyang 110034, China

<sup>c</sup> School of Basic Medicine, Shenyang Medical College, 146 Huanghe North Avenue, Shenyang 110034, China



## ARTICLE INFO

## Keywords:

Nanozyme  
Transition metal  
Catalytic property regulation  
Biomedical application  
Therapy

## ABSTRACT

Transition metal-based nanozymes, which exhibit intrinsic enzyme-like capacities, have several advantages over natural enzymes, including excellent stability, abundant metal sources, controllable activity, and inexpensive preparation processes. Nanozymes are characterized by interesting physicochemical properties, including photoluminescence, superparamagnetism, and special optical properties. Recently, various transition metal-based nanozyme platforms have been developed to target single or multiple substrates. The catalytic properties of nanozymes can be regulated by microenvironmental factors such as pH, oxygenation level, and concentration of H<sub>2</sub>O<sub>2</sub>, and also by a magnetic field, light, ultrasound, and heat. Thus, nanozyme signals can be maximized and tailored for disease diagnosis and treatment. Prompted by these inherent advantages, new approaches for diagnosis, treatment, and theranostics are emerging and gaining momentum. In this review, we summarize the preparation, catalytic mechanisms, and properties of transition metal-based nanozymes and highlight their emerging biomedical applications, including disease diagnosis, cancer therapy, imaging, and antibacterial infections. We anticipate that this review will be significant for improving our understanding of the capacities of metal-based nanozymes and motivating broader applications in several biomedical fields.

## 1. Introduction

Nanozymes are catalytic nanomaterials that convert enzyme

substrates into products, although they may have different catalytic mechanisms than their counterparts [1,2]. As emerging materials, nanozymes have unique physicochemical features and catalytic

**Abbreviations:** TMNs, transitionmetal-based nanozymes; NCs, nanoclusters; CDs, carbon dots; NWs, nanowires; NSs, nanosheets; AuNPs, gold nanoparticles; <sup>3</sup>O<sub>2</sub>, trilinear oxygen; HO<sub>2</sub>•, peroxyhydroxyl radicals; EMSI, electronic metal-support interaction; HEA, high-entropy alloy; US-HEANPs, ultra-small high-entropy alloy nanoparticles; POD, peroxidase; MOFs, metal-organic frameworks; TMB, 3,3,5,5'-tetra-methylbenzidine; ABTS, 2,2-azino-bis(3-ethylbenzothiazoline)-6-sulfonate; OXD, oxidase; CAT, catalase; SOD, superoxide dismutase; GOD, glucose oxidase; GPx, glutathione peroxidase; SPR, surface plasmon resonance; ELISA, enzyme-linked immunosorbent assays; OPD, o-phenylenediamine; HRP, horseradish peroxidase; SAzymes, single-atom nanozymes; M-oxide, metal-oxide; M-M, metal-metal; M-N<sub>4</sub>, metal-N<sub>4</sub>; M-N<sub>5</sub>, metal-N<sub>5</sub>; ROS, reactive oxygen species; DAzymes, Diatomic nanozymes; AuNRs, gold nanorods; •OH, hydroxyl radical; Cys, cysteine; CTAB, cetyltrimethylammonium bromide; GSH, glutathione; CM-PtNP, β-casein stabilized Pt nanoparticle; PCR, polymerase chain reaction; mSiO<sub>2</sub>, mesoporous silica; Pt NPs, platinum nanoparticles; PSMOF, photosensitized metal-organic framework; Ag NPs, silver nanoparticle; CuTA@Ag, copper-polyphenol colloidal spheres; SERS, surface enhanced Raman scattering; miRNA, microRNAs; AFP, alpha-fetoprotein; CEA, carcinoembryonic antigen; CA125, carbohydrate antigen 125; NDs, nano-dendrites; CTC, circulating tumor cells; PEC, photoelectrochemical; CDT, chemodynamic therapy; PTT, photothermal therapy; PDT, photodynamic therapy; RT, radiotherapy; SDT, sonodynamic therapy; MTO, mitoxantrone; TME, tumor microenvironment; HNCs, nitrogen-doped carbon nanosphere; FePc, iron phthalocyanine; TiO<sub>1-x</sub> NRs, titanium monoxide nanorods; NIR, near-infrared; RGD, tumor-specific peptide; PAI, Photoacoustic imaging; PTAs, photothermal switching agents; Ce6, chlorin e6; PET, positron emission tomography; SPECT, single photon emission computed tomography; NIRF, near-infrared fluorescence; MRSA, methicillin-resistant Staphylococcus aureus; HPO, haloperoxidase; DNase, deoxyribonuclease; <sup>1</sup>O<sub>2</sub>, singlet oxygen; eDNA, extracellular DNA; ZIF8, zeolitic imidazolate frameworks-8; Au@Ag-GO, gold-silver-graphene oxide; DMTU, dimethylthiourea; FEITC, β-phenylethyl isothiocyanate.

\* Corresponding authors.

E-mail addresses: [chemwangguannan@126.com](mailto:chemwangguannan@126.com) (G. Wang), [zhangyang@qdu.edu.cn](mailto:zhangyang@qdu.edu.cn) (Y. Zhang).

<https://doi.org/10.1016/j.ccr.2024.215771>

Received 3 September 2023; Accepted 26 February 2024

Available online 17 March 2024

0010-8545/© 2024 Elsevier B.V. All rights reserved.

properties similar to those of natural enzymes and have attracted significant attention in recent years [3–5]. Compared to natural enzymes, nanozymes have several advantages, including high stability, renewable precursor sources, adjustable activity, and low cost. In addition, nanozymes exhibit interesting physicochemical properties such as photoluminescence, supermagnetism, and photothermal properties [6–8]. Transition-metal-based nanozymes (TMNs) are a class of nanozymes that inherit the intrinsic properties of nanozymes, except for excellent magnetic, optical, electrical, and other properties with multi-valent electrons [9]. TMNs have been widely studied because of these advantages and have been evaluated for a variety of applications in environmental science, biomedicine, chemical and biosensing [10–12], bioimaging [13,14], cancer diagnosis and therapy [9], and antioxidant therapy [15–17]. In this review, we provide an overview of different categories of TMNs, their typical properties and catalytic mechanisms, and their potential biomedical applications.

The name “nanozyme” can be traced back to a 2004 study by Scrimin and colleagues in which triazacyclonane-functionalized gold nanoparticles (AuNPs) were used as catalysts of transphosphorylation reactions. Yan et al. (2007) found that magnetic Fe<sub>3</sub>O<sub>4</sub> NPs have peroxidase (POD)-like properties. Subsequently, researchers have shown that nanomaterials, including carbon-based nanomaterials, such as graphitic carbon, porous carbon, and carbon nanotubes [13,15,18–22] mimic the activity of natural enzymes. This is also the case for transition metal and transition metal-oxide NPs such as iron oxide [23–25], manganese [16,26,27], ceria [28–30], noble metal [31–35], and metal–organic frameworks (MOFs) [36,37]. Customized nanozymes, which imitate the catalytic properties and mechanisms of natural enzymes, have been developed to overcome some drawbacks of natural enzymes, particularly in terms of the eco-environment [9,38]. Furthermore, the scope of applications for nanozymes has expanded, particularly in biomedicine, owing to their more robust multicatalytic activity under wide pH and temperature conditions, facilitating possible breakthroughs in the field. Examples of this are the nano-CeO<sub>2</sub>, nano-MnO<sub>2</sub>, and nano-Fe<sub>3</sub>O<sub>4</sub> nanozymes, which can catalyze the oxidation of 3,3,5,5'-tetra-methylbenzidine (TMB) and 2,2-azino-bis(3-ethylbenzothiazoline)-6-sulfonate (ABTS) substrates to generate chromogenic products. Most artificial transition metals and metal-oxide nanomaterials have remarkable enzymatic properties, including typical oxidoreductases such as glucose oxidase (GOx), POD, oxidase (OXD), catalase (CAT), superoxide dismutase (SOD), and glutathione peroxidase (GPx) (Fig. 1). Other hydrolase-like activities such as urease, protease, esterase, and nuclease-like properties, which can catalyze the hydrolysis of carboxylic- and phosphoric-acid esters, are also exhibited by various transition metals and metal-oxide nanomaterials. However, few studies have classified TMNs by their mechanism of action on substrates and their emerging biomedical applications.

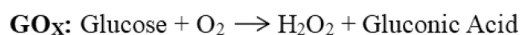
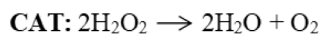
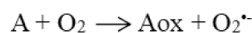
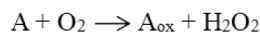


Fig. 1. Typical nanozyme reaction formulas.

Hence, we explored the classification of TMNs according to their modes of action, including self-acting, synergistic, and remotely controlled catalytic mechanisms. We also discuss the latest advances in the biomedical applications of nanozymes, including disease diagnosis, imaging, antibacterial applications, and cancer therapy. We examined strategies used to improve the efficacy of these nanozymes in various diseases. Finally, we analyze the current limitations and potential future directions for TMNs development, particularly in the biomedical field.

## 2. Catalytic properties of artificial TMNs

TMNs such as noble metal NPs and manganese-, iron-, copper-, and cerium-based NPs have been used to elucidate the catalytic abilities of OXD, POD, CAT, SOD, GOx, and GPx. In addition to single-NP systems, composites combining transition metal-based units with other nanounits have been developed, including Fe<sub>3</sub>O<sub>4</sub>-Pt and Au-Pt. It has been observed that TMNs often display synergistic effects that can significantly boost their catalytic performance when integrated with other nanozymes. Various natural metal enzymes have been identified in living organisms that play vital roles in complicated biocatalytic processes. Considering the inherent limitations of natural metallic enzymes, the development of artificial TMNs as potential substitutes for enzymes is promising. Most TMNs belong to the oxidoreductase family, and their intrinsic enzymatic activity is related to the atomic composition of the nanozyme surface and interior, with the exception of other influencing factors, including morphology and size, surface groups, pH, temperature, and reaction time. Although TMNs have been studied for several decades, there is still a lack of understanding of their catalytic mechanisms and kinetics. Herein, we review the typical catalytic mechanisms and kinetics of TMNs. Table 1 provides a classification and its typical bioapplications, which may help further our knowledge of TMNs.

### 2.1. Monometal nanozymes

Monometal nanozymes generally refer to noble metal NPs, which exhibit surface plasmon resonance (SPR), optical and photothermal conversion properties, and are chemically stable [59,63,154]. These nanozymes exhibit OXD, POD, CAT, and SOD activities [39,49]. For example, noble-metal NPs have been observed to catalyze the oxidation of substrates such as TMB in the presence of H<sub>2</sub>O<sub>2</sub> under acidic conditions because the reaction intermediate O\* exhibits POD activity instead of free radicals [43]. Additionally, these nanozymes can catalyze the decomposition of H<sub>2</sub>O<sub>2</sub> into H<sub>2</sub>O and O<sub>2</sub> under basic conditions, thereby replicating CAT activity [31,49]. Noble-metal NPs have also shown SOD-like activity, enabling them to quench O<sub>2</sub><sup>•−</sup> and adjust the levels of reactive oxygen, making them suitable for *in vivo* applications [31]. Researchers have conducted relevant studies on the catalytic mechanisms of noble metal nanozymes. The mechanisms of Au, Ag, Pt, and Pd have been investigated in terms of their POD and CAT activities using theoretical calculations and experimental verification [155]. H<sub>2</sub>O<sub>2</sub> molecules attach to Au (1 1 1) surfaces and undergo a decomposition reaction under acidic or neutral conditions, leading to the formation of highly oxidizing oxygen species denoted as O\* (\* indicates the substance adsorbed on the metal surface). O\* can then react with hydrogen atoms from the organic substrates, resulting in oxidation reactions that show POD activity. However, under alkaline conditions, hydroxyl groups were adsorbed onto the Au (1 1 1) surface, and in the presence of OH\*, H<sub>2</sub>O<sub>2</sub>\* underwent an acid decomposition reaction, resulting in the adsorbed oxygen species, O<sub>2</sub><sup>\*</sup>, which was released as O<sub>2</sub>; therefore, the catalyst showed CAT-like activity. Notably, OH\* acts as both an active site for CAT-like activity and an inhibitory site for POD-like activity. Subsequently, the mechanisms of the effects of Au, Ag, Pt, and Pd on OXD and SOD activity were also studied. Because trilinear oxygen (<sup>3</sup>O<sub>2</sub>) with a magnetic moment is the main component of O<sub>2</sub> in air, it does not readily react with organic substrates. However, when <sup>3</sup>O<sub>2</sub> is adsorbed onto a metal surface, the metal electrons enter the antibonding orbitals of <sup>3</sup>O<sub>2</sub>,

**Table 1**  
Current relative metal nanomaterials as enzyme analogues and emerging bioapplications.

Type	Nanomaterial	Enzyme-like	Application	Detection limit	Reference		
Monometal nanozyme	Au NCs	GOx,	Therapeutics for cancer		[39]		
	Au NPs	POD, CAT, SOD				[40,41]	
		Ag NPs	SOD, CAT			[42]	
		Pt NPs	POD	Detection of Hg <sup>2+</sup>	7.2 nM	[43]	
		Pt NCs	POD	Detection of glucose	0.28 μM	[44]	
		Pt-apoferritin NPs	POD, CAT	–	–	[45]	
		Pd NPs	POD	Detection of I, Antibacteria	0.19 nM	[32,46]	
		Pd NCs	SOD, CAT	–	–	[31]	
		Pd nanosheets	CAT, POD	Therapeutics for tumor	–	[47]	
		Ru NPs	POD, OXD	–	–	[48]	
		Ir NPs	POD, CAT, OXD	Oxidation of aromatic alcohols	–	[49]	
		Cu NCs	POD	Detection of H <sub>2</sub> O <sub>2</sub> and glucose	10 μM, 100 μM	[50]	
		Cu-CDs	POD, CAT	Antibacteria	–	[51]	
		Os NPs	POD	Detection of glucose and pyruvic acid	400 nM	[52]	
		Rh NPs	POD	Detection of H <sub>2</sub> O <sub>2</sub> and glucose	<0.75 μM	[53]	
		Mn(II)	OXD	–	–	[54]	
		FeNPs	OXD	Detection of dopamine	10 nM	[55]	
	Metal alloy nanozyme	Au <sub>2</sub> Pt	CAT	Therapeutics for tumor	–	[56]	
		AgPt NPs	CAT, POD	–	–	[57]	
Au-Pt NCs		OXD	–	–	[58]		
Fe-Pt NPs		OXD	–	–	[59]		
Pd/Pt NWs		OXD	Detection of acidphosphatase	0.06 U L <sup>-1</sup>		[60]	
NiPd NPs		CAT,POD, OXD	Detection of glucose	4.2 μM		[61]	
		Au@Pt nanorods	OXD, POD	Detection of H <sub>2</sub> O <sub>2</sub> , glucose, cholesterol	45 μM, 45 μM, 30 μM	[62]	
		Au@PtNPs	CAT	Detection of cocaine	0.33 μM	[63]	
		Au@PdPt nanodots	OXD	Detection of Fe <sup>2+</sup>	1.5 μM	[64]	
		PtCo NPs	OXD	Detection of cancer cells	–	[65]	
		Au@Ag nanodots	POD	Immunoassay for carcinoembryonic antigen	30 fg mL <sup>-1</sup>	[66]	
		Au@Pd nanodots	POD	Immunoassay for carcinoembryonic antigen	3 fg mL <sup>-1</sup>	[67]	
		Pd-Ir nanocubes	POD	Immunoassay for human prostate surface antigen	0.67 pgmL <sup>-1</sup>	[68]	
		Bi/Au NPs	POD	Detection of thrombin	2.5 pM	[69]	
		Bi/Pt NPs	POD	Detection of glucose	0.2 μM	[70]	
		AgM (Au, Pd, Pt) NPs	POD	Detection of ascorbic acid	6.7 μM	[71]	
		AgPt NCs	POD	Detection of thrombin	2.6 nM	[72]	
		PtCu nanoframe	POD	Phenol degradation	–	[73]	
		PtCu nanocages	POD, SOD, CAT, AAO	Detection of dehydroepiandrosterone	0.5 ngmL <sup>-1</sup>	[74]	
		Pd@Pt NPs	POD, CAT, OXD	Detection of <i>Salmonella</i>	58 CFU mL <sup>-1</sup>	[75]	
Metal oxide-based nanozyme		US-HEANPs	POD	Therapeutics for tumor	–	[76]	
		MnO <sub>2</sub> NSs	OXD	Detection of acid phosphatase	40 μU mL <sup>-1</sup>	[77]	
		MnO <sub>2</sub> NPs	POD, CAT, SOD	Immunoassays for goat anti-human IgG, Antioxidant	0.25 μg mL <sup>-1</sup> , 0.025 μg mL <sup>-1</sup>	[78,79]	
			MnO <sub>2</sub> nanoflakes	POD	Detection of glucose	1 μM	[26]
			Mn <sub>3</sub> O <sub>4</sub> NPs	OXD, POD, CAT, SOD	Detection of arsenic, Antioxidant	1.32 μg L <sup>-1</sup>	[80–82]
			Fe <sub>3</sub> O <sub>4</sub>	POD, CAT	Immunoassay for target Ag, Antioxidant	18 fg mL <sup>-1</sup> ,	[83,84]
			γ-Fe <sub>2</sub> O <sub>3</sub> NPs	POD, CAT	Antioxidant	–	[23]
		α-Fe <sub>2</sub> O <sub>3</sub> NPs	CAT	Antioxidant	–	[85]	
		CeO <sub>2</sub> NRs	OXD	Detection of GSH	–	[28]	
		CeO <sub>2</sub> NPs	POD,CAT, SOD	Antioxidant	–	[86–88]	
		CeO <sub>2</sub> nanocrystals	Phosphatase	–	–	[89]	
		CeO <sub>2-x</sub> nanorods	POD, hydrolase	Antibacteria	–	[90,91]	
		Co <sub>3</sub> O <sub>4</sub> NPs	CAT	Detection of H <sub>2</sub> O <sub>2</sub>	4.4 μM	[92]	
		Co <sub>3</sub> O <sub>4</sub> nanoflowers	POD, CAT, OXD, SOD	Detection of acid phosphatase and H <sub>2</sub> O <sub>2</sub>	0.062 U L <sup>-1</sup> , 2 μM	[93]	
		NiO nanoflowers	SOD	–	–	[94]	
		ZnO NPs	OXD, POD	Detection of carvedilol, L-cystine, L-proline, L-cysteine, L-histidine, dopamine, epinephrine, pyrogallallic acid, tannic acid, ascorbic acid, hydroquinone, pyrocatechol and <i>p</i> -aminophenol	3.25 nM, 0.85 ng/L, 0.91 ng/L, 0.79 ng/L, 0.56 ng/L, 0.8 ng/L, 0.74 ng/L, 0.43 ng/L, 0.27 ng/L, 0.38 ng/L, 0.65 ng/L, 0.11 ng/L, 0.89 ng/L	[95,96]	
		V <sub>2</sub> O <sub>5</sub> nanowires	POD	Antioxidant	–	[97]	
		V <sub>2</sub> O <sub>5</sub> NPs	POD	Antibacteria	–	[98]	
		VO <sub>2</sub> nanoplates	POD	–	–	[99]	
		V <sub>6</sub> O <sub>13</sub> nanotextiles	OXD, POD, CAT	Detection of glutathione, H <sub>2</sub> O <sub>2</sub> and glucose	0.63 μM, 6.41 μM, 0.02 μM	[100]	

(continued on next page)

Table 1 (continued)

Type	Nanomaterial	Enzyme-like	Application	Detection limit	Reference
Single-atom nanozymes	VO <sub>x</sub> nanoflakes	POD, CAT	Detection of glucose and H <sub>2</sub> O <sub>2</sub>	–	[101]
	Cu <sub>2</sub> O NPs	OXD	–	–	[102]
	CuO NPs	POD	Phenol degradation	–	[103]
	Cu <sub>5</sub> .4O NPs	SOD, CAT	Therapeutics for inflammation related diseases	–	[104]
	Cu <sub>x</sub> O NCs	SOD, CAT	Therapeutics for Parkinson's disease	–	[105]
	MoO <sub>3</sub>	OXD	Cytoprotection	–	[106]
	RuO <sub>2</sub> NPs	POD, CAT, SOD	Therapeutics for acute kidney injury	–	[107]
	FeN <sub>5</sub> SA/CNF	OXD	Antibacteria	–	[108]
	Fe SAEs	POD, OXD, CAT	Degrade phenol	–	[109]
	Fe-SAs/NC	POD, CAT, SOD	Detection of acetylcholinesterase, Cytoprotection	0.56 U L <sup>-1</sup>	[110,111]
	Fe-N-C SAzymes	OXD, POD	Detection of acetylcholinesterase, organo phosphorus compounds and glucose	0.014 mU mL <sup>-1</sup> , 0.97 ng mL <sup>-1</sup> , 8.2 μM	[112,113]
	CNT/FeNC SAN	POD	Detection of H <sub>2</sub> O <sub>2</sub> , glucose, and ascorbic acid	0.03 μM, 0.02 μM, 0.03 μM	[114]
	Fe-N-rGO	POD	Detection of acetylcholine and H <sub>2</sub> O <sub>2</sub>	20 nM	[115]
	SA-Fe/NG	POD	Detection of Cr(VI)	3 nM	[116]
	SAFNCs	POD	Antibacteria	–	[117]
	Pt/CeO <sub>2</sub>	POD, CAT, SOD	Therapeutics for neurotrauma	–	[118]
	Cu/HCSs	POD, CAT, SOD	Antibacteria	–	[119]
	Cu-N-C	POD	Detection of H <sub>2</sub> O <sub>2</sub> and glucose	0.12 μM, 0.58 μM	[120]
	Ti <sub>3</sub> (Al <sub>x</sub> Cu <sub>1-x</sub> )C <sub>2</sub>	POD	Detection of H <sub>2</sub> O <sub>2</sub>	0.06 μM	[121]
	PMCS	POD	Disinfection	–	[122]
	Mo <sub>5A</sub> -N <sub>x</sub> -C	POD	Detection of xanthine	–	[123]
	Fe-N/C SACs	POD, OXD, CAT	Antioxidant	–	[124]
	OxgenMCC-r	CAT	Therapeutics for tumor	–	[125]
	Co-MoS <sub>2</sub>	POD	–	–	[126]
	Co-PMCS	CAT, SOD, POD	Sepsis management	–	[127]
	MitoCAT-g	OXD	Therapeutics for cancer	–	[128]
	FeBNC SAzymes	POD	Detection of organo phosphorus pesticides	2.19 ngmL <sup>-1</sup>	[129]
Mo/Zn	POD	Detection of H <sub>2</sub> O <sub>2</sub>	24.4 μM	[130]	
Fe <sub>2</sub> NC@Se	SOD, OXD, CAT	Therapeutics for reperfusioninjury	–	[131]	
CuMn	CAT, OXD	Therapeutic for tumor	–	[132]	
M1/M2-NC (M = Fe, Co, Ni, Mn, Ru, Cu)	POD	Therapeutic for tumor	–	[133]	
Cu/GMP MOF	OXD	Detection of epinephrine	0.41 μg mL <sup>-1</sup>	[134]	
Ce-MOF	OXD	Detection of cysteine, homocysteine and glutathione	0.150 μM, 0.132 μM, 0.125 μM	[135]	
Co/2Fe MOF	OXD, POD	Detection of H <sub>2</sub> O <sub>2</sub>	5 μM	[136]	
Au/CuS composite	POD	Degrading pollutants	–	[137]	
Au-MOF	OXD, POD	Detection of glucose, glucose and lactate	8.5 μM, 4.2 μM, 5.0 μM	[138,139]	
FeS	POD	Detection of H <sub>2</sub> O <sub>2</sub>	92 nM	[140]	
Fe <sub>3</sub> S <sub>4</sub> NPs	POD	Detection of glucose	0.16 μM	[141]	
Fe <sub>2</sub> NPs	OXD, POD	Therapeutics for tumor	–	[142]	
MoS <sub>2</sub> nanoflowers	POD	Antibacteria	–	[143]	
MoS <sub>2</sub> -Pt <sub>74</sub> Ag <sub>26</sub> nanohybrids	POD	Detection of H <sub>2</sub> O <sub>2</sub> and glucose	0.4 μM, 0.8 μM	[144]	
MoS <sub>2</sub> -Lys NSs	POD	Antibacteria	–	[145]	
Fe-MOF	POD	Detection of H <sub>2</sub> O <sub>2</sub> and ascorbic acid	0.13 μM, 15 μM	[146]	
Cu-MOF	POD	Detection of alkaline phosphatase	0.19 UL <sup>-1</sup>	[147]	
Ni-MOF	POD	Detection of H <sub>2</sub> O <sub>2</sub>	8 nM	[148]	
Pt-MOF	POD, CAT	Detection of Hg <sup>2+</sup> , Therapeutics for cancer	0.35 nM	[149,150]	
Tb-MOF	POD	Detection of estrogen endocrine disruptors	50 pM	[151]	
CuS NCs	POD, CAT, SOD	Detection of acid phosphatase	0.01 U L <sup>-1</sup>	[152]	
MoS <sub>2</sub> @Au@BSANSs	POD, CAT, SOD	Antibacteria	–	[153]	

leading to its dissociation and the formation of O\* without a magnetic moment. O\* can oxidize organic substrates, resulting in monometal nanozymes exhibiting OXD-like activity. The superoxide anion •O<sub>2</sub><sup>-</sup> is a Brønsted base and susceptible to protonation, so it can be transformed into peroxyhydroxyl radicals (HO<sub>2</sub>•) in the solution. Once adsorbed onto the metal surface, HO<sub>2</sub>• undergoes atomic rearrangement, resulting in the production of O<sub>2</sub>\* and H<sub>2</sub>O<sub>2</sub>\*, thus displaying SOD-like activity. Notably, it was also found by theoretical calculations that the catalytic

activity increases with increasing adsorption energies of H<sub>2</sub>O<sub>2</sub> and <sup>3</sup>O<sub>2</sub> on the metal surface [156]. There have been many reports on enzyme-like catalysis by noble-metal nanozymes; however, few studies have been conducted on their catalytic mechanisms.

## 2.2. Metal alloy nanozymes

The catalytic properties of TMNs can be adjusted by fabricating

alloys with different elemental compositions (bimetallic and multimetallic alloys) [23,85,93]. Compared to monometallic nanozymes, metal-alloy nanozymes are more cost-effective and have been observed to show improved performance in biocatalytic reactions. For example, although small Pt NPs (<5 nm) exhibit excellent catalytic activity, SPR is rarely employed because it is located in the UV region. In contrast, Au nanorods exhibit a ratio-dependent longitudinal SPR and are often used in optical sensing, imaging, and hyperthermia treatment. Inspired by this, Guo et al. developed Au@Pt nanostructures and discovered that the OXD-, POD-, and CAT-like activities of Au@Pt were dependent on the composition [157]. Therefore, the Pt-containing nanostructure was demonstrated for sensing-based enzyme-linked immunosorbent assays (ELISA) by detecting mouse interleukin 2 (Fig. 2). The results revealed that the antibody was securely attached to the Au@Pt nanostructures, displaying strong biological detection capability, and this approach was more sensitive in the presence of H<sub>2</sub>O<sub>2</sub>. Moreover, the introduction of magnetic metals such as cobalt, iron, and nickel can yield multimetallic alloy nanozymes and further enhance the enzymatic properties of these alloys [61,65]. Mei et al. found that PtCuCo NPs can act as POD-like catalysts in the reaction between luminol and H<sub>2</sub>O<sub>2</sub> [158]. PtCuCo NPs catalyzed the rapid decomposition of H<sub>2</sub>O<sub>2</sub> and dissolved oxygen into highly reactive (hydroxyl radicals) •OH and O<sub>2</sub>•<sup>-</sup>. O<sub>2</sub>•<sup>-</sup> initiate an active oxygen chain reaction to form singlet oxygen (<sup>1</sup>O<sub>2</sub>). Simultaneously, luminol and H<sub>2</sub>O<sub>2</sub> are broken down to generate luminol<sup>•-</sup> and HO<sub>2</sub>. This triggered a reaction between the generated luminol<sup>•-</sup> and HO<sub>2</sub> with •OH, accelerating the production of luminol<sup>•-</sup>. Luminol<sup>•-</sup> then reacts with <sup>1</sup>O<sub>2</sub> and O<sub>2</sub>•<sup>-</sup> to form unstable 3-APA\*, which quickly returns to the ground state and emits bright light at 425 nm. Owing to the synergistic catalytic activity of PtCuCo, trimetallic nanozymes possess the highest activity among the studied particles. In summary, synergistic effects are the main reasons for the improved catalytic performance of metal-alloy nanozymes [62,159].

In addition to bimetallic and trimetallic nanozymes, high entropy

alloys (HEA) are a new type of alloy nanozymes developed in recent years, which are composed of five or more metals in equal or nearly equal proportions. The combination of multiple components in HEAs creates a stable single-phase solid-solution structure that can modify the electronic and geometric structures of the alloy materials to achieve outstanding catalytic performance. For example, Liang et al. developed ultrasmall HEA nanoparticles (US-HEANPs) through the carbonization of metallo-supramolecular precursors created by an aldol condensation reaction-based metal–ligand crosslinking technique [76]. This simple and versatile method produces US-HEANPs with remarkable POD-like activity. Because US-HEANPs have random mismatches, atomic occupancy, and original properties of the five different metal elements, electron transfer during the reaction was accelerated, thus accelerating the enzyme catalysis process and generating highly toxic •OH from endogenous H<sub>2</sub>O<sub>2</sub>. Furthermore, US-HEANPs exhibit a high photo-thermal conversion effect. However, reports on the production of HEAs with specific structures and investigations of their enzymatic catalytic activity are limited. Despite their remarkable catalytic performance, further research is required to achieve controllable synthesis methods and fully elucidate the catalytic mechanisms of HEAs as nanozymes for more widespread applications.

### 2.3. Metal-oxide nanozymes

Various metal oxides have been used to synthesize nanozymes. It has been reported that these metal oxide-based nanozymes have enzymatic activity similar to various enzymes, including POD, OXD, CAT, and SOD [93], due to their high surface energy and proportionately large surface area, as well as magnetic and fluorescence quenching properties [160]. Iron-oxide NPs were the first nanozymes to be discovered with intrinsic POD-like activity. It has been reported that Fe<sub>3</sub>O<sub>4</sub> can catalyze the oxidation of horseradish peroxidase (HRP) substrates such as TMB, 2,2'-diamino-azobenzene, or OPD, resulting in the formation of blue-, brown-

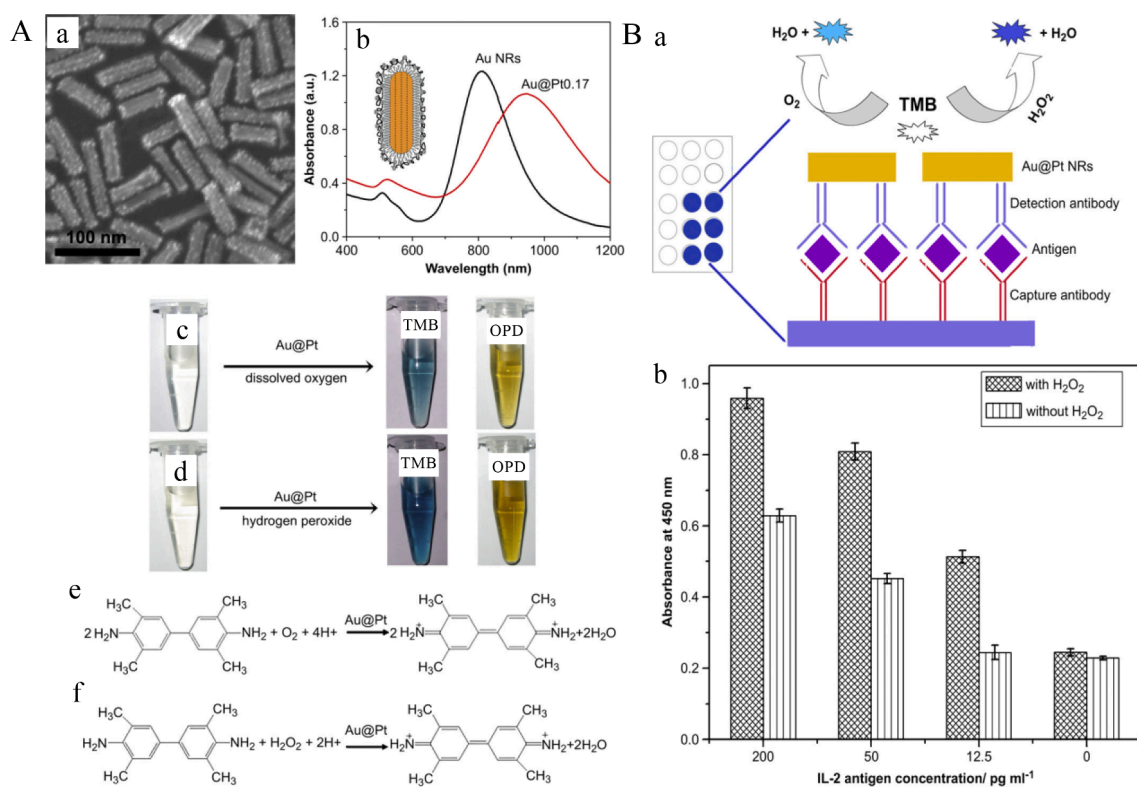


**Fig. 2.** (A) (a) SEM image of Au@Pt and (b) UV–vis–near-infrared (NIR) spectrum of Au@Pt. Color changed depiction of oxidizing TMB and OPD without (c) and with (d) the H<sub>2</sub>O<sub>2</sub>. Catalytic reaction of O<sub>2</sub> (e) and H<sub>2</sub>O<sub>2</sub> (f) by TMB reduction. (B) The ELISA depended on Au@Pt NRs (a) and Au@Pt 0.17 (b). Reprinted with permission from Ref. [157].

or orange-colored products [25]. DFT calculations were used to study the catalytic mechanisms and reaction kinetics of the iron-oxide surfaces with POD-like activities [161]. All surfaces analyzed were found to catalyze the reaction through a three-step mechanism involving the chemisorption of  $\text{H}_2\text{O}_2$  to form two hydroxyl adsorbates, followed by two reduction processes to remove the hydroxyl groups from the surface. In addition to iron-based nanomaterials, many other types of metal-oxide nanomaterials exhibit similar enzymatic properties. Moreover, electron transfer-related mechanisms have been employed to explain the enzymatic performance of metal oxide-based nanozymes [162]. For example,  $\text{CeO}_2$  mimics CAT [163]. The  $\text{H}_2\text{O}_2$  molecule first attaches to the  $2\text{Ce}^{4+}$  binding site of the oxygen vacancy site, resulting in a fully reduced oxygen vacancy site, with oxygen being produced from the released protons and two electrons being transferred to the two  $\text{Ce}^{4+}$ . Subsequently, the homolysis of the O–O bond leads to the binding of another  $\text{H}_2\text{O}_2$  molecule to the  $2\text{Ce}^{3+}$  site, which is a consequence of the transfer of two electrons and the uptake of two protons. The nanoceria surface returned to its initial  $\text{Ce}^{4+}$  sites after  $\text{H}_2\text{O}$  molecules were released. However, the proposed mechanisms for CAT-like properties have certain shortcomings because they do not consider real structural features [164]. Guo et al. explored the potential mechanism of CAT-like activity at the atomic and molecular levels [165]. The mechanisms of alkali- and acid-like dissociation and hydrogen peroxide association were considered by incorporating two  $\text{H}_2\text{O}_2$  molecules into the calculation model. Calculations of the thermochemical energies and associated activation barriers suggested that the most viable mechanism for the CAT-mimicking catalytic recycling of  $\text{Co}_3\text{O}_4$  is the bi-hydrogen peroxide associative mechanism. In addition,  $\text{CeO}_2$  can simulate POD [166] and SOD [167] because of the large number of empty oxygen sites and mixed valence states of  $3+$  and  $4+$  in cerium.  $\text{Co}_3\text{O}_4$  NPs show POD, OXD, and SOD-like activities [92,168,169].  $\text{V}_2\text{O}_5$  has shown intrinsic POD-like activity [170], which was attributed to the nanozyme surface properties and not to free orthovanadate anions. Furthermore,  $\text{Mn}_3\text{O}_4$  [171] and  $\text{MnO}_2$  [172] have been reported to be SOD mimics. The coupled electron-transfer model, polished catalytic cycle mechanism, and Langmuir–Hinshelwood and Eley–Rideal mechanisms are considered possible mechanisms for explaining the SOD mimetic properties of nanozymes [163,165,173,174].

#### 2.4. Single-atom nanozymes

With the advancement of high-angle annular dark-field scanning transmission electron microscopy (HAADF-STEM), the study of nanozymes has entered a new era of single-atom analyses. Single Pt atoms dispersed on  $\text{FeO}_x$  exhibit remarkable stability and activity for CO oxidation, thus leading to the concept of “single-atom catalysts,” namely a catalyst constructed by anchoring isolated metal atoms with catalytic activity on a solid support, with a uniform distribution of active sites and no obvious interaction between them [175–179]. Single-atom catalysts greatly improve the utilization rate of atoms and the density of active centers compared to traditional catalysts. Similarly, various single-atom nanozymes (SAzymes) have been developed, and this research area is becoming increasingly popular [114]. The typical structures of SAzymes include metal-oxide (M–oxide), metal–metal (M–M), metal- $\text{N}_4$  (M– $\text{N}_4$ ), and metal- $\text{N}_5$  (M– $\text{N}_5$ ) [108,180–182]. The main factors affecting the enzymatic properties of SAzymes are the active sites of M–N and the coordination structure of M–N–C groups (mainly Fe, Cu, Pt, and Zn) [183–186]. The main factors affecting the catalytic activity of SAzymes with the best electronic and geometric M–N–C coordination structures are the carrier morphology, molecular ligands, metal clusters, atomic dopants, defects, number and type of N atoms, and the heterozygous mode [187]. Researchers have discovered that SAzymes are more efficient than “conventional” nanozymes, with activity levels that are a factor of 3–100 times higher [180]. Yan et al. demonstrated that a Pt/ $\text{CeO}_2$  SAzymes had POD-like activity that was 3–10 times higher than that of Pt particles and  $\text{CeO}_2$  nanoclusters due to the ability

of  $\text{CeO}_2$  to strongly trap Pt single atoms [118]. Additionally, dispersing single Pt atoms on the  $\text{CeO}_2$  surface increases the utilization of single Pt atoms by up to 100 %. Moreover, the Pt/ $\text{CeO}_2$  nanozyme displayed higher CAT-like activity and four-fold higher SOD-like activity than Pt NPs and  $\text{CeO}_2$  nanoclusters (Fig. 3). In addition to mimicking POD, CAT, and SOD activities, SAzymes exhibit OXD and GPx activities. Researchers successfully synthesized iron SAzymes (Fe-N/C-CNT) containing an  $\text{FeN}_3$  active site, confirming that  $\text{FeN}_3$  is a key oxidative active site conferring significant OXD-like activity to Fe-N/C-CNT and that the catalytic mechanism may be based on the resulting reactive oxygen species (ROS) [183,188]. Huang et al. proposed a novel iron SAzyme ( $\text{FeN}_5$  SA/CNF) and assessed the catalytic activities of  $\text{FeN}_4$  SA/CNF and  $\text{MN}_5$  SA/CNF (where M denotes the metal: Mn, Fe, Co, Ni, or Cu) [108]. Moreover,  $\text{FeN}_5$  SA/CNF exhibited a stronger OXD-like activity than other NPs, such as  $\text{CeO}_2$ ,  $\text{Fe}_3\text{O}_4$ ,  $\text{MnO}_2$ ,  $\text{CuO}$ ,  $\text{Au}$ ,  $\text{Pd}$ , and  $\text{Pt}$ . Cao et al. synthesized Co/PMCS NPs that simulated the catalytic processes of SOD, CAT, and GPx to eliminate  $\text{O}_2^{\bullet}$  and  $\text{H}_2\text{O}_2$  [127]. Concurrently,  $\bullet\text{OH}$  was effectively reduced by the redox cycles, demonstrating the unprecedented activity of the nanozymes. Moreover, the SAzyme effectively eradicates  $\bullet\text{NO}$  through the collective action of coporphyrin centers, which is nearly impossible for nanozymes. The theoretical mechanisms of SAzyme catalysis can be elucidated using DFT because of the unique coordination environment of atomically dispersed metal catalysts. In M–N–C nanostructures, the isolated M– $\text{N}_x$  active sites act as the heart of metalloproteinases, and the presence of nitrogen is vital for their enzyme-like catalytic activities in SAzymes. The catalytic performance of SAzymes in a transition-metal oxide can be attributed to strong metal–support interactions between the isolated metal atoms and the support. To further elucidate the catalytic mechanism of SAzymes, they introduced the concept of electronic metal–support interaction (EMSI) to explain how the chemical and catalytic properties of the metal and support can be affected by electronic perturbations, specifically shifts in the energy of the d-band center. Overall, the catalytic activity of SAzymes is largely associated with the electronic states of the active site [189].

#### 2.5. Diatomic nanozymes

Diatomic nanozymes (DAzymes), particularly heteronuclear DAzymes, are nanoscale molecules composed of two different atoms held together by coordination bonds. This special structure provides remarkable catalytic performance, specificity, stability, and controllability. The high catalytic efficiency and specificity of DAzymes accelerate chemical reactions in organisms, and their high structural stability makes them resistant to inactivation during the catalytic process, making them useful for various applications in biomedicine and environmental science. Additionally, the catalytic activity can be regulated by adjusting the atomic type, coordination environment, and other factors to meet the requirements of different applications [190]. Zhou et al. developed multifunctional CuMn diatomic nanozymes loaded with the chemotherapeutic drug doxorubicin ( $\text{DOX}@CuMn$ -DAzymes) [132]. This system triggered a super-exchange interaction between the Cu and Mn atoms, resulting in an optimized electronic structure and the synergistic effect of  $\text{Cu}^{2+}$ – $\text{Mn}^{3+}$  diatomic pairs. The  $\text{DOX}@CuMn$  DAzymes had excellent CAT and OXD enzyme activities and could efficiently catalyze cascade reactions with endogenous  $\text{H}_2\text{O}_2$  as the starting reactant in an acidic tumor microenvironment. This highly active catalytic center accelerates the rate-fixing step of the cascade reaction, thereby promoting the subsequent generation of  $^1\text{O}_2$ . In addition,  $\text{DOX}@CuMn$  DAzymes exhibited remarkable 1064 nm laser-prompted photothermal performance, high DOX loading efficiency, and dual pH- and near infrared ray (NIR)-responsive DOX release. Song et al. presented a straightforward and universal method for synthesizing a DAzyme library with similar structures using formamide condensation and carbonization to demonstrate the POD-like catalytic properties of these materials [133]. The results revealed that  $\text{Fe-N}_4$  is a highly active site with

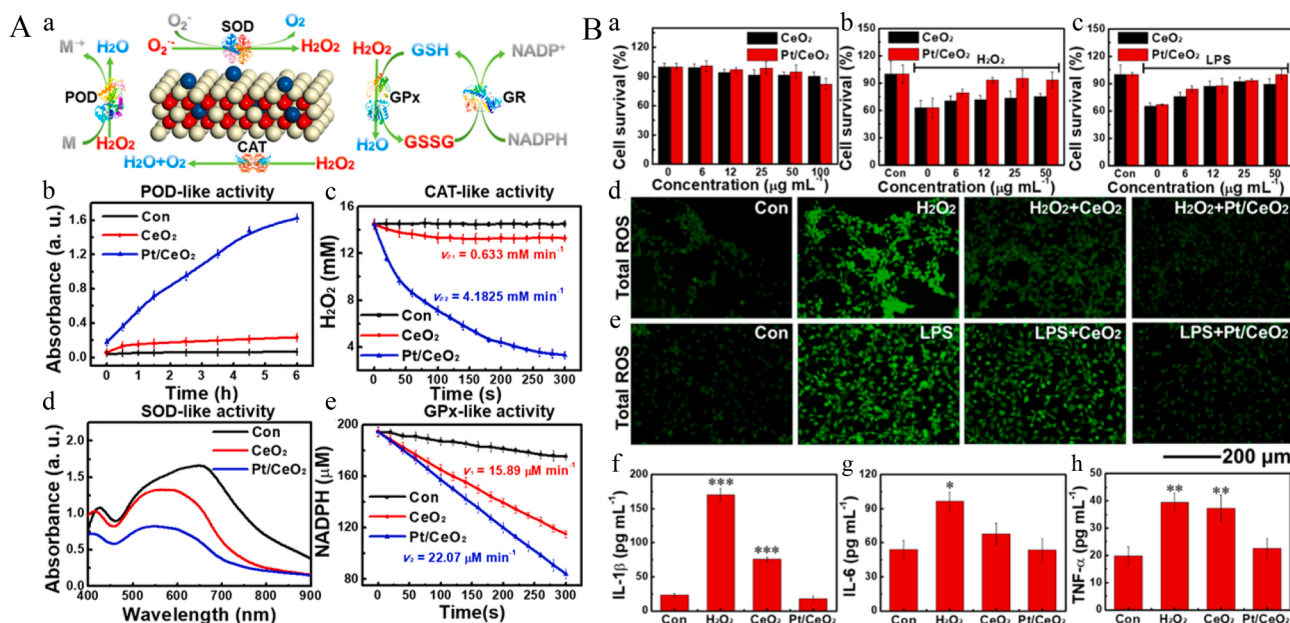


Fig. 3. (A) Schematic diagram of the enzymatic antioxidant defense system in the absence and presence of Pt/CeO<sub>2</sub> catalysis. (B) Survival rate of cells incubated with (a) nanozymes, (b) H<sub>2</sub>O<sub>2</sub>, and (c) LPS in the presence and absence of nanozymes through MTT determination. Fluorogram of total ROS in cells stained with DCFH-DA in the presence of (d) H<sub>2</sub>O<sub>2</sub> and (e) LPS and in the presence and absence of nanozymes. Levels of (f) IL-1 $\beta$ , (g) IL-6, and (h) TNF- $\alpha$  in cell determined with H<sub>2</sub>O<sub>2</sub> induction by ELISA. Reprinted with permission from Ref. [118].

outstanding POD-like activity, and the incorporation of heteronuclear metal atoms, particularly Co atoms, significantly enhances the catalytic efficiency. Theoretical calculations suggested that doping with Co heteronuclear sites modulates the d-band center of Fe<sub>1</sub>-NC, providing additional reaction sites and decreasing the reaction energy barrier of the entire catalytic pathway, thus facilitating the catalytic process. Additionally, upon doping with Fe and Co atoms, the photothermal performance of the amorphous NC improved with decreasing band gap. The synergetic effect between the homo- or heterobimetallic pairs in DAZymes is a key factor for improving the catalytic performance. However, few studies have thoroughly investigated and systematically verified the role of diatomic sites in nanozymes to explore their respective structure–activity relationships in biocatalytic reactions.

## 2.6. Other nanozymes

In addition to the metal- and metal oxide-based nanozymes, SAzymes, and DAZymes mentioned above, metal sulfides (e.g., FeS<sub>2</sub>, CuS, and MoS<sub>2</sub>), MOFs, and metallic core–shell nanostructures have been reported to exhibit enzymatic activity [136,191,192]. In this review, we focus on nanozymes based on metal sulfides and MOFs. In the last few years, metal sulfide-based nanozymes have been developed as substitutes for enzymes, offering benefits such as straightforward synthesis, a low bandgap for electron transfer, and adjustable catalytic effectiveness [193]. Among the many metal sulfide-based nanozymes, those that incorporate MoS<sub>2</sub> have been shown to have superior redox chemistry, photophysical properties, and excellent POD-like catalytic activity [143,194]. Lin et al. reported that layered MoS<sub>2</sub> nanosheets have POD-like activity, can produce  $\bullet\text{OH}$  through the decomposition of H<sub>2</sub>O<sub>2</sub>, and catalyze substrates such as OPD, ABTS, and TMB in color reactions [195]. In the reaction process, electrostatic effects cause TMB to be adsorbed on the surface of the nanosheets, resulting in electron transfer from the amino groups to the nanosheets, thus accelerating the electron transfer between the nanosheets and H<sub>2</sub>O<sub>2</sub> and increasing the reaction rate. Compared with other nanomaterials (such as Co<sub>3</sub>O<sub>4</sub>, TiO<sub>2</sub> nanotubes, Fe<sub>3</sub>O<sub>4</sub> NPs, and Pt nanotubes), MoS<sub>2</sub> nanosheets are characterized by higher catalytic activity and faster reaction rates over a wide pH range (2.0–7.5). Additionally, for MoS<sub>2</sub> nanosheets, the kinetic

results show a ping-pong mechanism, suggesting that MoS<sub>2</sub> tends to react with the substrate first, and then releases it to react with the other substrate. MOFs have also been studied for their outstanding physicochemical and thermal stabilities, high specific surface areas, and uniform cavity structures. The application of MOFs in nanozymes is based on two important aspects: (i) MOFs themselves have nanozyme activity, and (ii) MOFs act as carriers for various enzymes. Yang et al. prepared a bimetallic (Co/2Fe) organic framework with POD- and OXD-like activity [136]. The introduction of Co enhanced the oxidation activity of the MOF (Co/2Fe), resulting in a high affinity for TMB. ZIF-8 is a typical MOF used for nanozyme immobilization. Wu et al. immobilized GOD and POD in ZIF-8 to form a multienzyme system [196]. The rigidity and limitations of the MOF scaffold structure enhance the thermal stability of the embedded enzyme, thereby preventing protein hydrolysis and chelation. These composites exhibited impressive catalytic efficiencies in enzyme cascade reactions. Zhao et al. prepared Fe-based MOFs and constructed a cascade colorimetric system using Fe-based MOFs loaded with GOx to detect glucose [197]. Compared with HRP, this system showed a higher POD-like activity. Thus, MOFs have two functions: (i) as POD mimics and (ii) as supports for GOx. Moreover, the high activity of MOFs results from their large exposed surface areas, which provide abundant accessible catalytic sites and few diffusion barriers.

## 3. Regulation activity of TMNs

The activity of multiple nanozymes is determined by exogenous conditions (e.g., pH and temperature), size, morphology, composition, surface modification, ions or molecules, and external energy. Among these factors, the composition has the most significant influence on activity. The various factors affecting the enzymatic activity of nanozymes stem from (i) the effect of the number of nanozyme active sites and (ii) their influence on the activity of a single active site. In this section, we discuss how each factor affects nanozyme activity.

### 3.1. Exogenous condition

Nanozyme activity is influenced by the pH of the surrounding medium. The POD activity of nanozymes is usually more efficient in acidic

environments, whereas the CAT activity is more efficient in alkaline environments. Gao et al. analyzed the mechanism by which pH affects the activity of nanozymes, using noble-metal nanozymes as a model [155]. The results showed that pH changed the decomposition process of the reactants on the surface of the noble metal. Under acidic conditions,  $\text{H}_2\text{O}_2$  tends to undergo base-like decomposition on the metal surface, and the pre-adsorbed hydrogen combines with the obtained OH to form  $\text{H}_2\text{O}^*$  and  $\text{OH}^*$ . However, under alkaline conditions,  $\text{H}_2\text{O}_2$  tends to undergo acid-like decomposition due to the pre-adsorption of OH, producing  $\text{H}_2\text{O}^*$  and  $\text{O}_2^*$ . At different pH values, POD and CAT activities were altered through different decomposition pathways. In addition, Gu et al. reported pH-dependent POD and CAT-like activities of  $\text{Fe}_3\text{O}_4$  nanozymes [23]. Under acidic lysosome-mimicking conditions, nanozymes catalyze  $\text{H}_2\text{O}_2$  to generate  $\bullet\text{OH}$ . In neutral physiological environments,  $\text{Fe}_3\text{O}_4$  nanozymes can remove harmful  $\text{H}_2\text{O}_2$  through CAT-like activity (Fig. 4). Additionally, the catalytic efficiency of nanozymes is influenced by temperature. It was shown that  $\text{Fe}@\text{PCN-224}$  NPs exhibit optimal POD-like properties at pH 3.5 and a temperature of  $45^\circ\text{C}$  [198]. At lower temperatures,  $37$  and  $25^\circ\text{C}$ , the activity of the NP decreased to 90 % and 80 %, respectively. Although many novel nanozymes have displayed remarkable enzyme-like properties across a wide range of temperatures, their catalytic properties may be slightly diminished below the optimal temperature [199]. See (Fig. 5).

### 3.2. Size and morphology

The effectiveness of typical nanozymes depends on the particle size; as the particle size decreases, the specific surface area increases and the number of surface atoms increases, leading to a lack of coordination between the surface atoms. This in turn increases the number of surface-active sites, thus enhancing the catalytic efficiency of the nanozymes. Many studies have shown that nanozymes with smaller particle sizes exhibit higher catalytic capacities. Xi et al. synthesized Pd-Ir NPs with four sizes from 3.3 to 13.0 nm, which all exhibited POD-like properties [200]. A model system was used to investigate the size effects and it was shown that smaller NPs exhibited lower detection limits and better catalytic properties. Berret et al. measured the size-dependent properties of SOD-mimicking and CAT-mimicking  $\text{CeO}_2$  NPs within a size range of 4.5–28 nm [201]. Smaller particles displayed the highest catalytic efficiency, owing to an increase in the  $\text{Ce}^{3+}$  fraction. Interestingly, Liu et al. selected  $\beta$ -Casein to create a hybrid Au-based nanozyme of varying sizes (2.8, 4.2, and 8.7 nm) [202]. The 4.2-nm nanozyme exhibited the highest POD-like catalytic activity, while the 8.7-nm nanozyme had the lowest activity. This could be because the protein coating on the nanozyme affected the gap between the substrate and the nanozyme core. Furthermore, Gao et al. experimentally evaluated the POD-like

properties of  $\text{Fe}_3\text{O}_4$  NPs of different sizes [25]. The results showed that the catalytic performance decreased in the order of 30, 150, and 300 nm particles. This was ascribed to the higher surface-to-volume ratio of the smaller nanoparticles, which allowed them to combine better with the corresponding substrates. However, for a single nanoparticle, smaller particles with smaller surface areas exhibit poorer catalytic properties. The surface area of a single particle with a diameter of 300 nm is four times larger than that of a particle with a diameter of 150 nm. Therefore, the size effect can be used to modify the nanozymes to achieve optimal catalytic performance. However, size reduction alone is not a reliable method for controlling the catalytic properties of nanozymes because it exposes only a limited number of surface-active sites.

During the reaction, the morphology of the nanozymes changes owing to variations in the reaction conditions, which further affects catalyst performance [80]. The relationship between morphology and catalytic activity has been extensively studied, and the main influencing factors are surface area, pore size, and volume. Liu et al. explored the catalytic properties of  $\text{Fe}_3\text{O}_4$  NPs with three different morphologies (spherical, triangular, and octahedral) and found that three types of nanomaterials with similar sizes and different morphologies exhibited different catalytic activities; spherical and octahedral  $\text{Fe}_3\text{O}_4$  NPs showed the highest and lowest catalytic activities, respectively [203]. This may be due to the different arrangements of Fe atoms on the surfaces of nanoparticles with different morphological structures and crystal surfaces. In 2017, Mugesh et al. discovered that flower-shaped  $\text{Mn}_3\text{O}_4$  nanozymes had the highest enzyme-like properties among five types of  $\text{Mn}_3\text{O}_4$  nanozymes, owing to their larger size, high specific surface area, and pore size [81]. Furthermore, four types of  $\text{V}_2\text{O}_5$  nanozymes with different morphologies were analyzed by DFT calculations, indicating that the (010) crystal surface had the highest GPx activity [204].

### 3.3. Surface chemistry

Surface modification is a promising strategy for modifying materials or avoiding their aggregation by modifying specific groups or molecules on the surface of materials. Because of the changes in the nanozyme–substrate interactions and/or electron-transfer properties during the catalytic process, nanozyme activity can be improved through surface modification, which involves altering the electronic structure of surfaces, adjusting surface acidity, blocking surface access, and facilitating product desorption. In addition, because nanozymes are affected by salt ions and small molecules in the working system and are prone to aggregation, surface modification can also enhance nanozyme stability [205,206]. This section discusses the improvement of nanozyme activity by surface modification. Surface modification can influence the activity

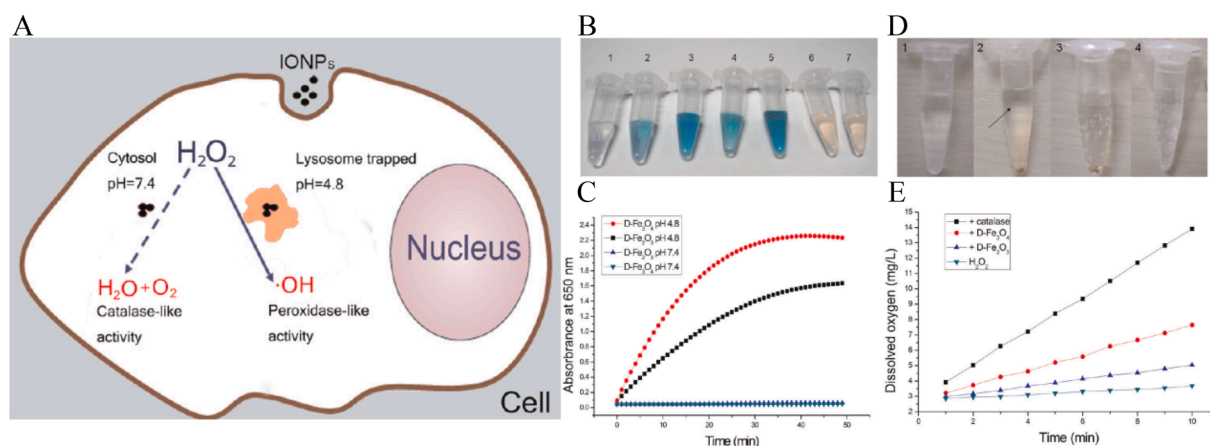
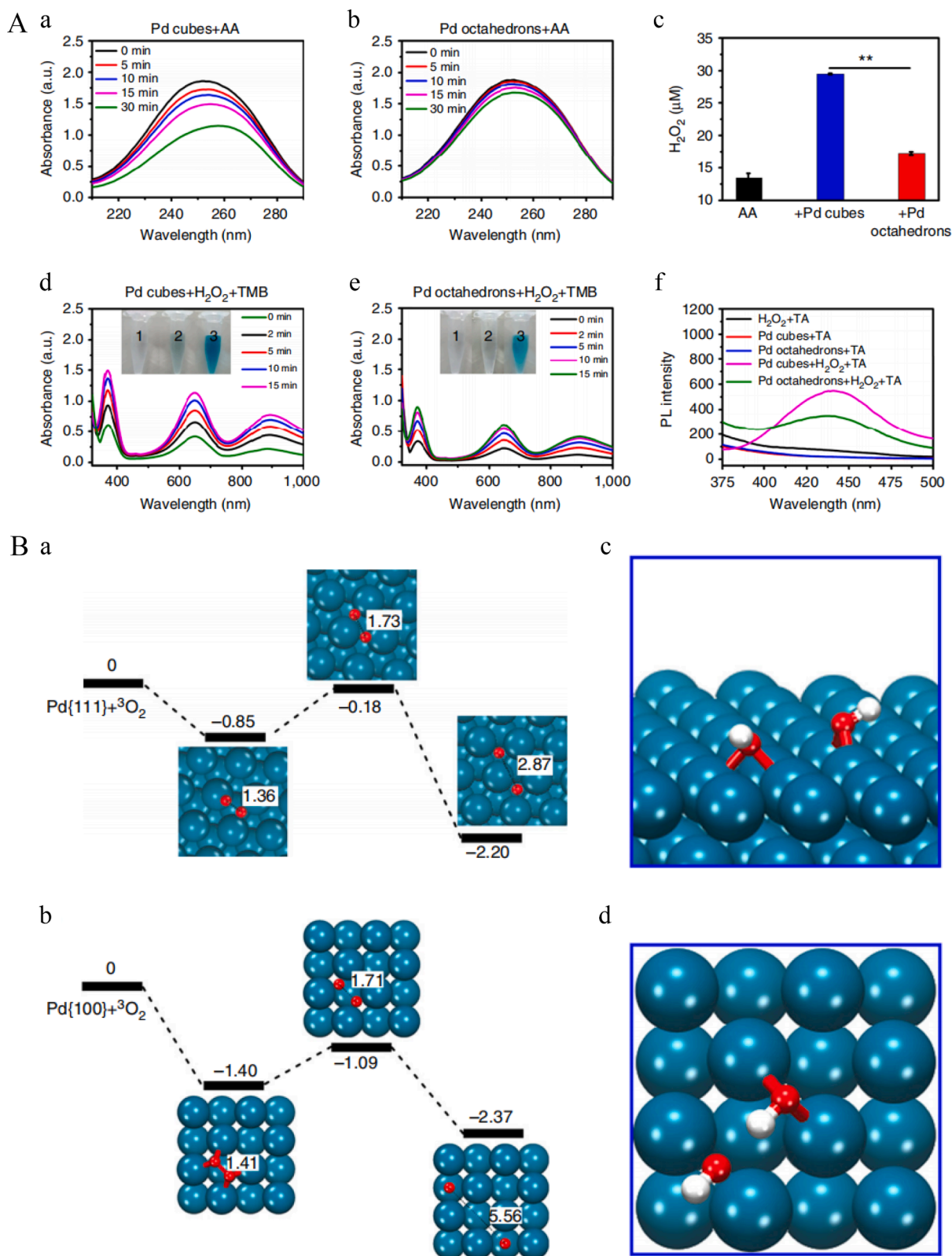


Fig. 4. (A) Scheme diagram of POD-like property induced cytotoxicity by IONPs. (B, C) POD-like property of IONPs. (D, E) CAT-like property of IONPs. Reprinted with permission from Ref. [23].



**Fig. 5.** (A) Effect of time on the AA absorbance in different environments (a, b). (c) The H<sub>2</sub>O<sub>2</sub> production in the catalytic system. Effect of time on TMB absorbance with Pd cubes (d) and the Pd octahedrons (e) catalyzing. (f) The fluorogram of •OH detection in the different systems. (B) The relative energies (eV) (a). The distances (Å) between O atoms (b). The adsorption structures of the two species containing oxygen with lowest-energy on the facets of Pd{111} and Pd{100} (c and d). Reprinted with permission from Ref. [46].

of nanozymes by regulating the adsorption of substrates. Yan et al. proposed the use of histidine residue-anchored  $\text{Fe}_3\text{O}_4$  nanozymes [207]. The affinity between the  $\text{H}_2\text{O}_2$  and imidazole group of histidine increased 10-fold owing to hydrogen bond formation, leading to an improved POD-like activity of the  $\text{Fe}_3\text{O}_4$  nanozymes and a 20-fold enhancement of the catalytic efficiency ( $k_{\text{cat}}/K_M$ ). Furthermore, CAT-like properties were improved by histidine modification. Furthermore, Wu et al. showed that oxidation of the TMB substrate, which is an indication of the POD activity of gold nanorods (AuNRs), could be significantly increased by coating the surface of cetyltrimethylammonium bromide (CTAB)-modified AuNRs [208]. The electrostatic attraction between the carboxyl group of cysteine and the protonated amino group of the TMB substrate enhances the POD activity of the AuNRs; this effect occurred only during the oxidation of the TMB substrate. Interestingly, surface modification by the introduction of glutathione (GSH) with two carboxylic groups inhibited the increase in

catalytic properties. This was attributed to the large molecular size of GSH, which increased the distance between AuNRs and TMB-GSH compared to that between TMB-Cys and AuNRs. Yue et al. chelated metal ions onto  $\text{CeO}_2$  nanorod surfaces to obtain functionalized ceria nanorod catalysts,  $\text{M}/\text{CeO}_2$  (where M represents  $\text{Fe}^{3+}$ ,  $\text{Co}^{2+}$ ,  $\text{Mn}^{2+}$ ,  $\text{Ni}^{2+}$ ,  $\text{Cu}^{2+}$ , or  $\text{Zn}^{2+}$ ) [209]. These metal ions all showed a positive effect on enhancing the POD-like performance, with  $\text{Mn(II)}/\text{CeO}_2$  exhibiting the best affinity for TMB because the surface carboxyl groups serve as substrate-binding sites. Recently, Liu et al. developed substrate-binding pockets on  $\text{Fe}_3\text{O}_4$  nanozymes with POD-like properties by growing molecularly imprinted polymers [154]. The authors reported moderate specificity for neutral monomers by imprinting an adsorbed substrate such as TMB and later introducing charged monomers. The imprinted substrate had a 100-fold greater specificity than the non-imprinted substrate compared to bare  $\text{Fe}_3\text{O}_4$ . The same method was successfully used to imprint the AuNPs (POD mimic) and nanoceria (OXD mimic)

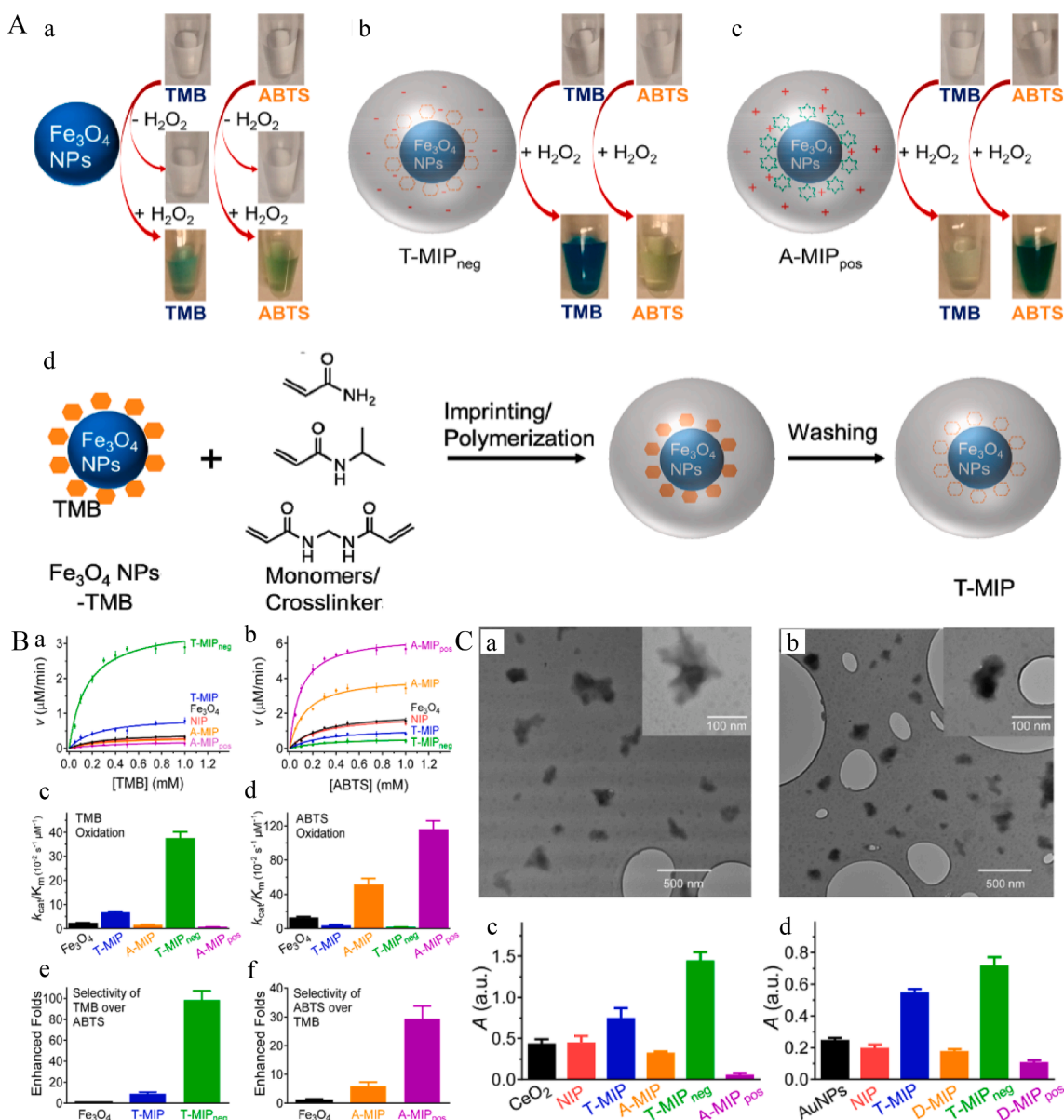


**Fig. 6.** (A) The activity and specificity of oxidating TMB and ABTS for (a)  $\text{Fe}_3\text{O}_4$  NPs, (b) T-MIP<sub>neg</sub> and (c) A-MIP<sub>pos</sub> nanogels in the presence and absence of  $\text{H}_2\text{O}_2$ . (d) Preparation diagram of T-MIP. (B) Catalytic rate of  $\text{Fe}_3\text{O}_4$  NPs and different nanogels used (a) TMB and (b) ABTS as substrates. The specificity of  $\text{Fe}_3\text{O}_4$  NPs and four imprinted nanogels catalytically oxidized (c) TMB and (d) ABTS. The increase fold of these five nanomaterials for oxidation of TMB over ABTS (e) and for oxidation of ABTS over TMB (f). (C) TEM images of (a) nanoceria and (b) AuNP imprinted T-MIP nanogels. Oxidating TMB by (c) free nanoceria and (d) AuNPs. Reprinted with permission from Ref. [154].

(Fig. 6). On the other hand, surface modification can also regulate the effect of nanozyme active sites by influencing electron transfer during catalysis. Liu et al. addressed the limitations of CeO<sub>2</sub> NPs by modifying the surface of CeO<sub>2</sub> with F<sup>-</sup> and obtained over 100-fold OXD-like activity compared to bare CeO<sub>2</sub>, which was ascribed to changes in the surface charge and accelerated electron transfer after introducing F<sup>-</sup> [210]. Berret et al. prepared six nanoparticles by associating CeO<sub>2</sub> cores with six types of polymer-grafted copolymers with distinct terminal groups [211]. The authors systematically investigated the SOD-, CAT-, POD-, and OXD-like catalytic properties of the nanoparticles. The interaction between the polymer and metal center may change the oxidation state of CeO<sub>2</sub>, thus inhibiting CAT- and OXD-like activity, and the synergistic interaction between the polymer and the nanoparticles can enhance the POD-like property, whereas the SOD-like property is not affected.

In addition, PEG-grafted copolymer-coated particles showed better performance for oxidoreductase-like enzymes than poly(acrylic acid)-coated particles. Huo et al. proposed that the critical factor in modulating the catalytic properties of nanozymes is the effect of functional groups on the electron-transfer capacity [212]. Therefore, they modified Co<sub>3</sub>O<sub>4</sub> nanoplates with amino, carboxyl, hydroxyl, and sulfhydryl groups, and systematically studied their POD mimetic properties and kinetic processes. All functional groups, except for the hydroxyl group, exhibited enhanced POD-like activities and the given order of activity. These results indicate that differences in the electron-transfer abilities of different functional groups are responsible for the distinct catalytic properties of functionalized nanozymes.

### 3.4. Composition

Generally, transition metals possess many easily lost single electrons, resulting in variable oxidation states in their electronic configurations, which enable transformations between various valence states, making them candidates for enzyme-like catalysis. Hence, the catalytic oxidation properties of TMNs can be adjusted by regulating specific metal components. For example, the orders of the different metals that oxidize TMB and glucose are (Pt, Ir, Pd, Rh, Ru, Au) and (Au, Pt, Ru, Ir, Pd, Rh), respectively. The catalytic oxidation capacity of TMNs is generally improved by alloying [213]. After the addition of different metals, changes in the geometry of the active sites in the raw material and charge transfer between them and the original metal affect the properties of TMNs [214]. Moreover, the properties of TMNs are significantly influenced by the fractions of the components. Xie et al. incorporated different metals into Ag NPs to form AgM (M = Au/Pd/Pt) alloys [71]. AgM alloys exhibited composition- and proportion-dependent POD activities, confirming that alloying effectively regulates the catalytic activity. To investigate the proportional adjustment of the components, Liu et al. studied various enzyme-like properties (e.g., POD, OXD, ferroxidase, CAT, and SOD) of PtRu NPs and the radical-scavenging properties of 1,1-diphenyl-2-picryl hydrazyl [215]. It was determined that the Pt/Ru molar ratio had a considerable effect on the enzyme-like activities of the PtRu NPs owing to alterations in electron transfer and electronic variation. The catalytic activities were in the order Pt<sub>90</sub>Ru<sub>10</sub> > Pt<sub>75</sub>Ru<sub>25</sub> > Pt > Pt<sub>40</sub>Ru<sub>6</sub>, implying that alloying Pt with Ru can improve both the pro- and anti-oxidant capacities. Another alloying method for TMNs is the formation of core-shell structure, where surface stresses and ligand effects exist between the outer and inner metals, affecting the overall *d*-band center of the material and the activity of the active site [216]. Xia et al. developed Pd@Ir cubes by coating them with extremely thin layers of Ir atoms [68]. This POD-like activity was significantly increased by the expansion of the Ir lattice caused by Pd, exhibiting catalytic constants over 20 and 400 times greater than those of the original Pd cubes and HRP, respectively. Moreover, the POD-like activity of Pd@Ir was related to the thickness of the outer metal layer.

Elemental doping is a practical way to regulate the enzymatic properties of TMNs. Among the various heteroatoms, the best catalytic activity enhancement was observed in the one-dimensional nanowires

made of CeO<sub>2</sub> or CeO<sub>2</sub>-based nanomaterials because of their rough and active (110) facets, which enable the generation of oxygen defects [217]. Zhang et al. introduced various metal elements (Ag, Cr, Co, Rh, Pd, Mn, and Ni) into CeO<sub>2</sub> NPs to prepare CeO<sub>2</sub> nanozymes and found that they exhibited activity similar to that of various enzymes [218]. The Cr/CeO<sub>2</sub> nanozymes showed the best performance because of the increase in the surface Ce<sup>3+</sup>/Ce<sup>4+</sup> ratio by Cr<sup>3+</sup> incorporation, resulting in an enzyme-like activity 3–5-fold higher than the corresponding levels with undoped CeO<sub>2</sub>. In addition, the number and type of doped atoms are critical for regulating the activity of nanozymes. Chen et al. synthesized a battery of Pr-modified ceria nanocubes by adjusting the Pr concentration [219]. Because the conduction-band position of Pr is lower, it can more easily accept electrons from the TMB reducing agent, resulting in improved OXD performance of the Pr-modified ceria NCs with increasing Pr concentration. Jampaiah et al. synthesized various Fe<sup>3+</sup>-doped CeO<sub>2</sub> nanorods (3, 6, 9, and 12 % Fe doping) and studied their POD-like and glucose detection properties [220]. The 6 % Fe<sup>3+</sup>-doped CeO<sub>2</sub> nanorods displayed a higher catalytic activity than the undoped and Fe<sup>3+</sup>-doped CeO<sub>2</sub> nanorods, and a superior catalytic activity for TMB oxidation, as confirmed by steady-state kinetic analysis.

### 3.5. Ions or molecules

In addition to H<sup>+</sup> or OH<sup>-</sup> ions in solution, other ions or molecules can be added to bind to the surface of the nanozymes, thereby affecting the stability of the nanozymes themselves or the binding of the nanozyme to the substrate. It is well established that both ions and molecules can adjust the catalytic properties of nanozymes by serving as modulators. Guo et al. investigated the effect of halide ions on the POD-linked activity of protein-modified Au NPs based on the Au-X interaction-directed binding of halide ions to Au NPs [221]. The catalytic activity of protein-modified Au NPs could be altered by halides because of the different Au-X interactions. The inhibitory effect of F<sup>-</sup>, Cl<sup>-</sup>, Br<sup>-</sup>, and I<sup>-</sup> on protein-modified Au NPs nanozymes was enhanced successively, similar to the reversible and irreversible inhibition of natural enzymes. It is likely that I<sup>-</sup> adsorbs strongly onto the Au nanozyme surface, which may block the binding sites on the nanozyme surface. Although binding at the active sites is a common inhibition principle, it does not apply to all ions, and the physicochemical mechanism needs to be analyzed in detail. Liu et al. prepared β-casein stabilized Pt NPs (CM-PtNPs) using β-casein as a model protein and systematically studied the effect of sulfide on the POD-like property of CM-PtNP [222]. The experimental data showed that sulfide has various regulatory influences on the POD-like properties of CM-PtNP for different reaction substrates. In the case of TMB as a reaction substrate, S<sub>2</sub> combines with CM-PtNP via Pt-S bonds, which blocks the active sites and switches off the activity. In the case of ABTS, the transition from Pt<sup>2+</sup> to Pt<sup>0</sup> was caused by sulfide binding to the Pt nanozyme surface, resulting in more active sites and enhanced enzymatic activity. In 2017, the effects of tungstate, molybdate, sulfate, and selenate ions (similar to phosphoric acid ions) on Ce nanozymes were investigated [156]. The results showed that the four ions had no influence on the surface valence state; tungstate and molybdate inhibited phosphatase activity by inhibiting the interaction between the ATP substrate and nanozymes, but did not affect CAT activity, whereas sulfate and selenate did not affect the activity. Small molecules, such as ATP, ADP, AMP, and other adenosine molecules in solution also bind to the surface of nanozymes [223–225]. These small molecules can enhance the POD-like activity by promoting H<sub>2</sub>O<sub>2</sub> oxidation and enhancing the interactions between •OH and the nanomaterials. However, when macromolecular substances (such as proteins) are bound to the surface of nanozymes, the binding of the substrate to the nanozymes is usually affected by steric hindrance, and the activity of the enzyme is inhibited. Self et al. reported that bovine serum proteins, which are commonly used in cell culture, inhibit the phosphatase activity of CeO<sub>2</sub> nanozymes [226]. When injected into the blood, nanozymes used for *in vivo* therapy encounter a large number of proteins that can produce a

protein crown on their surface, causing irreversible inhibition of activity and seriously hindering their application *in vivo*. Therefore, the effect of protein cap formation on nanozyme activity *in vivo* must be investigated before nanozymes can be viewed as an effective therapeutic option.

### 3.6. External energy

Nanozyme activity can be remotely regulated by external energy based on the physical and chemical performance of nanozymes. For example, the development of a light-controlled system may be a promising strategy for controlling the catalytic efficiency of nanozymes given the high temporal and spatial accuracy afforded by this technique. Prins et al. used light-responsive molecules to regulate the catalytic properties of nanozymes [227]. When 4-(phenylazo)-benzoic acid was exposed to light in the UV to visible spectrum, the conformation of the photo-responsive azobenzene group changed from *trans* to *cis*-structures, and these changes were reversible. When exposed to visible light, the *trans*-structure of 4-(phenylazo)-benzoic acid has a strong affinity for Au NP 1, thus hindering the binding of the substrate to the nanozyme and decreasing its catalytic activity. In contrast, under UV light, the *cis* structure of 4-(phenylazo)-benzoic acid has a lower affinity for Au because of its increased polarity, allowing the catalytic properties of Au NP 1 to be monitored efficiently by detecting the fluorescence intensity of the product. Zhang et al. combined AuNPs and  $\alpha$ -FeOOH microcrystals anchored on the surface of porous carbon, forming Au/ $\alpha$ -FeOOH-FPC catalysts with visible-light-driven enzymatic properties [159]. In this study, AuNPs catalyzed the oxidation of glucose with oxygen to produce  $H_2O_2$  and gluconic acid. The SPR effect facilitates the interaction between glucose molecules and oscillating local electromagnetic fields, which activate the glucose molecules and increase the production of  $H_2O_2$ . The light energy absorbed by AuNPs also generates heat, increasing the temperature to an optimal level for enzymatic reactions. Furthermore, hot electrons from plasmon-excited AuNPs accelerate charge separation at the Au/ $\alpha$ -FeOOH interface, resulting in efficient cycling of  $Fe^{3+}/Fe^{2+}$ . Additionally, the growth of  $\alpha$ -FeOOH nanocrystals on carbon frameworks facilitates electron transfer between carbon and  $\alpha$ -FeOOH, thus preventing the leaching of iron ions. Zhu et al. found that the catalytic properties of  $Fe_2O_3$  nanozymes, which are related to light,

are affected by the band gap and range of light absorption, which are responsible for forming a barrier and absorbing light energy [228]. Additionally, they observed that enzyme-like properties varied depending on the type of light excitation. Wang et al. observed that the catalytic properties of Au/Si/Azo were enhanced in the presence of UV illumination but suppressed in the presence of visible light [229]. These findings suggest that the isomerization of Azo regulates host-guest interactions between azo and cyclodextrin, which is essential for controlling catalytic activity when exposed to UV or visible light. Other forces, such as sound and heat, can also affect the performance of nanozymes. External control may promote the activity of single active sites by improving the thermal motion of reactants near the active site or by modifying the number of active sites by controlling their coverage by molecules. Lin et al. synthesized a disordered graphite nanozyme through carbonization and found that maximum enzyme activity was obtained at 60°C [230]. With the photothermal conversion ability of graphene, the specific activation of nanozymes in tumor treatment can be achieved using near-infrared light. Zheng et al. connected an ultrasound-sensitive agent, T790, to the surface of a Pd@Pt nanozyme (Fig. 7) [231]. T790 inhibits the CAT activity of Pd@Pt, and enzyme activity can be restored after ultrasonic stimulation, thus achieving targeted therapy with controllable tumor sites. The strong penetration ability of ultrasound enables it to be used *in vivo*, unlike light, which cannot penetrate the body.

## 4. Biomedical applications

An increasing number of TMNs have been demonstrated as potential substitutes for natural enzymes that they mimic. The accumulation of results from recent studies has deepened our understanding of TMN systems and has stimulated their biomedical applications. The applications of TMNs in this field include early diagnosis, imaging, and treatment of various diseases. Here, we highlight the various emerging applications of TMNs in biomedicine. By categorizing TMNs based on their particular applications, we highlight the most recent developments and future potential of this technology.

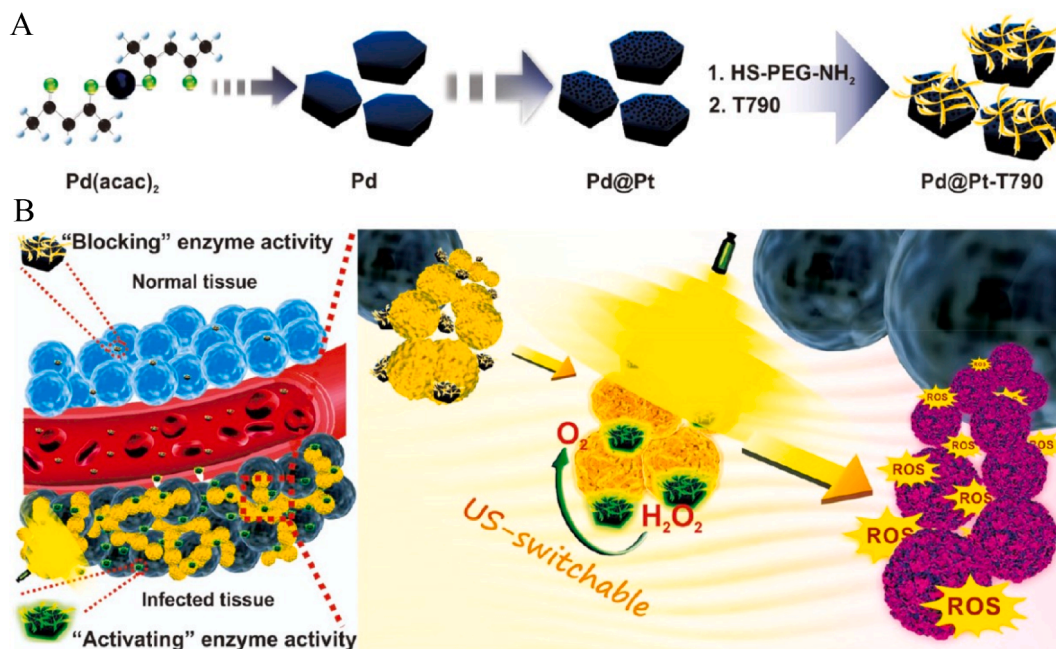
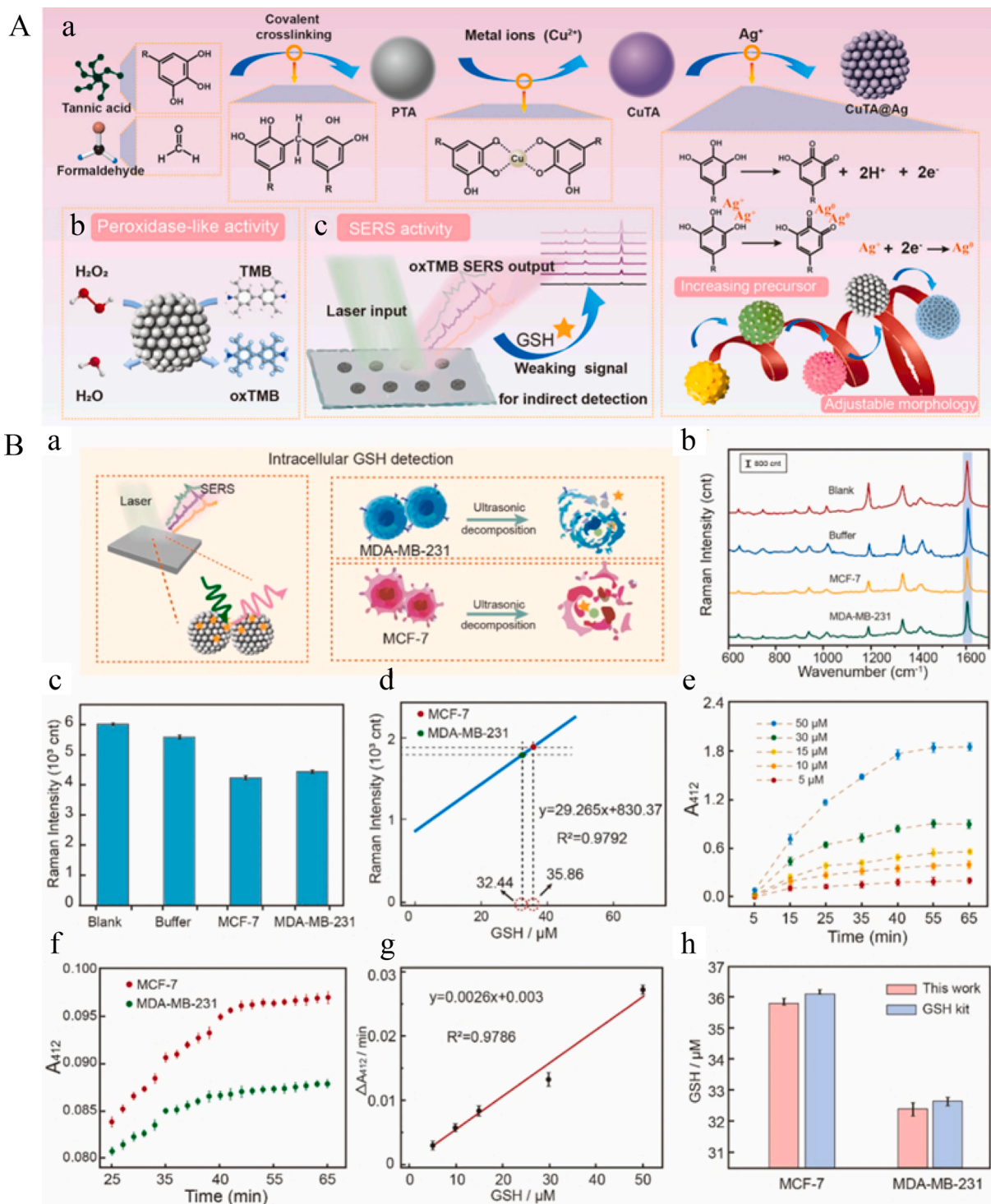


Fig. 7. (A) The synthesis scheme of Pd@Pt-T790 nanoplatform. (B) Pd@Pt-T790 was able to be effectively accumulated at the infection site through the influence of EPR. Reprinted with permission from Ref. [231].

## 4.1. Disease diagnosis

TMNs are multifunctional molecules that have both catalytic activity and unique physical and chemical properties such as magnetic, fluorescent, and photothermal properties. By combining nanozymes with early cancer diagnostic technology, they can be used to detect cancer-related genes, molecules, cells, and tissues, thus providing a novel

approach for enzyme-catalyzed reactions in cancer diagnosis. Here, we review the advances made in the *in vitro* detection of cancer-related genes, GSH and other cancer biomarkers, and cancer cells, and highlight the importance of cancer diagnosis *in vivo*. Other diseases including metabolic, infectious, neurodegenerative, cardiovascular, and inflammatory diseases are also reviewed.



**Fig. 8.** (A) (a) Synthesis process of CuTA@Ag, (b) POD-like activity (c) SERS detection by using Ag NPs deposited metal-polyphenol; (B) (a) SERS detection for cellular GSH of MCF-7. (b) SERS spectra and (c) Raman intensity of TMB (3 mM) on the CuTA@Ag-iv in the cytosol sample. (d) GSH levels in MCF-7, MDA-MB-231 cell lysates analyzed with SERS way. (e) Absorbance at 412 nm for different GSH concentrations employing the GSH kit. (f) GSH levels in cell lysates analyzed with kits. (g) Linear fitting curve of the standard kit. (h) SERS comparison between using CuTA@Ag and the standard kit. Reprinted with permission from Ref. [238].

#### 4.1.1. Cancer diagnosis

**4.1.1.1. Genes detection.** Genetic alterations are a key factor in the development of cancer, and both proto-oncogenes and tumor suppressor genes are necessary for the growth, proliferation, and regulation of cells. Nevertheless, when exposed to certain conditions such as viral infection, chemical carcinogens, or radiation, these genes are easily mutated, deleted, or inactivated, causing malignant cell transformation and tumor formation. Thus, the detection of cancer-related genes is one way to diagnose cancer [232]. Generally, the conventional method concentrates on amplifying genes through a polymerase chain reaction, identifying them with labeled nucleic acid probes, and converting them into detectable signals such as fluorescence, color, and current. However, probe labeling is time-consuming and increases the complexity of operations [233]. Wang et al. developed an easy, label-free DNA detection method using platinum-based nanozymes to detect the breast cancer gene BRCA1 [234]. Platinum NPs (Pt NPs) were loaded onto the surface of mesoporous silica (mSiO<sub>2</sub>) to form Pt@mSiO<sub>2</sub> nanomaterials. Pt NPs exhibit POD activity, which catalyzes the chromogenic reaction of the enzyme substrate TMB with H<sub>2</sub>O<sub>2</sub>. The single-stranded DNA probe (P1) was then adsorbed onto the surface of Pt@mSiO<sub>2</sub> via electrostatic interactions; the mSiO<sub>2</sub> channel was closed and the internal Pt NPs could not catalyze the reaction. However, when complementary DNA (T<sub>0</sub>) was specifically bound to P1 on the surface of Pt@mSiO<sub>2</sub>, the exposed Pt NPs catalyzed TMB oxidation. The sensitivity of the nanozyme signal amplification strategy for BRCA1 was 3 nM and it exhibited excellent single-base pair mismatch recognition ability. Compared to other detection methods, the nanozyme exhibited higher sensitivity and did not require a label probe, demonstrating its huge potential for clinical translational.

**4.1.1.2. GSH detection.** GSH is an important antioxidant in living systems and its content in cancer cells is higher than that in normal cells [235,236]. Various detection systems have been proposed for detecting GSH-dependent TMNs. Wei et al. provided a photosensitized metal-organic framework (PSMOF) that can imitate OXD-like structures controlled by light [237]. PSMOF can catalyze TMB oxidation into oxidized TMB in the presence of visible light irradiation, which has a strong absorbance at 652 nm and exhibits visible, distinguishable color changes, thus making it a colorimetric probe for the detection of GSH. The constructed platform was used to evaluate the GSH levels in the lysates of normal and cancer cells. These results are in agreement with the findings of a commercial GSH detection assay, which showed that the GSH content in cancer cells was approximately double that in normal cells. In addition, Ag NP/copper-polyphenol colloidal spheres (CuTA@Ag) were synthesized [238]. The nanozyme performance and surface-enhanced Raman scattering (SERS) properties were related to the size and density of the deposited Ag NPs. The SERS performance of CuTA@Ag was investigated using oxTMB, a catalytic product of the nanozymes, as a molecular probe (Fig. 8). The system exhibited good detection of GSH levels in cancer cells with satisfactory accuracy and reproducibility. Recently, we fabricated catalytically active protein-directed nanoflower-like artificial nanozymes (apo-TF-MnO<sub>x</sub> NFs) using a biomineralization method to develop a simple visible colorimetric sensor for GSH [239]. The experiments proved that the apo-TF-MnO<sub>x</sub> NFs exhibited POD, CAT, and SOD activities and realized the differential identification of GSH without invasive treatment, which is an advantage over other methods.

**4.1.1.3. Detection of other biomarkers.** Biomarkers play an important role in cancer research. In addition to GSH, biomarker classes specific to tumors involving microRNA (miRNA), DNA, RNA, or proteins have recently been identified, which are related to their potential application as therapeutic targets and in easy clinical diagnosis and follow-up monitoring [240]. Furthermore, researchers have focused on

identifying cancer biomarkers to link molecular mechanisms to clinical diagnosis and cancer therapy. Recently, TMNs have been used to detect various biomarkers. Li et al. utilized the miR-107 target as an activator to develop the self-assembly of Au nanospheres driven by miRNAs on the surface of hollow Au/Ag alloy nanocubes for prostate cancer diagnosis [241]. The prepared nanozymes were able to generate plasmonic-activated SERS signals in the presence of miR-107 and exhibited a novel self-assembled nanomaterial with only signal-amplifying performance. The Au nanospheres on the surface of hollow alloy nanocubes caused catalytic cascades of nanozymes for Raman signals. Additionally, TMNs can be used to detect protein-based cancer biomarkers (Fig. 9). Furthermore, Li et al. reported a novel immunosensor comprised of a Au-Ag composite nanocup array *meta*-SPR chip and an artificial nanozyme-labeled antibody [242]. The sensor was demonstrated for the ultrasensitive and selective detection of cancer biomarkers with a detection limit of alpha-fetoprotein of 21.74 fM, which is far lower than that of commercial enzyme-linked immunosorbent assay kits. The device was also tested for the quantification of carcinoembryonic antigen and carbohydrate antigen 125. Owing to its high speed, user-friendliness, and high throughput, this platform has the potential for rapid, high-throughput cancer screening or early diagnosis. An electrochemical sensor was designed by synthesizing a cysteine-histidine-Cu-modified jujube-like Cu<sub>2</sub>O nanozyme (CH-Cu@J-Cu<sub>2</sub>O) for the detection of mucin-1 on the surface of MCF-7 cells. The sensor had a linear range from 0.5 to 5000 pg mL<sup>-1</sup> and a limit of detection of 0.085 pg mL<sup>-1</sup> [243].

Meng et al. prepared a Pd@Ir core-shell nanozyme and proposed a colorimetric signal amplification method based on the bimetallic nanozyme-mediated *in situ*-catalyzed reporter deposition [244]. This method used gastric cancer biomarkers pepsinogen I and pepsinogen II as model targets and reached a cutoff value of 10 pg mL<sup>-1</sup>, 200 times lower than that without signal enhancement. A highly sensitive heterostructured BiVO<sub>4</sub>/CoPi photoelectrochemical (PEC) biosensor was developed for the detection of miRNA 141, with the aid of in-house-synthesized AuPt nanodendrites as the nanozyme [245]. Using a cyclic enzyme strategy, the PEC biosensor exhibited an impressively wide linear range of 5 fM to 1 pM and a low limit of detection of 0.17 fM (signal-to-noise ratio of 3). This breakthrough provides valuable insights into the sensitivity analysis of tumor-associated miRNAs in clinical settings.

**4.1.1.4. Cancer cell and tissue detection.** Recently, the precise and sensitive detection of tumor cells has become of utmost clinical importance for tracking the development of the disease and assisting the selection of efficient treatment methods to improve clinical results. Trau et al. used dual-functional Fe<sub>3</sub>O<sub>4</sub> nanozymes with magnetic properties and enzyme activity to establish a nanozyme immunoassay for the rapid separation and colorimetric detection of circulating tumor cells (CTC) in serum [246]. A carboxyl-modified Fe<sub>3</sub>O<sub>4</sub> nanozyme was covalently bound to melanoma-specific antibodies to construct a specific melanoma-recognizing Fe<sub>3</sub>O<sub>4</sub> nanozyme, which was then added to the patient's serum to enrich and separate CTCs based on the magnetic properties of Fe<sub>3</sub>O<sub>4</sub> (Fig. 10). Visual detection of CTCs was performed via the POD activity. This convenient, time-saving, and highly sensitive CTC detection method provides a diagnostic basis for the recurrence and metastasis of melanoma in clinical practice and is a good case for the multifunctional application of nanozymes. In 2023, Li et al. designed an ultrasensitive photothermal cell sensor that combined Fe<sub>3</sub>O<sub>4</sub>@PDA NPs and multifunctional Ti<sub>3</sub>C<sub>2</sub>@Au@Pt nanozymes to directly capture and detect breast cancer (BC)-CTCs [247]. DNA (P1) containing MUC1 inducers was adsorbed onto the surface of the Fe<sub>3</sub>O<sub>4</sub>@PDA-P1 capture nanoprobes via Ca<sup>2+</sup>-mediated DNA adsorption for effective BC-CTC capture. To increase the detection signal, a multifunctional two-dimensional core-shell Ti<sub>3</sub>C<sub>2</sub>@Au@Pt nanozyme was synthesized, which is an excellent photothermal nanomaterial and also catalyzes the production of oxTMB from TMB, thereby amplifying the temperature

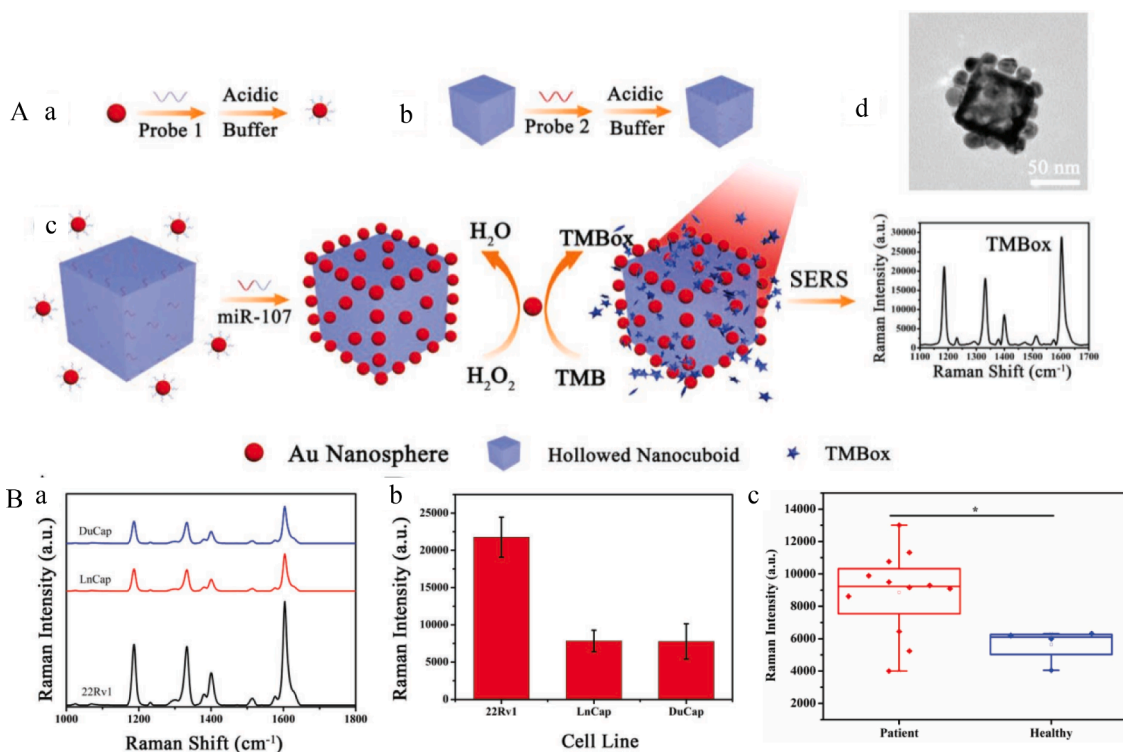


**Fig. 9.** The preparation of plasmonic nanostructures as SERS probe for miR-107 detection. (B) Raman detection for miR-107. (C) Differential detection for miR-107 in urine samples from PCa patients and healthy people by this plasmonic nanostructures, \* $P < 0.05$ . Reprinted with permission from Ref. [242].

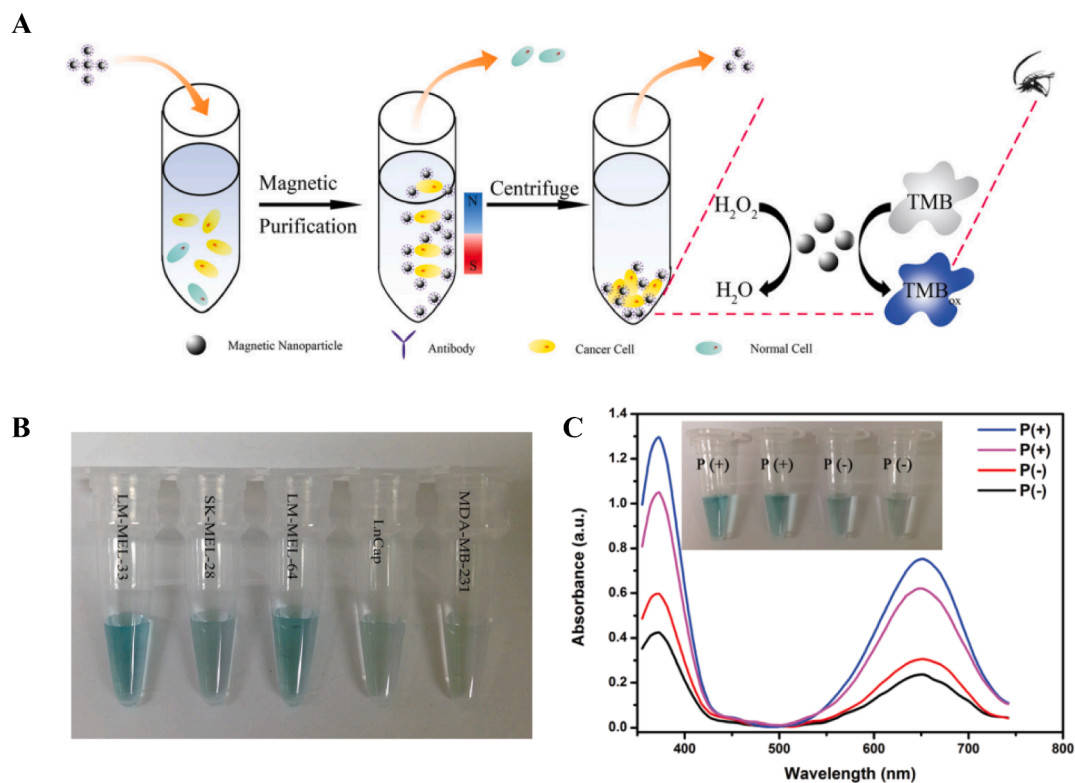


**Fig. 10.** (A) Visual CTC detection. (B) The cell suspensions with  $10^3$  MCSP over expressed cells,  $10^5$  LnCap cells and  $10^5$  MDA-MB-231 cells. (C) CTC detection in model patient bloods. p(+):  $10^3$  LM-MEL-33 cells were added into 7.5 mL healthy blood. p(-): no LM-MEL-33 cells were added into 7.5 mL healthy blood. Reprinted with permission from Ref. [246].

signal. Consequently, the recognition and binding of multiple adaptors are expected to enhance the detection sensitivity and accuracy. This cell sensor has great potential for accurate diagnosis and personalized medical therapy of early breast cancer.

Immunohistochemical detection is currently recognized as the “gold standard” for cancer diagnosis worldwide and is commonly used for pathological diagnosis. The basic process includes the specific binding of antibodies to tumor-related antigens, the specific recognition of tumor cells through the primary antibody, identification of the primary antibody by a second antibody labeled with biotin, and finally the binding of streptomycin labeled on HRP to biotin. Finally, POD was used to oxidize the chromogenic substrate to detect the tumor tissue. However, this immunoassay method requires various antibody incubations and repeated washing with a buffer solution, which has shortcomings such as complicated steps and long operation times, and the analysis of the results is limited by the subjective judgment of those performing the assay. Therefore, it is necessary to improve this method clinically. In 2012, Fan et al. developed a new method for the immunohistochemical detection of cancer using nanozymes [248]. They found for the first time that human heavy-chain ferritin can identify tumor organization and that the recognition level is accurately related to the degree of cancer

malignancy. A dual-function probe was developed that could recognize and visualize tumors and achieve the fast and sensitive detection of tumor tissues. Compared with the conventional immunohistochemical method, the new strategy: (i) has higher sensitivity and specificity; (ii) is more simple and repeatable; (iii) is faster (analysis in less than 1 h); (iv) has lower cost and eliminates the need for expensive, volatile antibodies. These results indicate that ferritin nanozymes are an effective new reagent for rapid, economical, and broad-spectrum tumor diagnosis. Subsequently, Pan et al. confirmed that increasing the size of the nanozyme wrapped in the H-ferritin shell in the ferritin nanozyme enhances its POD performance and staining effect on tumor tissues [249]. By loading an Fe-Co hybrid nanozyme into the H-ferritin shell, the POD-like activity of the ferritin nanozyme could be further enhanced, thus increasing the sensitivity of the ferritin nanozyme for tumor tissue detection [250]. These reports confirm the feasibility and universality of ferritin nanozymes in the pathological diagnosis of cancer.

#### 4.1.2. Diagnosis of other diseases

In addition to cancer diagnosis, scientists have developed new strategies for disease diagnosis based on TMNs, including metabolic, infectious, neuro degenerative, cardiovascular, and inflammatory

**Table 2**  
Nanozymes for other diseases diagnosis.

Diseases	Biomarker	Metal-based nanozymes	Activity	Method	Application	References		
Metabolic diseases	Glucose in blood and urine, purines, fats, proteins, etc	rGO-CMC-H@Pt NCs	POD	Electrochemical detection	1,5-anhydroglucitol	[251]		
		Cu-Pt	POD	Electrochemical detection	Glucose	[252]		
		Ch-Mn <sub>3</sub> O <sub>4</sub> NPs	POD	Colorimetric detection	Glucose and alpha-amylase	[253]		
		MoSe <sub>2</sub> /ZnO	GOD	Surface plasmon resonance	Glucose	[254]		
		RGO-PT/Pt@Pd NPs	POD	Colorimetric detection	1,5-anhydroglucitol	[255]		
		AuNP@AuNCs	POD GOD	Colorimetric detection	H <sub>2</sub> O <sub>2</sub> and glucose	[256]		
		BSA-PtNP@MnCo <sub>2</sub> O <sub>4</sub>	OXD POD	Colorimetric detection	Glutathione glucose	[257]		
		MnO <sub>2</sub> nanoflakes	POD GOD	Colorimetric detection	Glucose	[26]		
		Infectious diseases	Various pathogens	Fe <sub>3</sub> O <sub>4</sub>		Immunoassay	Ebola	
				CeO <sub>2</sub> NPs	OXD	Colorimetric detection	C. trachomatis	
BSA-Ag NCs	OXD			Colorimetric detection	Human immunodeficiency virus	[258]		
Antibodies-Fe <sub>3</sub> O <sub>4</sub>	POD			Colorimetric detection	Rotavirus	[259]		
Antibodies-Au@Pt NRs	POD			Colorimetric immunoassay	Rubella virus	[260]		
FeS <sub>2</sub>	POD			Colorimetric detection	SARS-CoV2	[261]		
PtNPs@Co <sub>3</sub> O <sub>4</sub> NCs	POD			Colorimetric immunoassay	Norovirus	[262]		
Pt@Au NPs	POD			Colorimetric immunoassay and smartphone	Zika virus	[263]		
Ag-TiO <sub>2</sub> SAN	POD			Adsorption	SARS-CoV2	[264]		
DNA-Ag/Pt NCs	POD			Electrochemical detection	VEGF	[265]		
Neurodegenerative disease	Acetylcholine, cysteine, ascular endothelial growth factor (VEGF), dopamine	PtNPs/GO	POD	Colorimetric detection	L-cysteine	[266]		
		Au/Ag NPs	POD	Fluorescence detection	Acetylcholine	[267]		
		DNA-Ag/Pt NCs	POD	Colorimetric detection	L-cysteine	[268]		
		PtCuSe	CAT SOD	Remove reactive oxygen species	Parkinson's disease	[269]		
		PtCu NAs	SOD	Remove reactive oxygen species	Parkinson's disease	[270]		
		Pt NPs	CAT	Digital volumetric bar-chart chip	B-type natriuretic peptide	[271]		
Cardiovascular disease	B-type natriuretic peptide, troponin T, homocysteine, ascorbic acid, thrombin, total cholesterol, etc.	MOF-818	OXD	Colorimetric detection	Troponin I	[272]		
		PtNCs	POD	Colorimetric detection	Thrombin	[273]		
		Fe <sub>3</sub> O <sub>4</sub> @C/Ni	POD	Colorimetric detection	Blood cholesterol	[274]		
		Mn@Co <sub>3</sub> O <sub>4</sub>	OXD	Colorimetric detection	Ascorbic acid	[275]		
			POD					

diseases. The relevant reports are listed in Table 2.

#### 4.2. Cancer therapy

To date, many nanozymes, such as metal nanozymes, metal oxide nanozymes, MOFs, and some non-metal nanozymes, have been designed and applied in biomedicine, particularly in cancer therapy. Depending on their catalytic mechanism, natural enzymes can be divided into hydrolases, oxidoreductases, lyases, transferases, ligases, isomerases, and translocases [276]. In this section, we summarize the oxidoreductase-like properties of nanozymes, including POD, OXD, CAT, and SOD, which are regularly used in tumor catalytic therapy, cascade catalytic therapy, and multifaceted synergistic therapies, mainly involving in chemodynamic therapy (CDT), immunotherapy, photothermal therapy (PTT), photodynamic therapy (PDT), radiotherapy (RT) and sonodynamic therapy (SDT) (Fig. 11).

##### 4.2.1. Catalytic therapy

In recent decades, a series of TMNs that act as POD-like nanozymes have been developed [204,264,277]. OXDs are known to catalyze oxidation–reduction reactions, producing either  $\text{H}_2\text{O}_2$  or the superoxide radical  $\text{O}_2^{\bullet-}$ . Among the different nanozymes,  $\text{CeO}_2$  nanoparticles have been widely researched for their OXD-like properties in the presence of  $\text{O}_2$  [28,278,279]. Recently, TMNs have been employed as toxic agents in the catalytic treatment of cancer, depending on the particular tumor microenvironment (TME), such as excessive  $\text{H}_2\text{O}_2$ , glucose, and acidity [280]. Through their POD- and OXD-like activities, toxic ROS are generated in a sequence of catalytic reactions, thereby hindering the survival and proliferation of cancer cells. Therefore, the cascading effects of OXD and POD-like nanozymes are generally employed to enhance the efficacy of cancer therapies [281,282]. As shown in Fig. 12, Fan et al. synthesized two nanozymes, FA-pyrite and Cy5.5-FA-pyrite with very high  $\text{H}_2\text{O}_2$  affinity, which led to a 4,144- and 3,086-fold increases in catalytic activity compared to  $\text{Fe}_3\text{O}_4$  nanozymes and natural HRP, respectively [283]. The pyrite nanozyme exhibited intrinsic GOx-like property, allowing it to catalyze the oxidation of reduced GSH and generate  $\text{H}_2\text{O}_2$ . Hence, the dual-functional pyrite nanozyme was used to develop a self-cascade platform that could produce large amounts of  $\bullet\text{OH}$  and reduce the level of reduced GSH, followed by the apoptosis and ferroptosis in cancer cells. This nanozyme exhibits specific

cytotoxicity against cancer cells and excellent biodegradability, thus ensuring its safety. These results suggested that the pyrite nanozymes are reliable therapeutic agents for the nanozyme-based catalytic treatment. To create an OXD-POD cascade platform, Chen et al. prepared hollow mesoporous Prussian blue (mGPB) with multi-enzymatic activity that which was coated with a cancer cell membrane and carried GOx [284].

Given the inherent hypoxic environment of tumors, OXD-like nanozymes can generally generate adequate  $\text{O}_2$  for cascade catalytic treatment when combined with CAT or CAT mimics. Wang et al. synthesized highly ordered  $\text{MnO}_2@\text{PtCo}$  nanoflowers by growing  $\text{MnO}_2$  on the surfaces of PtCo nanoparticles in situ [285]. Utilizing the CAT-like properties of  $\text{MnO}_2$  and the OXD-like properties of PtCo,  $\text{MnO}_2@\text{PtCo}$  nanoflowers can supply  $\text{O}_2$  to ease hypoxic conditions and increase ROS production in tumors, thereby providing excellent cancer therapy (Fig. 13).

Ling et al. prepared biodegradable  $\text{MoO}_{3-x}$  nanourchins (NUs) with CAT- and OXD-like properties [286]. In the TME, the CAT-like behavior of the  $\text{MoO}_{3-x}$  NUs can catalyze the decomposition of  $\text{H}_2\text{O}_2$  and provide abundant  $\text{O}_2$  for the next reaction. The high OXD-like ability of nanozymes can produce substantial amounts of cytotoxic  $\text{O}_2^{\bullet-}$  to induce cancer cell apoptosis. Importantly, when the  $\text{MoO}_{3-x}$  NU nanozyme is placed in blood or normal tissues with a neutral pH, they can quickly be decatalyzed, rendering them safe in the body. In another study, Jing et al. [287] designed a bimetallic FeCu PNzyme which was co-encapsulated with natural GOx and the anticancer drug mitoxantrone (MTO). The produced biocompatible formulation, FeCu-GOx PNzyme-MTO acted as both a carrier and a therapeutic reagent. The cascade catalytic treatment was initiated by the transformation of intratumoral gluconic acid to  $\text{H}_2\text{O}_2$  by GOx induction, which was then transformed into ROS by the FeCu nanozyme. SOD converts  $\text{O}_2^{\bullet-}$  into  $\text{O}_2$  and  $\text{H}_2\text{O}_2$ , which are key defense mechanisms against oxidative damage in organisms. Generally, the components and structures of natural SOD involve metals such as Cu, Zn, Fe, and Mn [288,289]. The CAT- and SOD-like cascade reactions of nanozymes are mainly used in cancer therapy to supply  $\text{H}_2\text{O}_2$  and  $\text{O}_2$  that then produce toxic ROS in cancer cells. Furthermore,  $\text{O}_2$  can improve the oxygen-depleted TME of cancer cells and is essential for  $\text{O}_2$ -dependent cancer therapies, such as SDT, RT, phototherapy, and immunotherapy. For example, Liang et al. prepared a Pt-TiO<sub>2</sub> heterostructure for improved SDT [290]. The additional  $\text{O}_2$

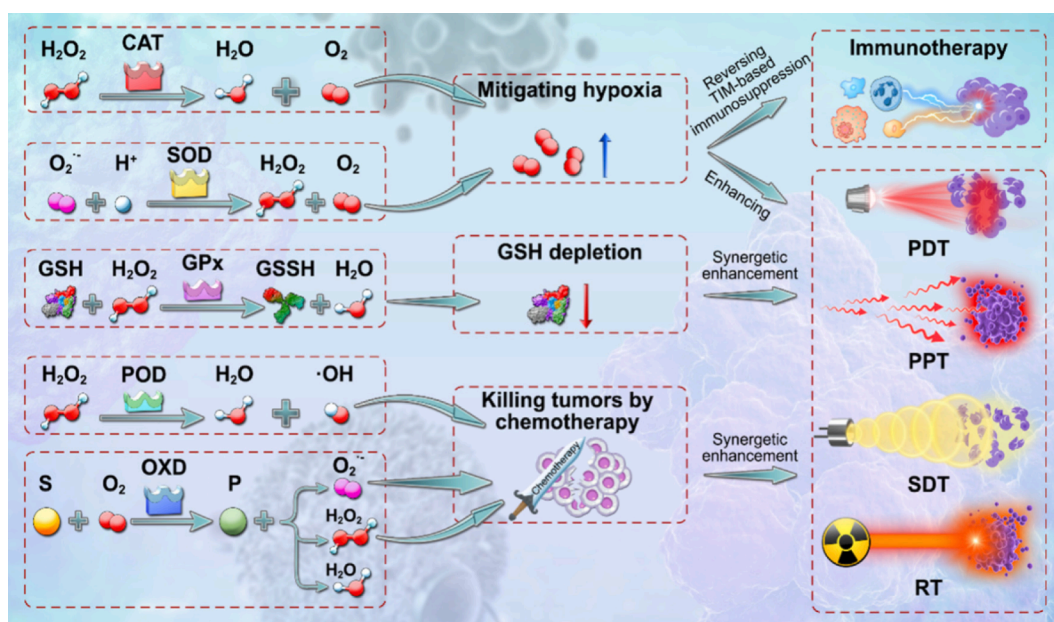
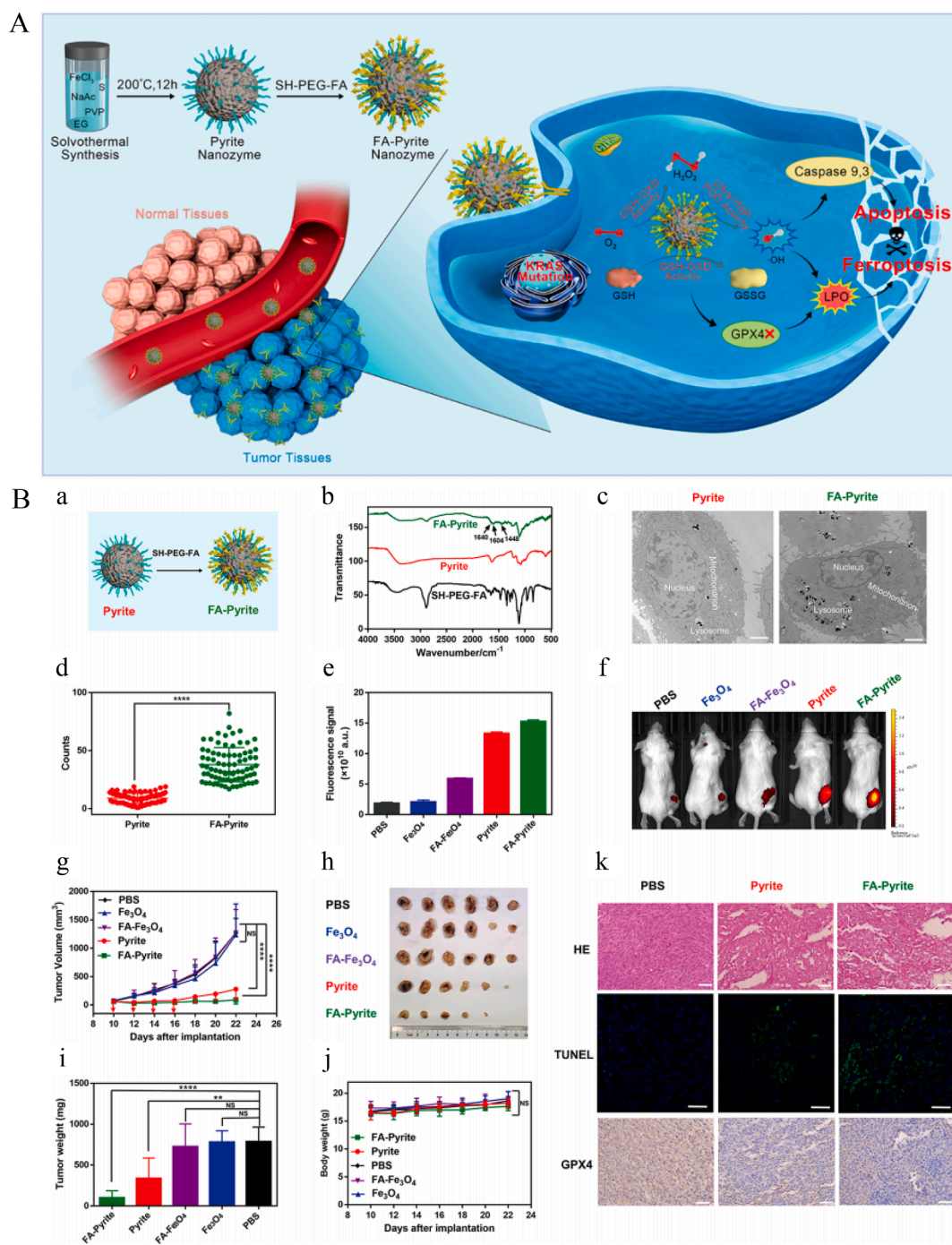


Fig. 11. Describe properties of oxidoreductases-mimic nanozymes and their anti-tumor applications. S is reduced state substances and P is the oxidation state production. Reprinted with permission from Ref. [276].



**Fig. 12.** (A) The synthesis of POD-like and GSH-OXD-like pyrite nanozymes and mechanism depiction of apoptosis-ferroptosis synergistic tumor therapy. (B) (a) The method of FA modified pyrite nanozymes; (b) The FTIR spectra of pyrite with and without FA modification; (c) TEM images of CT26 cells after co-incubating with pyrite and FA-pyrite, respectively. (d) Quantitative detection in CT26 cells; (e, f) Fluorescence detection and quantification of ROS in tumor areas. Tumor volume (g), images of stripped tumor tissue (h), stripped tumor weight (i) and body weight of mice (j) after different treatments. Tumor tissues staining by HE, TUNEL, and immunohistochemical analysis. Reprinted with permission from Ref. [283].

produced by the CAT-like activity of the Pt nanozyme enhances SDT.

#### 4.2.2. Multifaceted synergistic cancer therapy

In addition to the catalytic or cascade catalytic therapy effects arising from the inherent enzymatic activity of nanozymes, multi-enzymatic nanozymes are extensively applied as specific toxic reagents or adjuvants to facilitate CDT, immunotherapy, phototherapy, SDT, RT, and chemotherapy in multifaceted synergistic cancer treatment. Given that these methods have great potential for solid tumor therapy, many studies have focused on combining them with TME-responsive cascade

reaction systems to achieve improved synergistic therapeutic results. Table 3 summarizes typical studies.

CDT is characterized by the local decomposition of endogenous  $\text{H}_2\text{O}_2$  and the production of ROS by in situ activation of tumor sites in Fenton or Fenton-like reactions [304,305], where the produced ROS can trigger cancer cell death. Moreover, in a neutral microenvironment, the Fenton reaction is inhibited, and a low supply of  $\text{H}_2\text{O}_2$  is provided. Therefore, this method does not have a significant effect on normal cells or tissues. Some types of TMNs have been shown to facilitate CDT by repeating the action of Fenton reaction-activating enzymes, which kill cancer cells

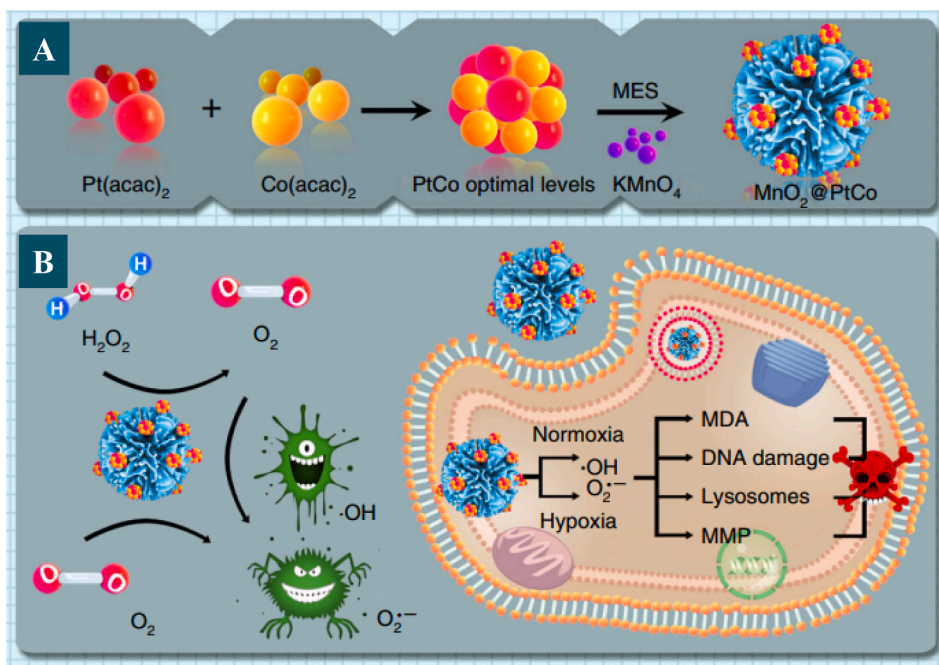


**Fig. 13.** (A) Preparation of MnO<sub>2</sub>@PtCo nanoflowers. (B) The diagram of the generation mechanism of ROS and cytotoxicity by MnO<sub>2</sub>@PtCo nanoflowers in relation to oxygen tension. Reprinted with permission from Ref. [285].

**Table 3**  
Typical reports on multifaceted synergistic cancer therapy.

Metal-based nanozymes	Activities	Therapeutic mode	Reference
Au@HCNs	POD, OXD	PTT, Catalytic therapy	[291]
Au-Ag@HA NPs	POD	Radiation, Nanozyme/ Ag combined therapy	[292]
PtPB nanozyme	CAT, POD	PTT, PDT	[293]
FePc/HNCS	POD, CAT	PDT, PTT	[294]
PtFe@Fe <sub>3</sub> O <sub>4</sub>	POD, CAT	Catalytic therapy, PTT	[289]
Ang-IR780-MnO <sub>2</sub> -PLGA	CAT	Chemotherapy, SDT	[295]
PEG-TiO <sub>1+x</sub> nanorods	HRP	CDT, SDT	[296]
Pt-CuS-P-TAPP	Catalyze decomposition of endogenous H <sub>2</sub> O <sub>2</sub>	PTT, SDT	[288]
Cu-CuFe <sub>2</sub> O <sub>4</sub> nanozyme	CAT, GSH peroxidase-like	CDT, SDT	[297]
TiO <sub>2</sub> -Fe <sub>3</sub> O <sub>4</sub> @PEG	Catalyze decomposition of endogenous H <sub>2</sub> O <sub>2</sub>	CDT, SDT	[298]
UPFB with Janus nanostructures	CAT	SDT, PDT, CDT	[299]
Mn-doped Ag <sub>2</sub> Se	CAT	Immunotherapy, RT, imaging	[300]
Porous platinum nanoparticles	CAT	Chemotherapy, RT	[301]
Ir@liposome	CAT	PTT, RT, imaging	[302]
HCeO <sub>2</sub> @ICG-RGD	Catalyze decomposition of endogenous H <sub>2</sub> O <sub>2</sub>	CDT, PTT	[303]

[306].

Phototherapy methods such as PTT and PDT are non-invasive cancer treatments that use light radiation to induce the death of cancer cells. PTT kills cancer cells by local hyperthermic damage under light radiation of a specific wavelength. In PDT, the light energy reacts with the surrounding O<sub>2</sub> to generate high levels of cytotoxic ROS to oxidize biomacromolecules and cause their dysfunction. In recent years, TMNs with multiple enzymatic abilities, particularly POD- and CAT-like

activities, have been proposed for tumor phototherapy [291–293,307]. Liu et al. developed a novel PtFe@Fe<sub>3</sub>O<sub>4</sub> nanozyme with improved POD- and CAT-like activities in an acidic TME [289]. As a result, combining photoenhanced tumor catalytic therapy with PTT using PtFe@Fe<sub>3</sub>O<sub>4</sub> has the potential to alleviate tumor TME hypoxia and eradicate tumors. A combination of PDT and PTT is more effective. Liu et al. developed a synergistic phototherapy system based on nanozymes with nitrogen-doped carbon nanospheres and iron phthalocyanine [294], demonstrating the potential of multifunctional nanozyme-dependent cancer therapy.

SDT is a non-invasive tumor therapeutic method that depends on ultrasound and sonosensitizers [308]. However, tumor hypoxia and insufficient singlet oxides significantly compromise the effectiveness of this treatment [309]. To overcome this, Lin et al. synthesized nanozyme Pt-CuS to achieve synergistic therapeutic modalities based on SDT [288]. As shown in Fig. 14, hollow CuS was loaded with sonosensitizer reagents for SDT, and the Pt nanozyme decomposed the intrinsic H<sub>2</sub>O<sub>2</sub> to produce O<sub>2</sub> to relieve tumor hypoxia, thus enhancing PDT (Fig. 14A). Furthermore, Pt-CuS with photothermal characteristics could both exert a PTT influence on tumor cells and aid the enzyme-like activity of Pt to produce O<sub>2</sub>, thereby enhancing the cancer cell apoptosis induced by SDT (Fig. 14B). Hence, this multifunctional system provides a synergistic approach for PTT and catalysis, highlighting the potential of SDT for tumor eradication. Some interesting strategies have been developed for the synergization of SDT with chemodynamic treatments.

Cheng et al. reported that titanium monoxide nanorods (TiO<sub>1+x</sub> NRs) are active in CDT via their Fenton-like catalytic activity, which could improve SDT [296]. The system produced more ROS than conventional sonosensitizers because of the oxygen vacancies in the TiO<sub>1+x</sub> NRs. In addition, the HRP-like activity of TiO<sub>1+x</sub> NRs can be used to catalyze the conversion of endogenous H<sub>2</sub>O<sub>2</sub> into •OH, thereby enabling CDT when combined with SDT. Based on the above review, the obvious advantages of SDT, such as its non-invasive and deep tissue penetration, have made it a powerful strategy for cancer therapy. Similar to PDT, SDT requires O<sub>2</sub> and nanozymes with multiple enzymatic functions can provide excess amounts of O<sub>2</sub>. In addition, nanozymes are ideal carriers for the transportation of sonosensitizers in the circulatory system.

RT has also been used in combination with nanozymes in cancer

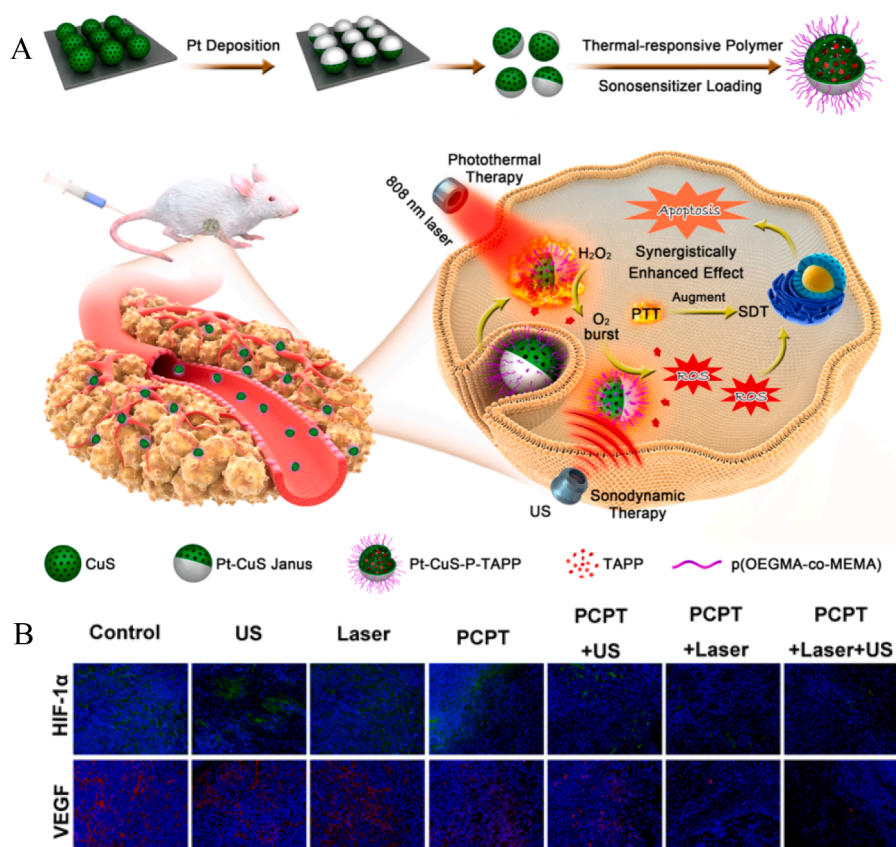


**Fig. 14.** (A) The synthesis of Pt-CuS-based nanozyme and for multi-mode cancer synergistic therapy involving in SDT by relieving tumor hypoxia and PTT. (B) The immunofluorescence images of tumor section as being treated differently for 24 h. The cell nuclei, tumor hypoxia areas and blood vessels were stained with DAPI (blue), HIF-1 $\alpha$  (green), and VEGF (red), respectively. Reprinted with permission from Ref. [288].

therapy. For instance, Liu et al. developed ultrasmall liposomal-coated Ir nanocrystals (Ir@liposomes), which exhibited high temperature/pH stability and CAT-like properties, particularly in the presence of NIR light, and could induce photothermally improved enzyme-like activity (Fig. 15). Thus, RT was achieved based on minimizing tumor hypoxia and the RT activity of Ir [302]. Recently, several types of multifunctional TMNs have been used in RT. Sun et al. designed a new nanozyme by introducing Mn ions into Ag<sub>2</sub>Se quantum dots that exhibited emission in the NIR-II window [300]. This nanozyme facilitated radiation deposition *in vivo*, which was attributed to the radiosensitivity of Ag. Moreover, a nanoprobe was developed by coupling the nanozyme with a tumor-specific peptide (RGD) for NIR-II imaging-guided RT of tumors. *In vivo* studies have shown that nanosystems can improve antitumor immunity, thereby noticeably inhibiting tumor growth.

#### 4.3. Imaging

TMNs possess enzymatic catalytic properties *in vivo* and have become increasingly popular in molecular imaging because of their unique properties such as various enzymatic properties, biocompatibility, and easy surface tenability. Nanozymes are generally used to improve imaging sensitivity and accuracy by combining different nanozymes with fluorescent, superparamagnetic, photoacoustic, and photothermal properties. Nanozymes can also recognize specific TME biomarkers, such as changes in metal ions and miRNA expression, which aid the early diagnosis of some cancers [310]. In addition, combining imaging strategies (e.g., magnetic resonance imaging (MRI), computerized tomography (CT), NIR imaging, photoacoustic imaging (PAI)) and therapeutic methods (e.g., PTT, PDT, and CDT) [311,312], nanozyme systems can provide a personalized diagnosis and indicate the best approach for

integrated diagnosis and therapy [313]. With a divergence in the fundamental concepts of these imaging techniques, we concentrated on recent advances in molecular imaging based on distinct types of nanozymes.

##### 4.3.1. Magnetic resonance imaging

Following the discovery of the POD-like activity of Fe<sub>3</sub>O<sub>4</sub>, the superparamagnetism of Fe<sub>3</sub>O<sub>4</sub> NPs has attracted considerable attention because of the short relaxation time of the surrounding protons, which makes this material suitable as a T2-weighted MRI agent [314]. Subsequently, Mooijjaart et al. discovered that Fe<sub>3</sub>O<sub>4</sub> NPs with dimensions below 5 nm are best for T1-weighted MRI because the T2 effect severely inhibits the magnetic moment, thus creating a strategy for the development of responsive T2/T1 switched MRI contrast agents [315]. Additionally, by utilizing the catalytic ability of TMNs, iron-mediated apoptosis of tumor cells can be induced through the Fenton reaction, which is beneficial for cancer treatment [316]. TMNs generally include Fe-based nanozymes [317], Mn-based nanozymes [318–320], and MOFs [321] containing transition elements. Hou et al. synthesized a T1/T2 switching MRI-guided cancer therapeutic agent based on the ROS produced by Fe<sub>3</sub>C<sub>2</sub>@Fe<sub>3</sub>O<sub>4</sub> NPs (Fig. 16) [317].

Mn-based nanozymes, which have the same features as POD, CAT, and SOD, can potentially be used as T1-weighted MRI contrast agents [322]. In the TME, MnO<sub>2</sub> reacts with H<sup>+</sup>, H<sub>2</sub>O<sub>2</sub>, and glutathione (GSH) to generate Mn<sup>2+</sup> ions and performs multiple functions in tumor diagnosis and therapy. It can be specifically activated in the TME and can precisely target tumors as an MR probe. MnO<sub>2</sub> nanozymes decompose excess H<sub>2</sub>O<sub>2</sub> into O<sub>2</sub> *in situ*, relieve hypoxia, and improve the efficacy of other therapies [318–320]. Moreover, combining these TMNs with classical and functional therapeutic agents, except for MRI and magnetic targeting, provides additional properties, such as PTT and PDT.

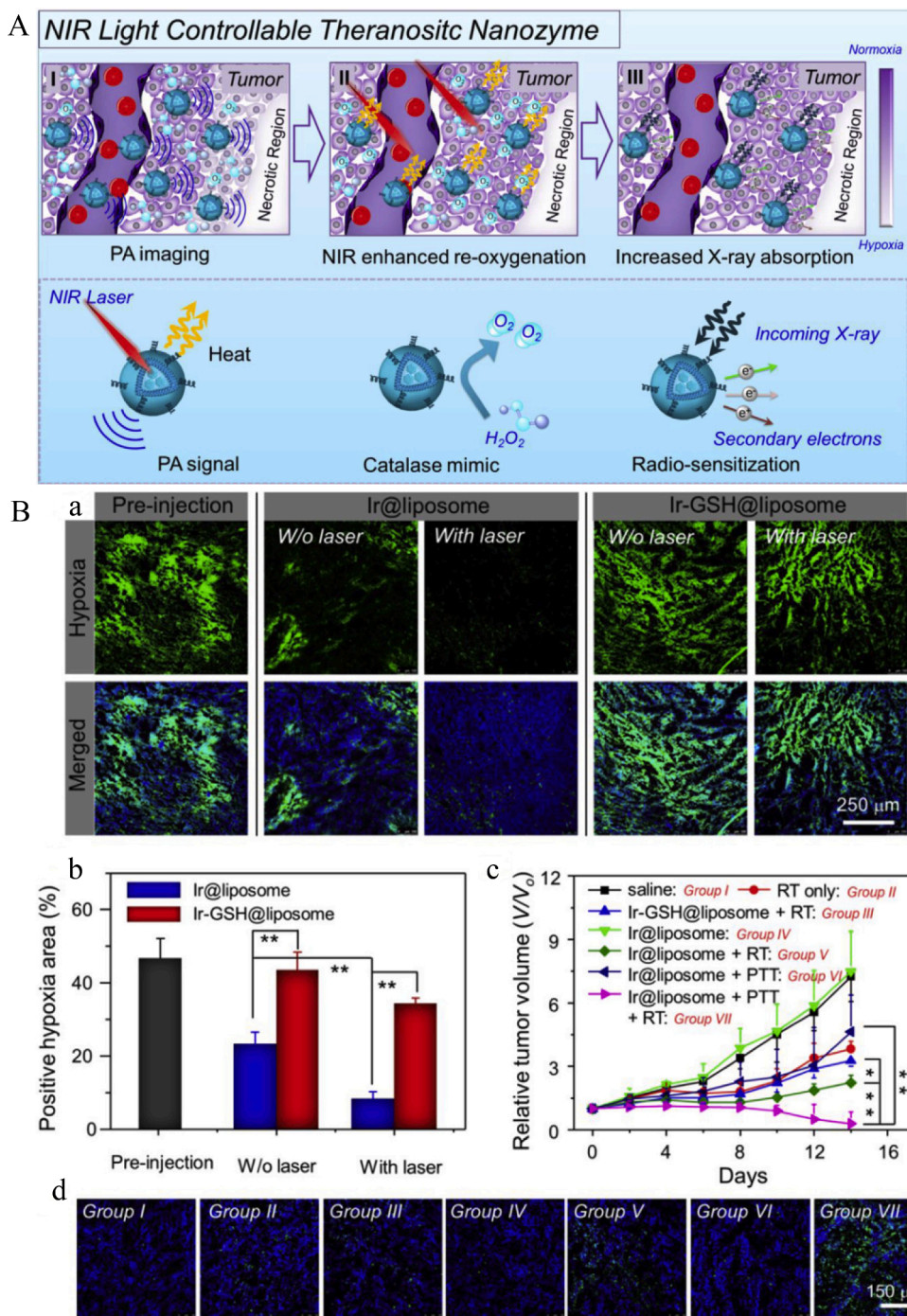


**Fig. 15.** (A) The schematic diagram of NIR-adjusted Ir@liposome nanozyme for cancer RT. (B) NIR light is used to reduce hypoxia in tumors and to synergistically enhance radiation therapy for cancer *in vivo*. Reprinted with permission from Ref. [303].

Consequently, TMNs have become novel nanoplatforms for personalized cancer imaging and theranostics.

#### 4.3.2. Photoacoustic imaging

PAI is a highly transformative, significant, and non-invasive imaging technique with high spatial resolution, excellent light absorption, and imaging depth [323,324]. Currently, the PTT effect stemming from photothermal switching agents (PTAs) is the focus of PAI [325,326]. PTAs can convert light energy into heat to raise the surrounding temperature, leading to a temporary thermoelastic expansion of the tissue, producing ultrasonic waves. Wang et al. developed a combined therapy nanoplatform ( $\text{Au}_2\text{Pt-PEG-Ce6}$ ) by covalent linking with the

photosensitizer chlorin e6 (Ce6), which catalyzed the transfer of  $\text{O}_2$  into  $^1\text{O}_2$ , remarkably improved  $^1\text{O}_2$  stability and preventing its premature release in complex organisms [56]. The system exhibited dual CAT and POD catalytic properties, producing  $\text{O}_2$  and  $\bullet\text{OH}$ , thus enhancing the PDT- and CDT-like activity. In addition,  $\text{Au}_2\text{Pt-PEG-Ce6}$  effectively realized the combination of PDT and PTT under laser irradiation at 650 and 808 nm. Liang et al. prepared a hollow Pt-CuS Janus structure, where the hollow structure of CuS provides an ideal space for the encapsulation of tetra-(4-aminophenyl) porphyrin molecules in carrier-out SDT [288]. Moreover, Pt imparts CAT-like activity to this system, and the production of  $\text{O}_2$  alleviates tumor hypoxia and enhances the generation of SDT-induced ROS. Additionally, the heat produced by

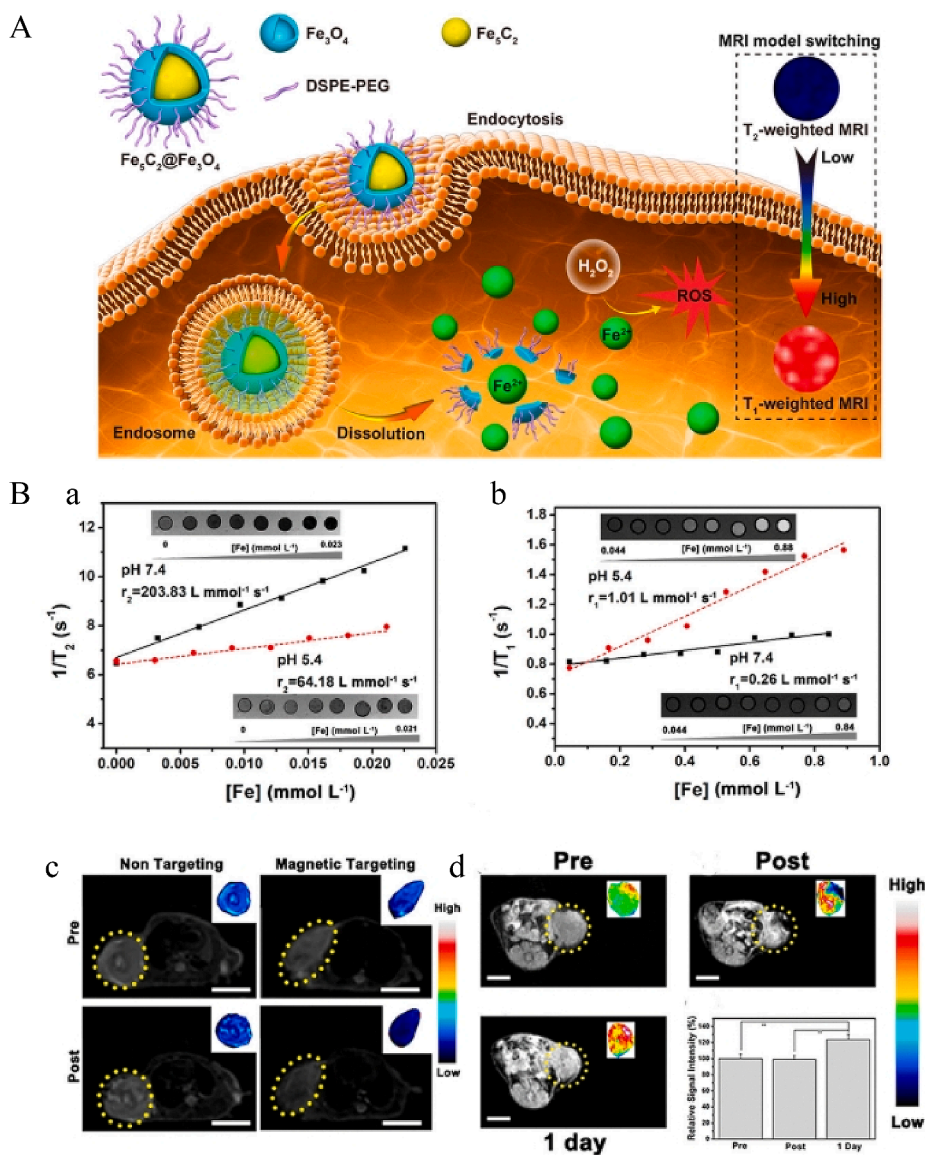


**Fig. 16.** (A) MRI of  $\text{Fe}_5\text{C}_2@\text{Fe}_3\text{O}_4$  NPs and T2/T1 signal-conversion performance. (B) (a,b) Effect of pH on MRI mode switching of PEG/ $\text{Fe}_5\text{C}_2@\text{Fe}_3\text{O}_4$ NPs. (c) T2-weighted MR images. (d) T1-weighted MR images. Reprinted with permission from Ref. [317].

808-nm laser irradiation can accelerate the CAT-like enzyme activity of Pt to produce more  $\text{O}_2$ , thus strengthening the effect of SDT. Furthermore, nanosystems have been improved to make them more effective thermal imaging agents for PA and NIR cancer therapy.

#### 4.3.3. Positron emission tomography

Positron emission tomography (PET) has been adopted in clinical practice over the past few decades owing to its high sensitivity, deep penetration, and the ability to quantitatively analyze signals. Combining PET with other imaging modes, such as PET/CT and PET/MRI, has been evaluated to overcome inherent limitations and optimize image quality [327]. Recently, TMNs such as iron oxide, manganese oxide, and Au nanoparticles, have been used as PET probes [328,329]. Yuan et al. applied the radio labeling strategy by thermally inducing PET  $89\text{Zr}^{4+}$  (or  $64\text{Cu}^{2+}$ ) and single photon emission computed tomography (SPECT)  $111\text{In}^{3+}$  to prepare radio-labeled Feraheme NPs for PET or SPECT [330]. Combining multiple imaging modalities can overcome the limitations of individual imaging technologies and provide comprehensive and precise imaging data [328]. Currently, PET/CT is a unique, clinically switching, and multimodal molecular imaging method. Other multiple modalities

such as MRI-PET/SPECT, MRI-MPI, and MRI-CT are still in the pre-clinical phase and require further assessment.

#### 4.3.4. Other optical-imaging methods

Optical imaging has the benefits of being highly sensitive and non-ionizing. Real-time imaging is a key component of molecular imaging. Nevertheless, *in vivo* optical imaging has drawbacks such as light scattering, intrinsic fluorescence, and the wavelengths being absorbed by adjacent tissues, lipids, etc [331]. Consequently, various advanced imaging techniques, including fluorescence imaging, bioluminescence imaging, and optical coherence tomography, have been developed to advance the field [332]. Near-infrared fluorescence (NIRF) is widely used to image animals *in vivo* [333]. Cui et al. successfully designed OMCAP@rBSA-FA@IR780 hybrid nanocomposites with favorable targeting and satisfactory healing effects by combining PTT and PDT with nanozyme oxidative treatment [334]. OMCAP@rBSA-FA@IR780 was used to eradicate cancer cells without recurrence after 30 days and conduct NIR fluorescence imaging. Interestingly, the well-protected Au NPs enclosed in the OMCAPs act as nanozymes to catalyze the reaction of  $\text{H}_2\text{O}_2$  to generate  $\bullet\text{OH}$  for synergistic cancer treatment. These results

demonstrate that combining NIR imaging, nanozyme catalysis, PTT, and PDT is an outstanding strategy for cancer therapy. To date, as many as 100 types of small NIR-II Au nanoclusters (<3 nm) have been studied because of their intrinsic fluorescence emission, high biocompatibility, and effective renal clearance.

Additionally, Au nanoclusters can generate toxic  $^1\text{O}_2$  under NIR laser irradiation, thus boosting PDT and killing cancer cells (Fig. 17). Bovine serum albumin (BSA) modified gold nanoclusters (BSA@Au) with NIR-II fluorescence and CAT-like properties were used as photosensitizers to achieve highly effective PDT [335]. BSA@Au with bright NIR-II fluorescence allowed PDT to be visualized in tumors with a high signal-to-noise ratio (7.3) in 4 T1 tumor-bearing mouse models. Moreover, the oxygen self-supply capability of BSA@Au increased the survival period of tumor-bearing mice, achieving a five-fold enhancement in PDT efficiency compared with that of the control group. This strategy was also used to treat bacterial infections. BSA@Au exhibited good potential as a new photosensitizer for enhanced cancer PDT and the treatment of bacterial infections.

#### 4.4. Antibacterial infections

Bacteria cause many infectious diseases that spread worldwide and affect millions of people each year. To counter this problem, several effective antibacterial materials have been developed to control the survival and growth of dangerous bacteria, such as antibiotics, metal

ions, and biocides [336,337]. However, these materials have drawbacks, such as high cost, eventual ineffective due to antibiotic resistance, and complex chemical processing [338]. Therefore, the need for alternative antimicrobials is becoming increasingly urgent. In recent decades, nanozyme-based antibacterial materials have attracted considerable attention. Unlike conventional antibacterial therapies, the antimicrobial mechanism of nanozymes does not cause drug resistance; rather, nanozymes can perform various antibacterial functions synergistically to effectively combat bacteria and biofilms [7]. Owing to their superior performance, antibacterial materials based on nanozymes have become a powerful method of combating bacterial infections. This section focuses on the antibacterial mechanisms and multimodal synergistic therapies using TMNs for treating bacterial infections (Table 4).

##### 4.4.1. Antibacterial mechanisms of nanozymes

Currently, antibacterial nanozyme systems are based on redox nanozymes, haloperoxidase (HPO)-like nanozymes, deoxyribonuclease (DNase)-like nanozymes, and NIR light-induced hyperthermia. Excessive ROS levels can lead to lipid peroxidation, protein oxidation, biofilm eradication, and DNA degradation in microbial cells through oxidative stress [356]. However, the development of drug resistance remains challenging. POD-like nanozymes produce highly oxidative  $\bullet\text{OH}$  in the presence of  $\text{H}_2\text{O}_2$  and a low concentration of  $\bullet\text{OH}$  can kill bacteria without damaging healthy tissues [357–359]. Based on these promising results, ferromagnetic nanoparticles are viewed as POD-like in terms of

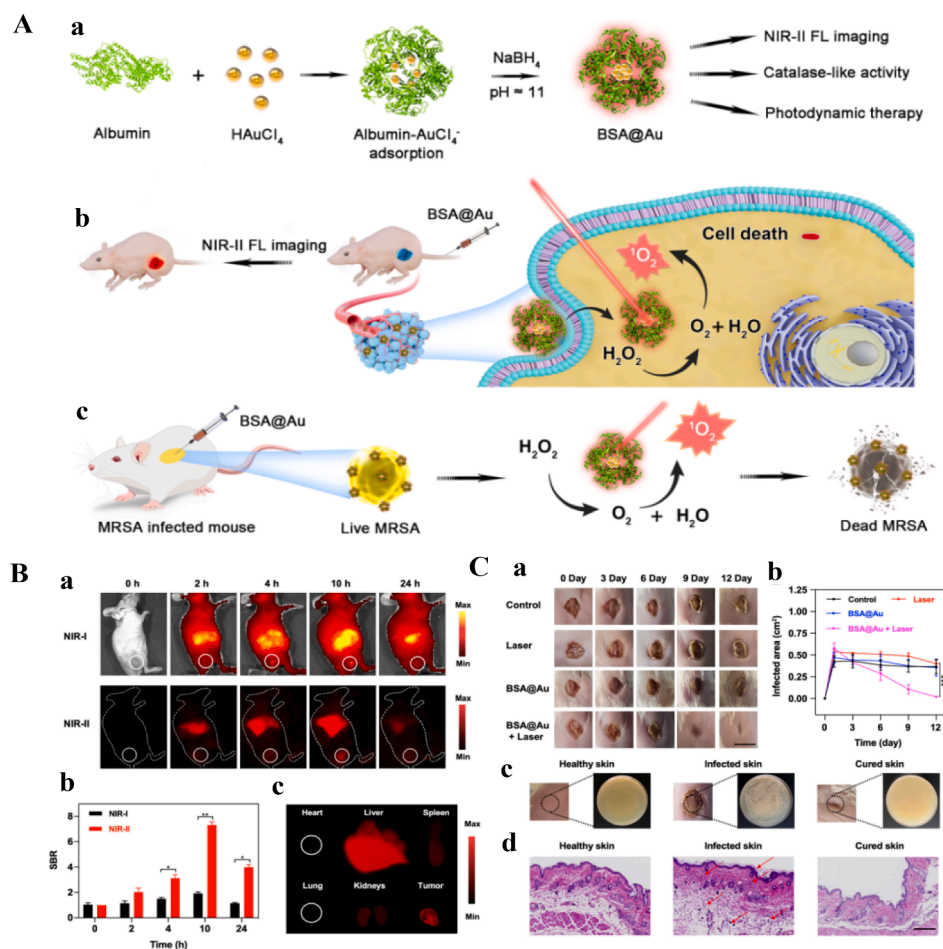


**Fig. 17.** (A) Description of NIR-II BSA@Au enhanced PDT. (a) Preparation of NIR-II BSA@Au. BSA@Au combining with PDT for breast cancer therapy (b) and methicillin-resistant Staphylococcus aureus (MRSA) infection (c); (B) (a) NIR-I and NIR-II FL images of 4 T1 tumor-bearing mice at different time. (b) SBR comparison between NIR-I and NIR-II FL images *in vivo*. (c) The NIR-II FL images of main organs and mature tumor at 10 h; (C) Anti-bacterial property investigation *in vivo* involving in images of the infectious wounds after treatment (a), wound areas (b). (c) The MRSA colonies on LB-agar plates from different states of skin tissue. (d) H&E staining analysis of wounds from different states of skin tissue. Reprinted with permission from Ref. [335].

**Table 4**  
Overview of antibacterial platform based on TMNs.

Metal-based nanozymes	Enzyme-like activities	Antibacterial mechanisms	Bacteria	Applications	References
Au-Au/IrO <sub>2</sub> @Cu(PABA)	GOX + POD	ROS	<i>E. coli</i> , <i>S. aureus</i>	Antibacterial agents	[339]
ZIF-8@Au-GOX	GOX + POD	•OH	MRSA, <i>S. aureus</i> <i>E. coli</i>	Wound healing	[340]
Cu <sub>2</sub> WS <sub>4</sub>	POD + OXD	ROS	<i>E. coli</i> , <i>S. aureus</i>	MRSA-infected wound healing	[341]
Au@AgAu alloy	POD + OXD	ROS	<i>E. coli</i> , <i>S. aureus</i>	Wound healing	[342]
ZnO/Ag/RGO	OXD	ROS + Ag <sup>+</sup>	<i>E. coli</i> , <i>S. aureus</i>	Bacteria combating	[343]
Ag/Fe <sub>3</sub> O <sub>4</sub>	POD	•OH + Ag <sup>+</sup>	<i>E. coli</i> , <i>S. aureus</i>	Wound healing	[344]
AgNPs/N-CD@ZnO	OXD	ROS + Ag <sup>+</sup>	<i>E. coli</i> , <i>S. aureus</i>	Wound healing	[345]
NH <sub>2</sub> -ML-88B(Fe)-Ag	POD	•OH + Ag <sup>+</sup>	<i>E. coli</i> , <i>S. aureus</i>	Wound healing	[346]
NA-Ag@Pt	POD	ROS	<i>E. coli</i> , <i>S. aureus</i>	Antibacterial agents	[347]
Au@CeO <sub>2</sub>	POD	ROS	<i>E. coli</i> , <i>S. aureus</i>	Antibacterial agents	[348]
Cu SAs/NPC	POD	•OH + PTT	<i>E. coli</i> , MRSA	Wound healing	[349]
AuPtNDs	POD	ROS + PTT	<i>E. coli</i> , <i>S. aureus</i>	Antibacterial therapy	[350]
Fe <sub>2</sub> C@Fe <sub>3</sub> O <sub>4</sub> -PEG	POD	•OH + magnetothermal effect	<i>E. coli</i> , <i>S. aureus</i>	Antibacterial therapy	[351]
Au@Cu <sub>2-x</sub> S	POD	ROS + PTT	<i>E. coli</i> , <i>Faecalis</i>	Root canal therapy	[352]
FePN SAzyme	POD	•OH + ROS+ PTT	<i>E. coli</i> , <i>S. aureus</i>	Wound healing	[353]
Cu <sub>x</sub> O-PDA	POD	•OH + PTT	<i>E. coli</i> , <i>S. aureus</i>	Wound healing	[354]
PDA-MnO <sub>2</sub> @Ce6/liposome	POD	•OH + ROS + CT + PDT	<i>E. coli</i> , <i>S. aureus</i>	Wound healing	[355]

their effectiveness in eliminating oxidative biofilms using H<sub>2</sub>O<sub>2</sub> [360]. Later, a set of TMNs was proposed as safe POD-like mimics for wound disinfection with H<sub>2</sub>O<sub>2</sub> at low doses [361–363]. In addition to the aforementioned POD-like mimics, some metal and metal-oxide nanomaterials exhibit OXD-like properties; that is, they can activate oxygen to produce ROS, such as •OH, O<sub>2</sub>•<sup>-</sup>, and <sup>1</sup>O<sub>2</sub> which impede the growth of bacteria and eradicate biofilms [364–370]. Subsequently, many OXD-like mimics with bactericidal activity have been reported, such as Au NPs [358], Pd NPs [46], and Pt/Ag nanoalloys [366,371], and their bactericidal activity is observed in the absence of H<sub>2</sub>O<sub>2</sub>. Many TMNs exhibit multiple enzyme-like activities against bacteria [341,372,373]. For example, Cu<sub>2</sub>WS<sub>4</sub> nanocrystals exhibit satisfactory OXD-like and POD-like activity, i.e., they produce ROS and act as efficient antibacterial agents to promote wound healing [341]. Zhou et al. prepared Pd nanocrystals with remarkable antibacterial performance via ROS production, depending on their facet-dependent OXD and POD-like properties [46]. Extracellular DNA (eDNA) is a structural component that plays an essential role in biofilm formation, including bacterial adhesion, growth, maturation, and maintenance of integrity in many bacterial species. Therefore, the development of DNase-like artificial enzymes for antibiofilm applications is urgently required. Nanomaterials that mimic DNase can effectively cleave eDNA to impede biofilm production and dissolve existing biofilms [374,375]. Qu et al. prepared passivated Au NPs on the surface of colloidal magnetic Fe<sub>3</sub>O<sub>4</sub>/SiO<sub>2</sub> with multiple Ce (IV) complexes to combat biofilms and kill bacteria [376]. Subsequently, bifunctional nanozyme-based synergistic platforms were developed by incorporating DNase- and POD-like mimics to combat biofilms [374]. The bifunctional MOF/Ce-based nanozymes hydrolyze eDNA, destroy established biofilms using Ce(IV) complexes (DNase mimetics), and kill bacteria in the presence of dispersed biofilms using POD-like MOF in the presence of H<sub>2</sub>O<sub>2</sub>. HPO mimics can impede the growth of biofilms and suspend them by intercepting quorum sensing through autoinducer quenching. Inspired by this principle, HPO-like nanozymes have been

evaluated for antibacterial therapy [98,377–380]. For example, the HPO-like activity of CeO<sub>2-x</sub> nanoparticles were found to depend on the aspect ratio of the nanoparticles, and the antibacterial activity was directly influenced by the level of HPO-like activity [380]. In addition, V<sub>2</sub>O<sub>5</sub> nanowires exhibit HPO-like properties and can efficiently inhibit bacterial growth; a 78 % decrease in *Escherichia coli* and a 96 % decrease in *Staphylococcus aureus* have been reported. Finally, hyperthermia induced by NIR, which is used as a non-invasive therapeutic strategy, has been applied in many fields, such as antibacterial and cancer therapy, owing to its high efficacy, broad-spectrum antibacterial activity, and minimal bacterial resistance [381–383]. Photothermal materials usually have a high light-to-heat switching capacity, which adsorbs NIR energy and generates localized hyperthermia, damaging membranes, proteins, and other endogenous bioactive matrices and irreversibly destroying bacteria.

#### 4.4.2. Multimodal synergistic therapies in combating bacterial infections

In recent decades, numerous TMN-based catalytic platforms have been developed with antibacterial activity and biofilm eradication functions [384,385]. Although these reports have shown acceptable disinfection effects, the clinical use of single-mode treatments is currently limited by the poor versatility of nanozyme platforms, low therapeutic efficiency, and narrow-spectrum antibacterial activity. Recently, synergistic systems based on TMNs have been developed and employed to increase antibacterial efficacy, targeting, and biosafety. Moreover, compared with a single antibacterial system, multimodal synergistic systems can achieve the effect of “1 + n > n + 1”, which reduces drug resistance and is useful in targeting specific substances for controlled treatments [386,387]. In this part, we summarize multimodal synergistic antibacterial systems based on TMNs, which are classified as: (i) a combination of various antibacterial mechanisms (including a blend of metal ions and redox-like mimics) [388,389], dual enzymatic antibacterial systems [374], antibacterial combined with PTT

[349,352,354]; and (ii) multifunctional platforms for the determination and restraint of bacterial growth [353,390].

In previous reports,  $\text{Ag}^+$  and  $\text{Zn}^{2+}$  showed good antibacterial effects and are not biotoxic like Ag and Zn NPs. Furthermore, photocatalytic sterilization is more useful. In the presence of NIR irradiation, photocatalysts boost the generation of abundant ROS to enhance antibacterial effects [388,389]. Wang et al. developed an acid-augmented dual-modal antibacterial system based on a nanozyme derived from zeolitic imidazolate framework-8 (ZIF8) (Fig. 18) [340]. Furthermore, Yang et al. prepared an Ag-based nanocomposite, ZnO/Ag/RGO, that was used as a green antibacterial agent for disinfection [343]. Some of the Ag NPs continuously released Ag ions under NIR irradiation, and the ZnO effectively generated ROS, thus providing a synergistic antibacterial effect against *E. coli* and *S. aureus*.

Huang et al. developed a new xerogel, N-CD@ZnO, which was shown to eradicate over 99 % of two strains of bacteria when exposed to NIR light, because of the combined action of the continual emission of  $\text{Ag}^+$  and the formation of ROS by N-CD@ZnO [345]. Moreover, the developed xerogel enhanced the healing of bacteria-infected wounds within 10 days. The triple-synergistic system integrates a glucose-induced cascade reaction with the release of  $\text{Zn}^{2+}$  to effectively eliminate *S. aureus* and *E. coli* [340]. Additionally, dual- or multi-functional platforms have been developed to combat bacterial infections [353]. A novel biofilm microenvironment (BME)-activated Fe-doped poly-diaminopyridine nanofusiform-mediated single-atom nanozyme (FePN SAzyme) for synergistic antibacterial PTT and CDT was developed. SAzyme PTT is activated by high levels of  $\text{H}_2\text{O}_2$  and accelerated by weak acids in the inflammatory environment. Furthermore, FePN SAzyme also enhanced CDT by producing  $\bullet\text{OH}$  from reactions with  $\text{H}_2\text{O}_2$  and consuming GSH, thus providing a more effective synergistic therapy. In

addition, the SAzyme catalyzes the decomposition of biofilm-overexpressing  $\text{H}_2\text{O}_2$  into  $\text{O}_2$ , which helps limit the hypoxia of the biofilm and increases the synergistic efficacy (Fig. 19).

## 5. Conclusions

The development of TMNs has received significant attention because they play a key role in life processes and have wide applications in biomedical fields. We conducted a comprehensive review of TMNs, which are superior to natural enzymes, and outlined a classification system based on the number and type of metal elements, internal and external factors that influence their enzyme-like properties, and rational design strategies. In addition, we discussed the latest advancements in their bioapplications. In terms of applications, the work presented herein attempts to enhance our understanding of TMNs and their relevant mechanisms. Emerging biomedical applications involving antibacterial treatments, imaging, disease diagnosis, and cancer therapy were outlined in detail. Breakthroughs have been made in TMN research and several advances in the knowledge of illnesses and nanotechnology have expanded the potential of nanozymes in biomedicine. The use of nanozymes in biomedicine is promising, particularly for the early detection of diseases, deep-tissue imaging, and multifunctional precision therapy.

## 6. Current limitations and challenges

Although breakthroughs have been achieved in nanozyme engineering, the field is still in its early stages and faces several challenges, including the following.

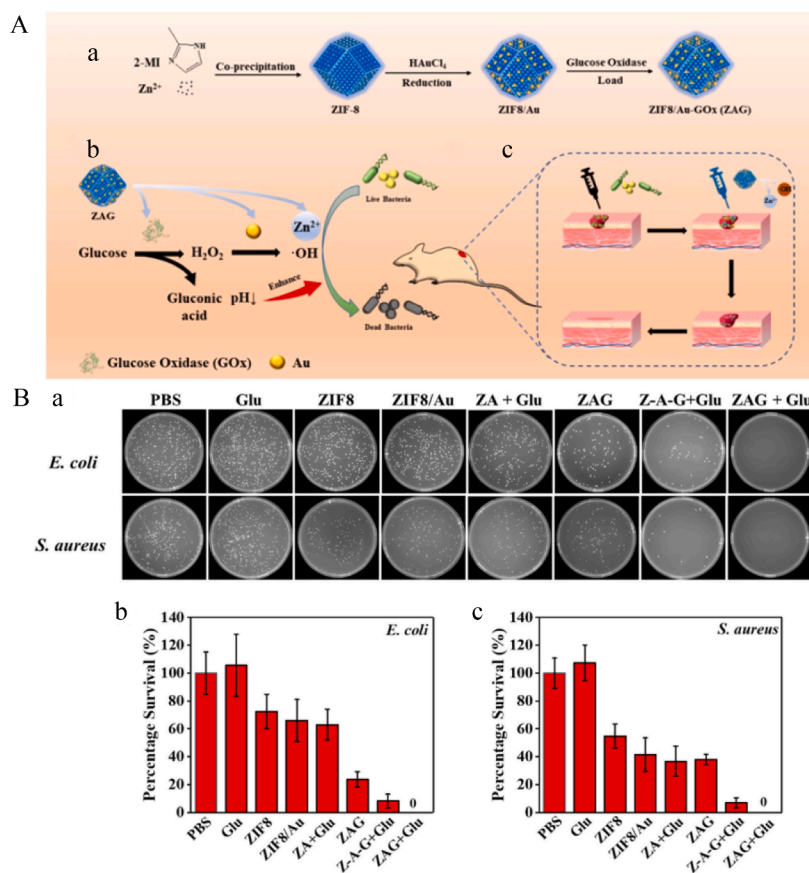


**Fig. 18.** (A) (a) The preparation of ZIF8/Au-GO<sub>x</sub> NPs. (b) Reaction mechanism of the strategy of antibacterial therapy with acid-augment and dual-modal. (c) Employing ZIF8/Au-GO<sub>x</sub> NPs for antibacterial treatment in mice; (B) (a) The images of *E. coli* and *S. aureus* treatment by various materials in solid agar plate, and (b), (c) the corresponding percentage viability. Reprinted with permission from Ref. [340].

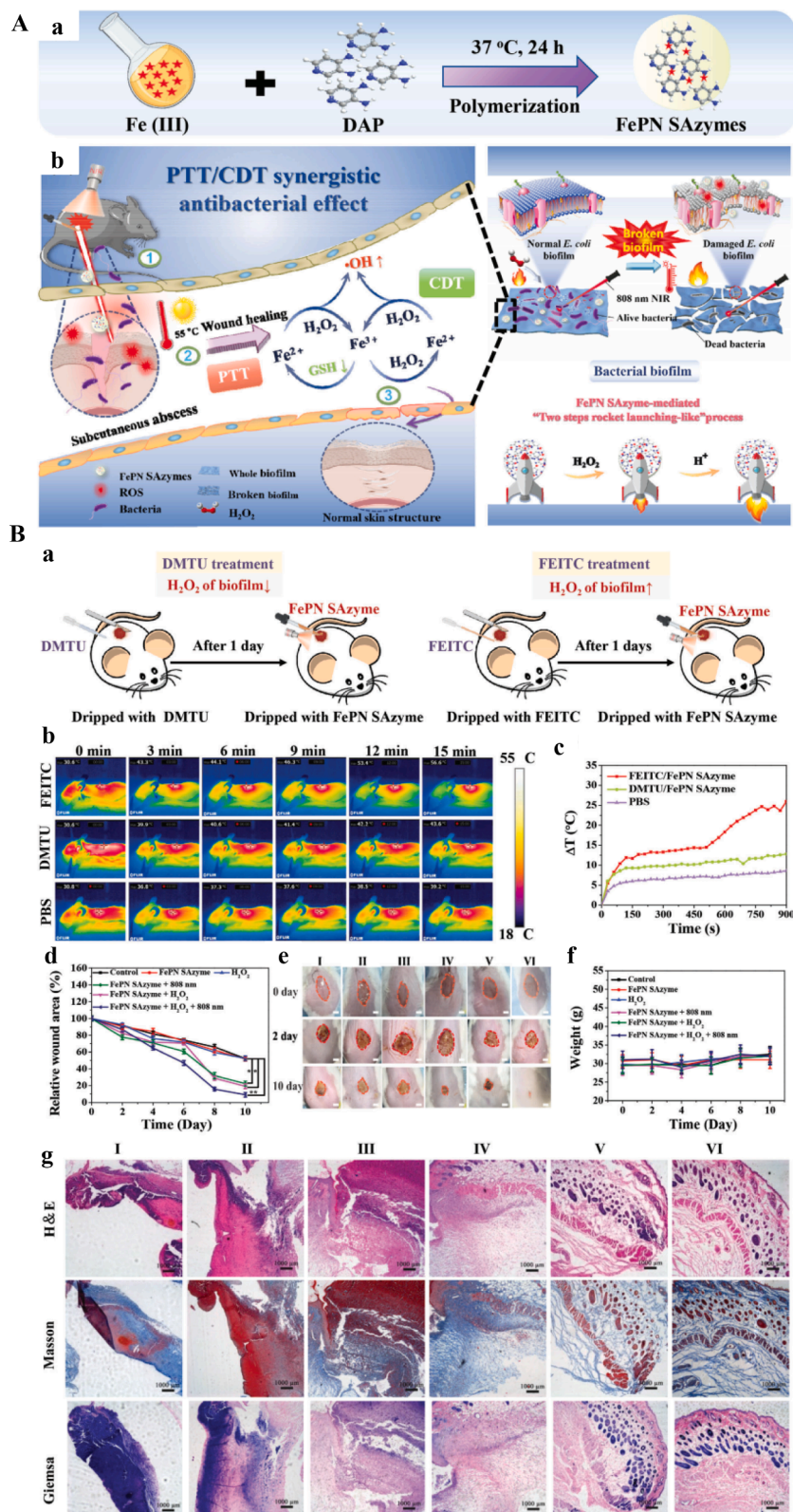


**Fig. 19.** A (a) Preparation of FePN SAzyme. (b) Schematic illustration of the FePN SAzyme as SANs for synergistic antibacterias. B (a) Schematic illustration of dimethylthiourea (DMTU) and  $\beta$ -phenylethyl isothiocyanate (FEITC) therapy. (b) Photothermal images and (c) curves of *E. coli*-infected mice with different treatments under the 808 nm laser irradiation ( $1.0 \text{ W cm}^{-2}$ ). (d) Relative wound area and (e) photographs of wound on the mice at different time points. (f) Body weights of mice after different treatments. (g) Histological, Masson, and Giemsa analysis of skin tissues harvested from different group mice. Reprinted with permission from Ref. [353].

- i. To date, TMN research has mainly focused on hydrolases and oxidoreductases; however, there is an urgent need to explore the activity of other types of enzymes, including transferases, isomerases, lyases, and synthetases, and discover new materials.
- ii. To gain a deeper understanding of the catalytic mechanism of nanozymes, it is essential to investigate novel nanozyme materials and analyze their catalytic properties. Specific catalytic theories must be established for each material type. Research on high-entropy alloys and diatomic nanozymes is limited. The design and fabrication of exceptional nanozyme catalysts remain a challenge.
- iii. Theoretical calculations and experimental verification are necessary to explore the mechanisms of TMNs. These approaches can be used to analyze the binding, reaction, and release of substrates as well as the structure–activity relationships of nanozymes. In future studies, a database for predicting nanozyme activity should be established to facilitate the screening, optimization, and design of nanozymes.
- iv. TMNs have remarkable detection, diagnostic, and treatment capabilities, and research on their uniqueness and irreplaceability should be intensified. To achieve biomedical conversion and clinical implementation, the biosafety of nanozyme-based treatments must be investigated *in vivo*. The targeting, biocompatibility, biodegradability, biodistribution, immunogenicity, and pharmacokinetics of nanozymes should be reliably assessed *in vivo*. The results of such studies will also be invaluable for optimizing the design and use of TMNs in various biomedical applications. Furthermore, the synthesis of highly homogeneous nanozymes and nanozyme mimics inspired by the fixed structure and molecular weight of small-molecule clinical products is a prerequisite for advancing their clinical application.
- v. Research on the utilization of TMNs has progressed, beginning with *in vitro* detection and environmental management. Recently, research has been extended to the realm of *in vivo* diagnosis and treatment, and current results suggest that nanozymes have great potential in biomedicine. To further realize the “Healthy World Strategy,” it is essential to expedite the development of nanozymes in areas such as biochemical testing and biosensing, diagnosis and treatment of cancer and other major diseases, antibacterial activity, antioxidant activity, biofilm removal, gene editing, and nanorobotics.
- vi. In recent years, machine learning-assisted high-throughput screening has rapidly developed. Such methods enable the prediction of key factors affecting the preparation of metal-based nanozymes to assist in the development of nanozymes with exceptional performance. Additionally, such modeling methods enable the prediction of nanozyme activity and the structure–activity relationships with target substances.

#### CRedit authorship contribution statement

**Dandan Zhang:** Conceptualization, Funding acquisition, Writing – review & editing. **Qing Chen:** Validation, Investigation. **Qunxiang Ren:** Data curation, Investigation. **Wenbin Zhong:** Visualization. **Hongjin Zhang:** Visualization, Investigation. **Guannan Wang:** Supervision, Conceptualization. **Yang Zhang:** Conceptualization, Writing – original draft, Project administration, Funding acquisition, Supervision.

#### Declaration of competing interest

The authors declare that they have no known competing financial interests or personal relationships that could have appeared to influence the work reported in this paper.

#### Data availability

No data was used for the research described in the article.

#### Acknowledgements

This work was financially supported by Shenyang Science and Technology Talent Special Project (RC230022), Science Research Foundation of Education Department for Liaoning Province (LJKMZ20221790 and SYYX202005), National Natural Science Foundation of China (Grant No. 22304123), PhD Start-up Foundation of Liaoning Province (2021-BS-284).

#### References

- [1] Y. Huang, J. Ren, X. Qu, *Chem. Rev.* 119 (2019) 4357–4412.
- [2] M. Liang, X. Yan, *Acc. Chem. Res.* 52 (2019) 2190–2200.
- [3] D. Jiang, D. Ni, Z.T. Rosenkrans, P. Huang, X. Yan, W. Cai, *Chem. Soc. Rev.* 48 (2019) 3683–3704.
- [4] H. Wang, K. Wan, X. Shi, *Adv. Mater.* 31 (2019) 1805368.
- [5] M. Zandieh, J. Liu, *Adv. Mater.* (2023) 2211041.
- [6] H. Wei, E. Wang, *Chem. Soc. Rev.* 42 (2013) 6060–6093.
- [7] J. Wu, S. Li, H. Wei, *Chem. Commun.* 54 (2018) 6520–6530.
- [8] J. Wu, X. Wang, Q. Wang, Z. Lou, S. Li, Y. Zhu, L. Qin, H. Wei, *Chem. Soc. Rev.* 48 (2019) 1004–1076.
- [9] X. Yang, Y. Yang, F. Gao, J.J. Wei, C.G. Qian, M.J. Sun, *Nano Lett.* 19 (2019) 4334–4342.
- [10] J. Xie, H. Cao, H. Jiang, Y. Chen, W. Shi, H. Zheng, Y. Huang, *Anal. Chim. Acta* 796 (2013) 92–100.
- [11] X. Cheng, L. Huang, X. Yang, A.A. Elzatahry, A. Alghamdi, Y. Deng, *J. Colloid Interface Sci.* 535 (2019) 425–435.
- [12] M. Zandieh, J. Liu, *Angewandte Chemie-International Edition* 61 (2022) e202212013.
- [13] Y. Li, W. Ma, J. Sun, M. Lin, Y. Niu, X. Yang, Y. Xu, *Carbon* 159 (2020) 149–160.
- [14] P. Wang, T. Wang, J. Hong, X. Yan, M. Liang, *Front. Bioeng. Biotechnol.* 8 (2020) 15.
- [15] Q. Li, T.T. Wu, O.U. Akakuru, N.N. Song, W. Liu, W. Jiang, K.L. Fan, *Adv. Funct. Mater.* 33 (2023) 2214826.
- [16] M. Lyu, M. Luo, J.Y. Li, O.U. Akakuru, X.W. Fan, Z. Cao, K.L. Fan, W. Jiang, *Adv. Funct. Mater.* 33 (2023) 2306930.
- [17] J. Yang, R.F. Zhang, H.Q. Zhao, H.F. Qi, J.Y. Li, J.F. Li, X.Y. Zhou, A.Q. Wang, K. L. Fan, X.Y. Yan, T. Zhang, *Exploration* 2 (2022) 20210267.
- [18] S. Li, X. Zhao, R. Gang, B. Cao, H. Wang, *Anal. Chem.* 92 (2020) 5152–5157.
- [19] X. Niu, Q. Shi, W. Zhu, D. Liu, H. Tian, S. Fu, N. Cheng, S. Li, J.N. Smith, D. Du, Y. Lin, *Biosens. Bioelectron.* 142 (2019) 111495.
- [20] P. Zhang, D. Sun, A. Cho, S. Weon, S. Lee, J. Lee, J.W. Han, D.P. Kim, W. Choi, *Nat. Commun.* 10 (2019) 940.
- [21] Y. Sang, Y. Huang, W. Li, J. Ren, X. Qu, *Chem.-A Euro. J.* 24 (2018) 7259–7263.
- [22] Y. Song, X. Wang, C. Zhao, K. Qu, J. Ren, X. Qu, *Chem.-A Euro. J.* 16 (2010) 3617–3621.
- [23] Z. Chen, J.J. Yin, Y.T. Zhou, Y. Zhang, L. Song, M. Song, S. Hu, N. Gu, *ACS Nano* 6 (2012) 4001–4012.
- [24] J. Chen, Q. Wang, L. Huang, H. Zhang, K. Rong, H. Zhang, S. Dong, *Nano Res.* 11 (2018) 4905–4913.
- [25] L. Gao, J. Zhuang, L. Nie, J. Zhang, Y. Zhang, N. Gu, T. Wang, J. Feng, D. Yang, S. Perrett, X. Yan, *Nat. Nanotechnol.* 2 (2007) 577–583.
- [26] L. Han, H. Zhang, D. Chen, F. Li, *Adv. Funct. Mater.* 28 (2018) 1800018.
- [27] Q. Chen, B. Hu, D.D. Zhang, Q.X. Ren, M.M. Wang, P.F. Li, Y. Zhang, *Talanta* 266 (2024) 124967.
- [28] L. Huang, W. Zhang, K. Chen, W. Zhu, X. Liu, R. Wang, X. Zhang, N. Hu, Y. Suo, J. Wang, *Chem. Eng. J.* 330 (2017) 746–752.
- [29] R. Singh, S. Singh, *Colloids and Surfaces B-Biointerfaces* 132 (2015) 78–84.
- [30] R. Singh, S. Singh, *Colloids and Surfaces B-Biointerfaces* 175 (2019) 625–635.
- [31] C. Ge, G. Fang, X. Shen, Y. Chong, W.G. Wamer, X. Gao, Z. Chai, C. Chen, J.J. Yin, *ACS Nano* 10 (2016) 10436–10445.
- [32] S.B. He, F.Q. Chen, L.F. Xiu, H.P. Peng, H.H. Deng, A.L. Liu, W. Chen, G.L. Hong, *Anal. Bioanal. Chem.* 412 (2020) 499–506.
- [33] M. Sharifi, S.H. Hosseinali, P. Yousefvand, A. Salihi, M.S. Shelcha, F.M. Aziz, A. Jouyatalaei, A. Hasan, M. Falahati, *Materials Science & Engineering C-Materials for Biological Applications* 108 (2020) 110422.
- [34] X. Liu, Y. Pan, J. Yang, Y. Gao, T. Huang, X. Luan, Y. Wang, Y. Song, *Nano Res.* 13 (2020) 653–660.
- [35] M. Moglianetti, E. De Luca, D. Pedone, R. Marotta, T. Catelani, B. Sartori, H. Amenitsch, S.F. Retta, P.P. Pompa, *Nanoscale* 8 (2016) 3739–3752.
- [36] Q. Chen, H.J. Zhang, H. Sun, Y.Z. Yang, D.D. Zhang, X. Li, L. Han, G.N. Wang, Y. Zhang, *Food Chem.* (2024) 138383.
- [37] L. Jiao, Y. Wang, H.L. Jiang, Q. Xu, *Adv. Mater.* 30 (2018) 1705112.
- [38] Y. Gao, Y. Zhou, R. Chandrawati, *ACS Appl. Nano Mater.* 3 (2020) 1–21.
- [39] C.P. Liu, T.H. Wu, C.Y. Liu, K.C. Chen, Y.X. Chen, G.S. Chen, S.Y. Lin, *Small* 13 (2017) 1700278.
- [40] W. Luo, C. Zhu, S. Su, D. Li, Y. He, Q. Huang, C. Fan, *ACS Nano* 4 (2010) 7451–7458.

- [41] W. He, Y.T. Zhou, W.G. Warner, X. Hu, X. Wu, Z. Zheng, M.D. Boudreau, J.J. Yin, *Biomaterials* 34 (2013) 765–773.
- [42] M.S. Khan, N.A. Qureshi, F. Jabeen, M.S. Asghar, M. Shakeel, M. Fakhar-e-Alam, *Biol. Trace Elem. Res.* 176 (2017) 416–428.
- [43] W. Li, B. Chen, H. Zhang, Y. Sun, J. Wang, J. Zhang, Y. Fu, *Biosens. Bioelectron.* 66 (2015) 251–258.
- [44] L. Jin, Z. Meng, Y. Zhang, S. Cai, Z. Zhang, C. Li, L. Shang, Y. Shen, *ACS Appl. Mater. Interfaces* 9 (2017) 10027–10033.
- [45] J. Fan, J.J. Yin, B. Ning, X. Wu, Y. Hu, M. Ferrari, G.J. Anderson, J. Wei, Y. Zhao, G. Nie, *Biomaterials* 32 (2011) 1611–1618.
- [46] G. Fang, W.F. Li, X.M. Shen, J.M. Perez-Aguilar, Y. Chong, X.F. Gao, Z.F. Chai, C. Y. Chen, C.C. Ge, R.H. Zhou, *Nat. Commun.* 9 (2018) 129.
- [47] S. Li, B. Xu, M. Lu, M. Sun, H. Yang, S. Liu, Z. Huang, H. Liu, *Adv. Mater.* 34 (2022) 2202609.
- [48] G.J. Cao, X. Jiang, H. Zhang, T.R. Croley, J.J. Yin, *RSC Adv.* 7 (2017) 52210–52217.
- [49] G. Jin, J. Liu, C. Wang, W. Gu, G. Ran, B. Liu, Q. Song, *Applied Catalysis B-Environmental* 267 (2020) 118725.
- [50] L. Hu, Y. Yuan, L. Zhang, J. Zhao, S. Majeed, G. Xu, *Anal. Chim. Acta* 762 (2013) 83–86.
- [51] M. Liu, L. Huang, X. Xu, X. Wei, X. Yang, X. Li, B. Wang, Y. Xu, L. Li, Z. Yang, *ACS Nano* 16 (2022) 9479–9497.
- [52] S. He, L. Yang, P. Balasubramanian, S. Li, H. Peng, Y. Kuang, H. Deng, W. Chen, *J. Mater. Chem. A* 8 (2020) 25226–25234.
- [53] T.G. Choleva, V.A. Gatselou, G.Z. Tsogas, D.L. Giokas, *Microchim. Acta* 185 (2018) 1–9.
- [54] J. Zhang, S. Wu, X. Lu, P. Wu, J. Liu, *Nano Lett.* 19 (2019) 3214–3220.
- [55] Q. Chen, C. Liang, X. Zhang, Y. Huang, *Talanta* 182 (2018) 476–483.
- [56] M. Wang, M. Chang, Q. Chen, D. Wang, C. Li, Z. Hou, J. Lin, D. Jin, B. Xing, *Biomaterials* 252 (2020) 120093.
- [57] M. Gharib, A. Kornowski, H. Noei, W.J. Parak, I. Chakraborty, *ACS Mater. Lett.* 1 (2019) 310–319.
- [58] C.X. Zhang, Y.C. Gao, H.W. Li, Y. Wu, *ACS Applied Nano Materials* 3 (2020) 9318–9328.
- [59] K. Shah, S. Bhagat, D. Varade, S. Singh, *Colloids and Surfaces a-Physicochemical and Engineering Aspects* 553 (2018) 50–57.
- [60] L. Jin, Y. Sun, L. Shi, C. Li, Y. Shen, *J. Mater. Chem. B* 7 (2019) 4561–4567.
- [61] Q. Wang, L. Zhang, C. Shang, Z. Zhang, S. Dong, *Chem. Commun.* 52 (2016) 5410–5413.
- [62] J. Liu, X. Hu, S. Hou, T. Wen, W. Liu, X. Zhu, J.J. Yin, X. Wu, *Sensors and Actuators B-Chemical* 166 (2012) 708–714.
- [63] Z. Zhu, Z. Guan, S. Jia, Z. Lei, S. Lin, H. Zhang, Y. Ma, Z.Q. Tian, C.J. Yang, *Angewandte Chemie-International Edition* 53 (2014) 12503–12507.
- [64] K. Zhang, X. Hu, J. Liu, J.J. Yin, S. Hou, T. Wen, W. He, Y. Ji, Y. Guo, Q. Wang, X. Wu, *Langmuir: the ACS Journal of Surfaces and Colloids* 27 (2011) 2796–2803.
- [65] S. Cai, C. Qi, Y. Li, Q. Han, R. Yang, C. Wang, *J. Mater. Chem. B* 4 (2016) 1869–1877.
- [66] Y. Zhang, F. Lu, Z. Yan, D. Wu, H. Ma, B. Du, Q. Wei, *Microchim. Acta* 182 (2015) 1421–1429.
- [67] Y. Zhang, X. Pang, D. Wu, H. Ma, Z. Yan, J. Zhang, B. Du, Q. Wei, *Analyst* 141 (2016) 337–345.
- [68] X. Xia, J. Zhang, N. Lu, M.J. Kim, K. Ghale, Y. Xu, E. McKenzie, J. Liu, H. Yet, *ACS Nano* 9 (2015) 9994–10004.
- [69] C.W. Lien, C.C. Huang, H.T. Chang, *Chem. Commun.* 48 (2012) 7952–7954.
- [70] G.W. Wu, Y.M. Shen, X.Q. Shi, H.H. Deng, X.Q. Zheng, H.P. Peng, A.L. Liu, X. H. Xia, W. Chen, *Anal. Chim. Acta* 971 (2017) 88–96.
- [71] W. He, X. Wu, J. Liu, X. Hu, K. Zhang, S. Hou, W. Zhou, S. Xie, *Chem. Mater.* 22 (2010) 2988–2994.
- [72] C. Zheng, A.X. Zheng, B. Liu, X.L. Zhang, Y. He, J. Li, H.H. Yang, G. Chen, *Chem. Commun.* 50 (2014) 13103–13106.
- [73] J. Li, X. Li, W. Feng, L. Huang, Y. Zhao, Y. Hu, K. Cai, *Mater. Lett.* 229 (2018) 193–197.
- [74] H. Yang, Q. He, J. Pan, M. Lin, Z. Lao, Q. Li, X. Cui, S. Zhao, *Sensors and Actuators B-Chemical* 351 (2022) 130905.
- [75] X. Wang, Y. Xu, N. Cheng, Q. Zhang, Z. Yang, B. Liu, X. Wang, K. Huang, Y. Luo, *Sensors and Actuators B-Chemical* 364 (2022) 131907.
- [76] Y.J. Ai, M.Q. He, H. Sun, X.M. Jia, L. Wu, X.Y. Zhang, H.B. Sun, Q.L. Liang, *Adv. Mater.* 35 (2023) 2302335.
- [77] J. Ge, J.H. Yu, H. Yang, D. Yang, R. Cai, *J. Mater. Chem. B* 8 (2020) 11090–11095.
- [78] X. Liu, Q. Wang, H. Zhao, L. Zhang, Y. Su, Y. Lv, *Analyst* 137 (2012) 4552–4558.
- [79] Y. Huang, Z. Liu, C. Liu, E. Ju, Y. Zhang, J. Ren, X. Qu, *Angewandte Chemie-International Edition* 55 (2016) 6646–6650.
- [80] J. Wang, H. Tao, T. Lu, Y. Wu, *J. Colloid Interface Sci.* 584 (2021) 114–124.
- [81] N. Singh, M.A. Savanur, S. Srivastava, P. D'Silva, G. Muges, *Angewandte Chemie-International Edition* 56 (2017) 14267–14271.
- [82] J. Yao, Y. Cheng, M. Zhou, S. Zhao, S. Lin, X. Wang, J. Wu, S. Li, H. Wei, *Chem. Sci.* 9 (2018) 2927–2933.
- [83] W. Li, G.C. Fan, F. Gao, Y. Cui, W. Wang, X. Luo, *Biosens Bioelectron.* 127 (2019) 64–71.
- [84] L. Gao, K. Fan, X. Yan, *Theranostics* 7 (2017) 3207–3227.
- [85] M. Hu, K. Korschelt, P. Daniel, K. Landfester, W. Tremel, M.B. Bannwarth, *ACS Appl. Mater. Interfaces* 9 (2017) 38024–38031.
- [86] Q. Bao, P. Hu, Y. Xu, T. Cheng, C. Wei, L. Pan, J. Shi, *ACS Nano* 12 (2018) 6794–6805.
- [87] M. Li, P. Shi, C. Xu, J. Ren, X. Qu, *Chem. Sci.* 4 (2013) 2536–2542.
- [88] C. Korsvik, S. Patil, S. Seal, W.T. Self, *Chem. Commun.* (2007) 1056–1058.
- [89] M.J. Manto, P. Xie, C. Wang, *ACS Catal.* 7 (2017) 1931–1938.
- [90] K. Herget, P. Hubach, S. Pusch, P. Deglmann, H. Goetz, T.E. Gorelik, I.Y. A. Gural'skiy, F. Pfitzner, T. Link, S. Schenk, M. Panthoef, V. Ksenofontov, U. Kolb, T. Opatz, R. Andre, W. Tremel, *Adv. Mater.* 29 (2017) 1603823.
- [91] K. Korschelt, R. Schwidetzky, F. Pfitzner, J. Strugatchi, C. Schilling, M. von der Au, K. Kirchoff, M. Panthoef, I. Lieberwirth, M.N. Tahir, C. Hess, B. Meermann, W. Tremel, *Nanoscale* 10 (2018) 13074–13082.
- [92] J. Mu, L. Zhang, M. Zhao, Y. Wang, *J. Mol. Catal. A Chem.* 378 (2013) 30–37.
- [93] X. Liu, L. Yan, H. Ren, Y. Cai, C. Liu, L. Zeng, J. Guo, A. Liu, *Biosens. Bioelectron.* 165 (2020) 460–466.
- [94] J. Mu, X. Zhao, J. Li, E.C. Yang, X.J. Zhao, *J. Mater. Chem. B* 4 (2016) 5217–5221.
- [95] P. Biparva, S.M. Abedirad, S.Y. Kazemi, *Talanta* 130 (2014) 116–121.
- [96] S.F. Li, X.M. Zhang, W.X. Du, Y.H. Ni, X.W. Wei, *J. Phys. Chem. C* 113 (2009) 1046–1051.
- [97] A.A. Vernekar, D. Sinha, S. Srivastava, P.U. Paramasivam, P. D'Silva, G. Muges, *Nat. Commun.* 5 (2014) 1–13.
- [98] F. Natalio, R. Andre, A.F. Hartog, B. Stoll, K.P. Jochum, R. Wever, W. Tremel, *Nat. Nanotechnol.* 7 (2012) 530–535.
- [99] L.M. Zhang, F. Xia, Z.D. Song, N.A.S. Webster, H.J. Luo, Y.F. Gao, *RSC Advance* 5 (2015) 61371–61379.
- [100] H. Li, T. Wang, Y. Wang, S. Wang, P. Su, Y. Yang, *Ind. Eng. Chem. Res.* 57 (2018) 2416–2425.
- [101] A. Zeb, X. Xie, A.B. Yousaf, M. Imran, T. Wen, Z. Wang, H.L. Guo, Y.F. Jiang, I. A. Qazi, A.W. Xu, *ACS Appl. Mater. Interfaces* 8 (2016) 30126–30132.
- [102] M. Chen, Z. Wang, J. Shu, X. Jiang, W. Wang, Z.H. Shi, Y.W. Lin, *Inorg. Chem.* 56 (2017) 9400–9403.
- [103] Y.B. Feng, L. Hong, A.L. Liu, W.D. Chen, G.W. Li, W. Chen, X.H. Xia, *Int. J. Environ. Sci. Technol.* 12 (2015) 653–660.
- [104] T. Liu, B. Xiao, F. Xiang, J. Tan, Z. Chen, X. Zhang, C. Wu, Z. Mao, G. Luo, X. Chen, *J. Deng, Nat. Commun.* 11 (2020) 2788.
- [105] C. Hao, A. Qu, L. Xu, M. Sun, H. Zhang, C. Xu, H. Kuang, *J. Am. Chem. Soc.* 141 (2019) 1091–1099.
- [106] R. Ragg, F. Natalio, M.N. Tahir, H. Janssen, A. Kashyap, D. Strand, S. Strand, W. Tremel, *ACS Nano* 8 (2014) 5182–5189.
- [107] Z. Liu, L. Xie, K. Qiu, X. Liao, T.W. Rees, Z. Zhao, L. Ji, H. Chao, *ACS Appl. Mater. Interfaces* 12 (2020) 31205–31216.
- [108] L. Huang, J. Chen, L. Gan, J. Wang, S. Dong, *Sci. Adv.* 5 (2019) eaav5490.
- [109] C. Zhao, C. Xiong, X. Liu, M. Qiao, Z. Li, T. Yuan, J. Wang, Y. Qu, X. Wang, F. Zhou, Q. Xu, S. Wang, M. Chen, W. Wang, Y. Li, T. Yao, Y. Wu, Y. Li, *Chem. Commun.* 55 (2019) 2285–2288.
- [110] M. Wang, L. Liu, X. Xie, X. Zhou, Z. Lin, X. Su, *Sensors and Actuators B-Chemical* 313 (2020) 128023.
- [111] W. Ma, J. Mao, X. Yang, C. Pan, W. Chen, M. Wang, P. Yu, L. Mao, Y. Li, *Chem. Commun.* 55 (2019) 159–162.
- [112] Y. Wu, L. Jiao, X. Luo, W. Xu, X. Wei, H. Wang, H. Yan, W. Gu, B.Z. Xu, D. Du, Y. Lin, C. Zhu, *Small* 15 (2019) 1900632.
- [113] M. Chen, H. Zhou, X. Liu, T. Yuan, W. Wang, C. Zhao, Y. Zhao, F. Zhou, X. Wang, Z. Xue, T. Yao, C. Xiong, Y. Wu, *Small* 16 (2020) 2002343.
- [114] N. Cheng, J.C. Li, D. Liu, Y. Lin, D. Du, *Small* 15 (2019) 1901485.
- [115] M.S. Kim, J. Lee, H.S. Kim, A. Cho, K.H. Shim, T.N. Le, S.S.A. An, J.W. Han, M. I. Kim, J. Lee, *Adv. Funct. Mater.* 30 (2020) 1905410.
- [116] Y. Mao, S. Gao, L. Yao, L. Wang, H. Qu, Y. Wu, Y. Chen, L. Zheng, *J. Hazard. Mater.* 408 (2021) 124898.
- [117] M. Huo, L. Wang, H. Zhang, L. Zhang, Y. Chen, J. Shi, *Small* 15 (2019) 1901834.
- [118] R. Yan, S. Sun, J. Yang, W. Long, J. Wang, X. Mu, Q. Li, W. Hao, S. Zhang, H. Liu, Y. Gao, L. Ouyang, J. Chen, S. Liu, X.D. Zhang, D. Ming, *ACS Nano* 13 (2019) 11552–11560.
- [119] J. Xi, G. Wei, L. An, Z. Xu, Z. Xu, L. Fan, L. Gao, *Nano Lett.* 19 (2019) 7645–7654.
- [120] Z. Lin, L. Zheng, W. Yao, S. Liu, Y. Bu, Q. Zeng, X. Zhang, H. Deng, X. Lin, W. Chen, *J. Mater. Chem. B* 8 (2020) 8599–8606.
- [121] Y. Li, M. Li, J. Lu, B. Ma, Z. Wang, L.Z. Cheong, K. Luo, X. Zha, K. Chen, P.O. A. Persson, L. Hultman, P. Eklund, C. Shen, Q. Wang, J. Xue, S. Du, Z. Huang, Z. Chai, Q. Huang, *ACS Nano* 13 (2019) 9198–9205.
- [122] B. Xu, H. Wang, W. Wang, L. Gao, S. Li, X. Pan, H. Wang, H. Yang, X. Meng, Q. Wu, L. Zheng, S. Chen, X. Shi, K. Fan, X. Yan, H. Liu, *Angewandte Chemie-International Edition* 58 (2019) 4911–4916.
- [123] Y. Wang, G. Jia, X. Cui, X. Zhao, Q. Zhang, L. Gu, L. Zheng, L.H. Li, Q. Wu, D. J. Singh, D. Matsumura, T. Tsuji, Y.T. Cui, J. Zhao, W. Zheng, *Chem* 7 (2021) 436–449.
- [124] M. Lu, C. Wang, Y. Ding, M. Peng, W. Zhang, K. Li, W. Wei, Y. Lin, *Chem. Commun.* 55 (2019) 14534–14537.
- [125] D. Wang, H. Wu, S.Z.F. Phua, G. Yang, W.Q. Lim, L. Gu, C. Qian, H. Wang, Z. Guo, H. Chen, Y. Zhao, *Nat. Commun.* 11 (2020) 357.
- [126] Y. Wang, K. Qi, S. Yu, G. Jia, Z. Cheng, L. Zheng, Q. Wu, Q. Bao, Q. Wang, J. Zhao, X. Cui, W. Zheng, *Nano-Micro Letters* 11 (2019) 102.
- [127] F. Cao, L. Zhang, Y. You, L. Zheng, J. Ren, X. Qu, *Angewandte Chemie-International Edition* 59 (2020) 5108–5115.
- [128] N. Gong, X. Ma, X. Ye, Q. Zhou, X. Chen, X. Tan, S. Yao, S. Huo, T. Zhang, S. Chen, X. Teng, X. Hu, J. Yu, Y. Gan, H. Jiang, J. Li, X.J. Liang, *Nat. Nanotechnol.* 14 (2019) 379–387.
- [129] L. Jiao, W. Xu, Y. Zhang, Y. Wu, W. Gu, X. Ge, B. Chen, C. Zhu, S. Guo, *Nano Today* 35 (2020) 100971.

- [130] C.B. Ma, Y.P. Xu, L.X. Wu, Q. Wang, J.J. Zheng, G.X. Ren, X.Y. Wang, X.F. Gao, M. Zhou, M. Wang, H. Wei, *Angewandte Chemie-International Edition* 61 (2022) e202116170.
- [131] R. Tian, H. Ma, W. Ye, Y. Li, S. Wang, Z. Zhang, S. Liu, M. Zang, J. Hou, J. Xu, Q. Luo, H. Sun, F. Bai, Y. Yang, J. Liu, *Adv. Funct. Mater.* 32 (2022) 2204025.
- [132] K. Li, Y. Miao, K. Song, S. He, G. Zhang, G.I.N. Waterhouse, S. Guan, S. Zhou, *Chem. Eng. J.* 471 (2023) 144693.
- [133] R. Zeng, Y. Li, X. Hu, W. Wang, Y. Li, H. Gong, J. Xu, L. Huang, L. Lu, Y. Zhang, D. Tang, J. Song, *Nano Lett.* 23 (2023) 6073–6080.
- [134] H. Liang, F. Lin, Z. Zhang, B. Liu, S. Jiang, Q. Yuan, J. Liu, *ACS Appl. Mater. Interfaces* 9 (2017) 1352–1360.
- [135] R. Dalapati, B. Sakthivel, M.K. Ghosalya, A. Dhakshinamoorthy, S. Biswas, *CrstEngComm* 19 (2017) 5915–5925.
- [136] H. Yang, R. Yang, P. Zhang, Y. Qin, T. Chen, F. Ye, *Microchim. Acta* 184 (2017) 4629–4635.
- [137] Q. Cai, S. Lu, F. Liao, Y. Li, S. Ma, M. Shao, *Nanoscale* 6 (2014) 8117–8123.
- [138] Y. Huang, M. Zhao, S. Han, Z. Lai, J. Yang, C. Tan, Q. Ma, Q. Lu, J. Chen, X. Zhang, Z. Zhang, B. Li, B. Chen, Y. Zong, H. Zhang, *Adv. Mater.* 29 (2017) 1700102.
- [139] Y. Hu, H. Cheng, X. Zhao, J. Wu, F. Muhammad, S. Lin, J. He, L. Zhou, C. Zhang, Y. Deng, P. Wang, Z. Zhou, S. Nie, H. Wei, *ACS Nano* 11 (2017) 5558–5566.
- [140] Z. Dai, S. Liu, J. Bao, H. Jui, *Chem.-A Euro. J.* 15 (2009) 4321–4326.
- [141] C. Ding, Y. Yan, D. Xiang, C. Zhang, Y. Xian, *Microchim. Acta* 183 (2016) 625–631.
- [142] S. Wang, Q. Zhang, N. Zeng, P. Qi, C. Huang, Q. Huang, *Front. Oncol.* 12 (2022) 1–8.
- [143] W. Yin, J. Yu, F. Lv, L. Yan, L.R. Zheng, Z. Gu, Y. Zhao, *ACS Nano* 10 (2016) 11000–11011.
- [144] S. Cai, Q. Han, C. Qi, Z. Lian, X. Jia, R. Yang, C. Wang, *Nanoscale* 8 (2016) 3685–3693.
- [145] D. Ma, C. Xie, T. Wang, L. Mei, X. Zhang, Z. Guo, W. Yin, *ChemBiochem* 21 (2020) 2373–2380.
- [146] L. Ai, L. Li, C. Zhang, J. Fu, J. Jiang, *Chem.-A Euro. J.* 19 (2013) 15105–15108.
- [147] C.H. Wang, J. Gao, Y.L. Cao, H.L. Tan, *Anal. Chim. Acta* 1004 (2018) 74–81.
- [148] J. Chen, Y. Shu, H. Li, Q. Xu, X. Hu, *Talanta* 189 (2018) 254–261.
- [149] H. Li, H. Liu, J. Zhang, Y. Cheng, C. Zhang, X. Fei, Y. Xian, *ACS Appl. Mater. Interfaces* 9 (2017) 40716–40725.
- [150] Y. Zhang, F. Wang, C. Liu, Z. Wang, L. Kang, Y. Huang, K. Dong, J. Ren, X. Qu, *ACS Nano* 12 (2018) 651–661.
- [151] L. Wang, Y. Chen, *ACS Appl. Mater. Interfaces* 12 (2020) 8351–8358.
- [152] Y. Zhang, S. Yang, J. Wang, Y. Cai, L. Niu, X. Liu, C. Liu, H. Qi, A. Liu, *Talanta* 233 (2021) 122594.
- [153] Y. Li, R. Fu, Z. Duan, C. Zhu, D. Fan, *Small* 18 (2022) 2200165.
- [154] Z. Zhang, X. Zhang, B. Liu, J. Liu, *J. Am. Chem. Soc.* 139 (2017) 5412–5419.
- [155] J. Li, W. Liu, X. Wu, X. Gao, *Biomaterials* 48 (2015) 37–44.
- [156] X.M. Shen, W.Q. Liu, X.J. Gao, Z.H. Lu, X.C. Wu, X.F. Gao, *J. Am. Chem. Soc.* 137 (2015) 15882–15891.
- [157] W. He, Y. Liu, J. Yuan, J.J. Yin, X. Wu, X. Hu, K. Zhang, J. Liu, C. Chen, Y. Ji, Y. Guo, *Biomaterials* 32 (2011) 1139–1147.
- [158] S. Mei, B. Liu, X. Xiong, X. Hun, *J. Pharm. Biomed. Anal.* 186 (2020) 113280.
- [159] X.T. Ding, Z. Zhao, Y.F. Zhang, M.L. Duan, C.Z. Liu, Y.H. Xu, *Small* 19 (2023) 2207142.
- [160] B. Liu, J. Liu, *Trac-Trends in Analytical Chemistry* 121 (2019) 115690.
- [161] X.M. Shen, Z.Z. Wang, X.F. Gao, Y.L. Zhao, *ACS Catal.* 10 (2020) 12657–12665.
- [162] X. Liu, X. Wang, Q. Han, C. Qi, C. Wang, R. Yang, *Talanta* 203 (2019) 227–234.
- [163] I. Celardo, J.Z. Pedersen, E. Traversa, L. Ghibelli, *Nanoscale* 3 (2011) 1411–1420.
- [164] C. Xu, X. Qu, *NPG Asia Mater.* 6 (2014) e90.
- [165] S. Guo, Y. Han, L. Guo, *Catal. Surv. Asia* 24 (2019) 70–85.
- [166] M. Ornatka, E. Sharpe, D. Andreescu, S. Andreescu, *Anal. Chem.* 83 (2011) 4273–4280.
- [167] Y. Li, X. He, J.J. Yin, Y. Ma, P. Zhang, J. Li, Y. Ding, J. Zhang, Y. Zhao, Z. Chai, Z. Zhang, *Angewandte Chemie-International Edition* 54 (2015) 1832–1835.
- [168] W. Qin, L. Su, C. Yang, Y. Ma, H. Zhang, X. Chen, *J. Agric. Food Chem.* 62 (2014) 5827–5834.
- [169] X. Liu, L. Yan, H. Ren, Y. Cai, C. Liu, L. Zeng, J. Guo, A. Liu, *Biosens. Bioelectron.* 165 (2020) 112342.
- [170] R. André, F. Natálio, M. Humanes, J. Leppin, K. Heinze, R. Wever, H.C. Schröder, W.E.G. Müller, W. Tremel, *Adv. Funct. Mater.* 21 (2010) 501–509.
- [171] N. Singh, M. Geethika, S.M. Eswarappa, G. Magesh, *Chemistry* 24 (2018) 8393–8403.
- [172] Y. Yu, Y.N. Zhang, Y. Wang, W.X. Chen, Z.J. Guo, N.N. Song, M.M. Liang, *Nano Res.* 16 (2023) 10763–107695.
- [173] J. Liu, X. Hu, S. Hou, T. Wen, W. Liu, X. Zhu, X. Wu, *Chem. Commun.* 47 (2011) 10981–10983.
- [174] S. Guo, L. Guo, *J. Phys. Chem. C* 123 (2019) 30318–30334.
- [175] B. Qiao, A. Wang, X. Yang, L.F. Allard, Z. Jiang, Y. Cui, J. Liu, J. Li, T. Zhang, *Nat. Chem.* 3 (2011) 634–641.
- [176] Z. Li, D. Wang, Y. Wu, Y. Li, *Natl. Sci. Rev.* 5 (2018) 673–689.
- [177] L. Jiao, H. Yan, Y. Wu, W. Gu, C. Zhu, D. Du, Y. Lin, *Angewandte Chemie-International Edition* 59 (2020) 2565–2576.
- [178] N. Cheng, S. Stambula, D. Wang, M.N. Banis, J. Liu, A. Riese, B. Xiao, R. Li, T. K. Sham, L.M. Liu, G.A. Botton, X. Sun, *Nat. Commun.* 7 (2016) 13638.
- [179] J. Liu, M. Jiao, L. Lu, H.M. Barkholtz, Y. Li, Y. Wang, L. Jiang, Z. Wu, D.J. Liu, L. Zhuang, C. Ma, J. Zeng, B. Zhang, D. Su, P. Song, W. Xing, W. Xu, Y. Wang, Z. Jiang, G. Sun, *Nat. Commun.* 8 (2017) 15938.
- [180] J. Pei, R. Zhao, X. Mu, J. Wang, C. Liu, X.D. Zhang, *Biomater. Sci.* 8 (2020) 6428–6441.
- [181] Y. He, S. Hwang, D.A. Cullen, M.A. Uddin, L. Langhorst, B. Li, S. Karakalos, A. J. Kropf, E.C. Wegener, J. Sokolowski, M. Chen, D. Myers, D. Su, K.L. More, G. Wang, S. Litster, G. Wu, *Energ. Environ. Sci.* 12 (2019) 250–260.
- [182] M. Zhou, Y. Jiang, G. Wang, W. Wu, W. Chen, P. Yu, Y. Lin, J. Mao, L. Mao, *Nat. Commun.* 11 (2020) 3188.
- [183] Y. Wang, Z. Zhang, G. Jia, L. Zheng, J. Zhao, X. Cui, *Chem. Commun.* 55 (2019) 5271–5274.
- [184] L. Nie, D. Mei, H. Xiong, B. Peng, Z. Ren, X.I.P. Hernandez, A. DeLaRiva, M. Wang, M.H. Engelhard, L. Kovarik, A.K. Datye, Y. Wang, *Science* 358 (2017) 1419–1423.
- [185] M. Kluecker, M.N. Tahir, R. Ragg, K. Korschelt, P. Simon, T.E. Gorelik, B. Barton, S.I. Shylin, M. Panthofer, J. Herzberger, H. Frey, V. Ksenofontov, A. Moeller, U. Kolb, J. Grin, W. Tremel, *Chem. Mater.* 29 (2017) 1134–1146.
- [186] Z. Kou, W. Zang, P. Wang, X. Li, J. Wang, *Nanoscale Horiz.* 5 (2020) 757–764.
- [187] Z. Shi, W. Yang, Y. Gu, T. Liao, Z. Sun, *Adv. Sci.* 7 (2020) 2001069.
- [188] X. Zhang, G. Li, G. Chen, D. Wu, X. Zhou, Y. Wu, *Coord. Chem. Rev.* 418 (2020) 213376.
- [189] L.H. Shen, D.X. Ye, H.B. Zhao, J.J. Zhang, *Anal. Chem.* 93 (2021) 1221–1231.
- [190] T.T. Cui, Y.P. Wang, T. Ye, J. Wu, Z.Q. Chen, J. Li, Y.P. Lei, D.S. Wang, Y.D. Li, *Angewandte Chemie-International Edition* 61 (2022) e202115219.
- [191] J. Liu, L. Meng, Z. Fei, P.J. Dyson, L. Zhang, *Biosens. Bioelectron.* 121 (2018) 159–165.
- [192] K. Zhao, W. Gu, S. Zheng, C. Zhang, Y. Xian, *Talanta* 141 (2015) 47–52.
- [193] W. Song, B. Zhao, C. Wang, Y. Ozaki, X. Lu, *J. Mater. Chem. B* 7 (2019) 850–875.
- [194] T. Chen, H. Zou, X. Wu, C. Liu, B. Situ, L. Zheng, G. Yang, *ACS Appl. Mater. Interfaces* 10 (2018) 12453–12462.
- [195] T. Lin, L. Zhong, L. Guo, F. Fu, G. Chen, *Nanoscale* 6 (2014) (1862) 11856.
- [196] X. Wu, J. Ge, C. Yang, M. Hou, Z. Liu, *Chem. Commun.* 51 (2015) 13408–13411.
- [197] Z. Zhao, J. Pang, W. Liu, T. Lin, F. Ye, S. Zhao, *Microchim. Acta* 186 (2019) 295.
- [198] T. Li, P. Hu, J. Li, P. Huang, W. Tong, C. Gao, *Colloids Surf A Physicochem Eng Asp* 577 (2019) 456–463.
- [199] A.P. Nagvenkar, A. Gedanken, *ACS Appl. Mater. Interfaces* 8 (2016) 22301–22308.
- [200] Z. Xi, W. Gao, X. Xia, *ChemBiochem: A Euro. J. Chem. Biol.* 21 (2020) 2440–2444.
- [201] V. Baldim, F. Bedioui, N. Mignet, I. Margail, J.F. Berret, *Nanoscale* 10 (2018) 6971–6980.
- [202] Y. Liu, Y. Xiang, D. Ding, R. Guo, *RSC Adv.* 6 (2016) 112435–112444.
- [203] S. Liu, F. Lu, R. Xing, J.J. Zhu, *Chem.-A Euro. J.* 17 (2011) 620–625.
- [204] S. Ghosh, P. Roy, N. Karmodak, E.D. Jemmis, G. Magesh, *Angewandte Chemie-International Edition* 57 (2018) 4510–4515.
- [205] L. Guerrini, R.A. Alvarez-Puebla, N. Pazos-Perez, *Materials* 11 (2018) 1154.
- [206] G.H. Tang, J.Y. He, J.W. Liu, X.Y. Yan, K.L. Fan, *Exploration* 1 (2021) 75–89.
- [207] K. Fan, H. Wang, J. Xi, Q. Liu, X. Meng, D. Duan, L. Gao, X. Yan, *Chem. Commun.* 53 (2017) 424–427.
- [208] R. Cai, X. Gao, C. Zhang, Z. Hu, Y. Ji, J. Liu, X. Wu, *Nanotechnology* 32 (2021) 458702.
- [209] Y. Yue, H. Wei, J. Guo, Y. Yang, *Colloids Surf A Physicochem Eng Asp* 610 (2021) 125715.
- [210] B. Liu, Z. Huang, J. Liu, *Nanoscale* 8 (2016) 13562–13567.
- [211] V. Baldim, N. Yadav, N. Bia, A. Grailot, C. Loubat, S. Singh, A.S. Karakoti, J. F. Berret, *ACS Appl. Mater. Interfaces* 12 (2020) 42056–42066.
- [212] J. Hao, J. Hao, J. Mu, Y. Wang, *ACS Appl. Bio. Mater.* 4 (2021) 3443–3452.
- [213] J.X. Chen, Q. Ma, M.H. Li, D.Y. Chao, L. Huang, W.W. Wu, Y.X. Fang, S.J. Dong, *Nat. Commun.* 12 (2021) 3375.
- [214] F. Tao, *Chem. Soc. Rev.* 41 (2012) 7977–7979.
- [215] C. Liu, Y. Yan, X. Zhang, Y. Mao, X. Ren, C. Hu, W. He, J.J. Yin, *Nanoscale* 12 (2020) 3068–3075.
- [216] J.R. Kitchin, J.K. Norskov, M.A. Barteau, J.G. Chen, *J. Chem. Phys.* 120 (2004) 10240–10246.
- [217] J. Wang, S. Lin, Z. Han, Y. Liu, *RSC Adv.* 5 (2015) 28619–28623.
- [218] S. Zhang, Y. Liu, S. Sun, J. Wang, Q. Li, R. Yan, Y. Gao, H. Liu, S. Liu, W. Hao, H. Dai, C. Liu, Y. Sun, W. Long, X. Mu, X.D. Zhang, *Theranostics* 11 (2021) 2806–2821.
- [219] L. Jiang, S. Fernandez-Garcia, M. Tinoco, Z. Yan, Q. Xue, G. Blanco, J.J. Calvino, A.B. Hungria, X. Chen, *ACS Appl. Mater. Interfaces* 9 (2017) 18595–18608.
- [220] D. Jampaiah, T. Srinivasa Reddy, A.E. Kandjani, P.R. Selvakannan, Y.M. Sabri, V. E. Coyle, R. Shukla, S.K. Bhargava, *J. Mater. Chem. B* 4 (2016) 3874–3885.
- [221] Y. Liu, Y. Xiang, Y. Zhen, R. Guo, *Langmuir* 33 (2017) 6372–6381.
- [222] Y. Liu, Y. Zheng, D. Ding, R. Guo, *Langmuir: the ACS Journal of Surfaces and Colloids* 33 (2017) 13811–13820.
- [223] J. Shah, R. Purohit, R. Singh, A.S. Karakoti, S. Singh, *J. Colloid Interface Sci.* 456 (2015) 100–107.
- [224] N.V.S. Vallabani, A.S. Karakoti, S. Singh, *Colloids and Surfaces B-Biointerfaces* 153 (2017) 52–60.
- [225] J.G. You, Y.T. Wang, W.L. Tseng, *ACS Appl. Mater. Interfaces* 10 (2018) 37846–37854.
- [226] J.M. Dowding, S. Das, A. Kumar, T. Dosani, R. McCormack, A. Gupta, T.X. T. Sayle, D.C. Sayle, L. von Kalm, S. Seal, W.T. Self, *ACS Nano* 7 (2013) 4855–4868.
- [227] S.G. Neri, C. Martin, L.J. Pezzato, *J. Am. Chem. Soc.* 139 (2017) 1794–1797.
- [228] M. Zhu, Y. Dai, Y. Wu, K. Liu, X. Qi, Y. Sun, *Nanotechnology* 29 (2018) 465704.
- [229] F. Wang, E. Ju, Y. Guan, J. Ren, X. Qu, *Small* 13 (2017) 1603051.
- [230] X. Xiong, Y. Tang, C. Xu, Y. Huang, Y. Wang, L. Fu, C. Lin, D. Zhou, Y. Lin, *Small* 16 (2020) 2004129.

- [231] D. Sun, X. Pang, Y. Cheng, J. Ming, S. Xiang, C. Zhang, P. Lv, C. Chu, X. Chen, G. Liu, N. Zheng, *ACS Nano* 14 (2020) 2063–2076.
- [232] L.X. Luo, X.P. Guo, X.X. Xi, T. Bao, Y.B. Li, Z. Wu, X.H. Zhang, S.F. Wang, W. Wen, *Sensors and Actuators B-Chemical* 381 (2023) 133444.
- [233] Z. Wang, X. Yang, J. Feng, Y. Tang, Y. Jiang, N. He, *Analyst* 139 (2014) 6088–6091.
- [234] A. Paul, S. Paul, *Frontiers in Bioscience-Landmark* 19 (2014) 605–618.
- [235] X. Zhang, F.G. Wu, P. Liu, N. Gu, Z. Chen, *Small* 10 (2014) 5170–5177.
- [236] B. Niu, K. Liao, Y. Zhou, T. Wen, G. Quan, X. Pan, C. Wu, *Biomaterials* 277 (2021) 121110.
- [237] Y. Liu, M. Zhou, W. Cao, X. Wang, Q. Wang, S. Li, H. Wei, *Anal. Chem.* 91 (2019) 8170–8175.
- [238] Y. Li, P. Li, Y. Chen, Y. Wu, J. Wei, *Biosens. Bioelectron.* 228 (2023) 115200.
- [239] D.D. Zhang, H.J. Zhang, H. Sun, Y.Z. Yang, W.B. Zhong, Q. Chen, Q.X. Ren, G. Jin, Y. Zhang, *Talanta* 266 (2024) 124967.
- [240] A.B. Chinen, C.M. Guan, J.R. Ferrer, S.N. Barnaby, T.J. Merkel, C.A. Mirkin, *Chem. Rev.* 115 (2015) 10530–10574.
- [241] J.R. Li, K.M. Koo, Y.L. Wang, M. Trau, *Small* 15 (2019) 1904689.
- [242] R. Li, H. Fan, H. Zhou, Y. Chen, Q. Yu, W. Hu, G.L. Liu, L. Huang, *Adv. Sci.* 10 (2023) 2301658.
- [243] Z. Li, H. Li, X. Geng, G. Dai, Z. Chu, F. Luo, F. Zhang, Q. Wang, *ACS Appl. Nano Mater.* 5 (2022) 2204–2213.
- [244] X. Meng, W. Zuo, P. Wu, Y. Song, G.J. Yang, S. Zhang, J. Yang, X. Zou, W. Wei, D. Zhang, J. Dai, Y. Ju, *Nano Lett.* (2023), <https://doi.org/10.1021/acs.nanolett.3c03118>.
- [245] G.Q. Wang, J.J. Wei, R. Hu, L.P. Mei, A.J. Wan, J.J. Feng, *Biosens. Bioelectron.* 215 (2022) 114552.
- [246] J. Li, J. Wang, Y. Wang, M. Trau, *Analyst* 142 (2017) 4788–4793.
- [247] L.M. Yang, H. Guo, T. Hou, J.A. Zhang, F. Li, *Biosens. Bioelectron.* 234 (2023) 115346.
- [248] K. Fan, C. Cao, Y. Pan, D. Lu, D. Yang, J. Feng, L. Song, M. Liang, X. Yan, *Nat. Nanotechnol.* 7 (2012) 459–464.
- [249] Y. Cai, C. Cao, X. He, C. Yang, L. Tian, R. Zhu, Y. Pan, *Int. J. Nanomed.* 10 (2015) 2619–2634.
- [250] T. Zhang, C. Cao, X. Tang, Y. Cai, C. Yang, Y. Pan, *Nanotechnology* 28 (2017) 045704.
- [251] G. Li, G. Wu, J. Huang, B. Wang, H. Li, W. Chen, J. Liang, M. Tan, Z. Zhou, *Bioelectrochemistry* 147 (2022) 108204.
- [252] S.N. Prasad, S.R. Anderson, M.V. Joglekar, A.A. Hardikar, V. Bansal, R. Ramanathan, *Biosens. Bioelectron.* 212 (2022) 114386.
- [253] L. Roy, S. Mondal, N. Bhattacharyya, R. Ghosh, A. Banerjee, S. Singh, A. Chattopadhyay, S.A. Ahmed, R.S. Jassas, M.M. Al-Rooqi, Z. Moussa, I. Althagafi, D. Bhattacharya, K. Bhattacharya, A.K. Mallick, S.K. Pal, *Sci. Rep.* 13 (2023) 17306.
- [254] R. Chen, C.C. Guo, G.L. Lan, P. Luo, J.M. Yi, W. Wei, *Biosens. Bioelectron.* 237 (2023) 115469.
- [255] G.Y. Li, X.H. Li, W.F. Xu, S.N. Li, X.H. Tan, J.T. Liang, Z.D. Zhou, *Anal. Bioanal. Chem.* (2023), <https://doi.org/10.1007/s00216-023-04975-2>.
- [256] J. Chen, W. Wu, L. Huang, Q. Ma, S. Dong, *Chem.-A Euro. J.* 25 (2019) 1944 11940–11941.
- [257] M. Liu, J. Mou, X. Xu, F. Zhang, J. Xia, Z. Wang, *Talanta* 220 (2020) 121374.
- [258] G.L. Wang, L.Y. Jin, X.M. Wu, Y.M. Dong, Z.J. Li, *Anal. Chim. Acta* 871 (2015) 1–8.
- [259] M.A. Woo, M.I. Kim, J.H. Jung, K.S. Park, T.S. Seo, H.G. Park, *Int. J. Mol. Sci.* 14 (2013) 9999–10014.
- [260] T. Zhang, F. Tian, L. Long, J. Liu, X. Wu, *Int. J. Nanomed.* 13 (2018) 4795–4805.
- [261] X. Meng, S. Zou, D. Li, J. He, L. Fang, H. Wang, X. Yan, D. Duan, L. Gao, *Biosens. Bioelectron.* 217 (2022) 114739.
- [262] I.M. Khoris, T. Kenta, A.B. Ganganboina, E.Y. Park, *Biosens. Bioelectron.* 215 (2022) 114602.
- [263] Y.P. Hsu, N.S. Li, Y.T. Chen, H.H. Pang, K.C. Wei, H.W. Yang, *Biosens. Bioelectron.* 151 (2020) 111960.
- [264] D. Wang, B. Zhang, H. Ding, D. Liu, J. Xiang, X.J. Gao, X. Chen, Z. Li, L. Yang, H. Duan, J. Zheng, Z. Liu, B. Jiang, Y. Liu, N. Xie, H. Zhang, X. Yan, K. Fan, G. Nie, *Nano Today* 40 (2021) 101243.
- [265] X.M. Fu, Z.J. Liu, S.X. Cai, Y.P. Zhao, D.Z. Wu, C.Y. Li, J.H. Chen, *Chin. Chem. Lett.* 27 (2016) 920–926.
- [266] X.Q. Lin, H.H. Deng, G.W. Wu, H.P. Peng, A.L. Liu, X.H. Lin, X.H. Xia, W. Chen, *Analyst* 140 (2015) 5251–5256.
- [267] C.I. Wang, W.T. Chen, H.T. Chang, *Anal. Chem.* 84 (2012) 9706–9712.
- [268] L.L. Wu, L.Y. Wang, Z.J. Xie, N. Pan, C.F. Peng, *Sensors and Actuators B-Chemical* 235 (2016) 110–116.
- [269] H. Xu, X. Ding, L. Li, Q. Li, Z. Li, H. Lin, *Front. Bioeng. Biotechnol.* 11 (2023) 1208693.
- [270] Y.Q. Liu, Y. Mao, E. Xu, H. Jia, S. Zhang, V.L. Dawson, T.M. Dawson, Y.M. Li, Z. Zheng, W. He, X. Mao, *Nano Today* 36 (2021) 101027.
- [271] Y. Li, J. Xuan, Y.J. Song, P. Wang, L.D. Qin, *Lab Chip* 15 (2015) 3300–3306.
- [272] R.T. Wen, C.H. Zhou, J.Y. Tian, J.S. Lu, *Talanta* 252 (2023) 123830.
- [273] Y. Zhang, W. Ren, H.Q. Luo, N.B. Li, *Biosens. Bioelectron.* 80 (2016) 463–470.
- [274] H.Z. Peng, J.X. Zhang, C.X. Zeng, C.Q. Zhou, Q.N. Li, N. Lu, L.H. Wang, *ACS Applied Bio Materials* 3 (2020) 5111–5119.
- [275] R.D. Isho, N.M.S. Mohammad, K.M. Omer, *Anal. Biochem.* 654 (2022) 114818.
- [276] Q. Li, T. Wu, X. Fan, X. Guo, W. Jiang, K. Fan, *Mater. Des.* 224 (2022) 111430.
- [277] S. Sahar, A. Zeb, C. Ling, A. Rajja, G. Wang, N. Ullah, X.M. Lin, A.W. Xu, *ACS Nano* 14 (2020) 3017–3031.
- [278] R. Pautler, E.Y. Kelly, P.J.J. Huang, J. Cao, B. Liu, J. Liu, *ACS Appl. Mater. Interfaces* 5 (2013) 6820–6825.
- [279] J. Zhang, J. Wang, J. Liao, Y. Lin, C. Zheng, J. Liu, *ACS Appl. Mater. Interfaces* 13 (2021) 50236–50245.
- [280] Y. Ai, Z.N. Hu, X. Liang, H.B. Sun, H. Xin, Q. Liang, *Adv. Funct. Mater.* 32 (2022) 2110432.
- [281] J. Liu, A. Wang, S. Liu, R. Yang, L. Wang, F. Gao, H. Zhou, X. Yu, J. Liu, C. Chen, *Angewandte Chemie-International Edition* 60 (2021) 25328–25338.
- [282] M. Huo, L. Wang, Y. Chen, J. Shi, *Nat. Commun.* 8 (2017) 357.
- [283] X. Meng, D. Li, L. Chen, H. He, Q. Wang, C. Hong, J. He, X. Gao, Y. Yang, B. Jiang, G. Nie, X. Yan, L. Gao, K. Fan, *ACS Nano* 15 (2021) 5735–5751.
- [284] Y. Chen, Z.H. Li, J.J. Hu, S.Y. Peng, L. Rong, Y. Sun, X.Z. Zhang, *Nanoscale Horiz.* 5 (2020) 283–293.
- [285] Z. Wang, Y. Zhang, E. Ju, Z. Liu, F. Cao, Z. Chen, J. Ren, X. Qu, *Nat. Commun.* 9 (2018) 3334.
- [286] X. Hu, F. Li, F. Xia, X. Guo, N. Wang, L. Liang, B. Yang, K. Fan, X. Yan, D. Ling, *J. Am. Chem. Soc.* 142 (2020) 1636–1644.
- [287] X. Jing, L. Meng, S. Fan, T. Yang, N. Zhang, R. Xu, X. Zhao, H. Yang, Z. Yang, D. Wang, Y. Liang, G. Zhou, W. Ji, J. She, *Chem. Eng. J.* 442 (2022) 136096.
- [288] S. Liang, X. Deng, Y. Chang, C. Sun, S. Shao, Z. Xie, X. Xiao, P.A. Ma, H. Zhang, Z. Cheng, J. Lin, *Nano Lett.* 19 (2019) 4134–4145.
- [289] S. Li, L. Shang, B. Xu, S. Wang, K. Gu, Q. Wu, Y. Sun, Q. Zhang, H. Yang, F. Zhang, L. Gu, T. Zhang, H. Liu, *Angewandte Chemie-International Edition* 58 (2019) 12624–12631.
- [290] C. Ren, X. Hu, Q. Zhou, *Adv. Sci.* 5 (2018) 1700595.
- [291] L. Fan, X. Xu, C. Zhu, J. Han, L. Gao, J. Xi, R. Guo, *ACS Appl. Mater. Interfaces* 10 (2018) 4502–4511.
- [292] Y. Chong, J. Huang, X. Xu, C. Yu, X. Ning, S. Fan, Z. Zhang, *Bioconjug. Chem.* 31 (2020) 1756–1765.
- [293] Z.H. Li, Y. Chen, Y. Sun, X.Z. Zhang, *ACS Nano* 15 (2021) 5189–5200.
- [294] H. Yang, B. Xu, S. Li, Q. Wu, M. Lu, A. Han, H. Liu, *Small* 17 (2021) 2007090.
- [295] S. Liu, W. Zhang, Q. Chen, J. Hou, J. Wang, Y. Zhong, X. Wang, W. Jiang, H. Ran, D. Guo, *Nanoscale* 13 (2021) 14049–14066.
- [296] X. Wang, X. Zhong, L. Bai, J. Xu, F. Gong, Z. Dong, Z. Yang, Z. Zeng, Z. Liu, L. Cheng, *J. Am. Chem. Soc.* 142 (2020) 6527–6537.
- [297] C.C. Gong, J.M. Zhao, X.D. Meng, Z. Yang, H.F. Dong, *Chem. Eng. J.* 435 (2022) 135083.
- [298] W. Xu, C. Dong, H. Hu, X. Qian, L. Chang, Q. Jiang, L. Yu, Y. Chen, J. Zhou, *Adv. Funct. Mater.* 31 (2021) 2103134.
- [299] Z. Wang, B. Liu, Q. Sun, L. Feng, F. He, P. Yang, S. Gai, Z. Quan, J. Lin, *ACS Nano* 15 (2021) 12342–12357.
- [300] M. Wang, H. Li, B. Huang, S. Chen, R. Cui, Z.J. Sun, M. Zhang, T. Sun, *Adv. Healthc. Mater.* 10 (2021) 2100090.
- [301] Y. Li, K.H. Yun, H. Lee, S.H. Goh, Y.G. Suh, Y. Choi, *Biomaterials* 197 (2019) 12–19.
- [302] L. Feng, Z. Dong, C. Liang, M. Chen, D. Tao, L. Cheng, K. Yang, Z. Liu, *Biomaterials* 181 (2018) 81–91.
- [303] H. Tan, Y. Li, J. Ma, P. Wang, Q. Chen, L. Hu, *Pharmaceutics* 14 (2022) 1717.
- [304] Y. Liu, M. Yao, W. Han, H. Zhang, S. Zhang, *Chemistry-a European Journal* 27 (2021) 13418–13425.
- [305] W. Zhang, J. Liu, X. Li, Y. Zheng, L. Chen, D. Wang, M.F. Foda, Z. Ma, Y. Zhao, H. Han, *ACS Nano* 15 (2021) 19321–19333.
- [306] P. Yang, J. Tao, F. Chen, Y. Chen, J. He, K. Shen, P. Zhao, Y. Li, *Small* 17 (2021) 2005865.
- [307] K. Lv, L. Wang, Y. Ma, F. Zhang, W. Guo, K. Yu, F. Qu, H. Lin, *Biomaterials Advances* 136 (2022) 212778.
- [308] W. Duan, B. Li, W. Zhang, J. Li, X. Yao, Y. Tian, J. Zheng, D. Li, J. Nanobiotechnol. 20 (2022) 217.
- [309] M. Wysocki, B. Czarczynska-Goslinska, D. Ziental, M. Michalak, E. Guzel, L. Sobotta, *ChemMedChem* 17 (2022) e202200185.
- [310] M.A. Iqbal, S. Arora, G. Prakasam, G.A. Calin, M.A. Syed, *Mol. Aspects Med.* 70 (2019) 3–20.
- [311] Y. Huang, J.C. Hsu, H. Koo, D.P. Cormode, *Theranostics* 12 (2022) 796–816.
- [312] X. Huang, N. Lan, Y. Zhang, W. Zeng, H. He, X. Liu, *Front. Chem.* 10 (2022) 842712.
- [313] S. Khan, M. Sharifi, S.H. Bloukh, Z. Edis, R. Siddique, M. Falahati, *Talanta* 224 (2021) 121805.
- [314] C. Cao, H. Zou, N. Yang, H. Li, Y. Cai, X. Song, J. Shao, P. Chen, X. Mou, W. Wang, X. Dong, *Adv. Mater.* 33 (2021) 2106996.
- [315] A.L. Sukstanskii, D.A. Yablonskiy, *Magn. Reson. Med.* 89 (2023) 370–383.
- [316] J. Wahsner, E.M. Gale, A. Rodriguez-Rodriguez, P. Caravan, *Chem. Rev.* 119 (2019) 957–1057.
- [317] J. Yu, F. Zhao, W.L. Gao, X. Yang, Y.M. Ju, L.Y. Zhao, W.S. Guo, J. Xie, X.J. Liang, X.Y. Tao, J. Li, Y. Ying, W.C. Li, J.W. Zheng, L. Qiao, S.B. Xiong, X.Z. Mou, S. L. Che, Y.L. Hou, *ACS Nano* 13 (2019) 10002–10014.
- [318] X. Cai, Q. Zhu, Y. Zeng, Q. Zeng, X. Chen, Y. Zhan, *Int. J. Nanomed.* 14 (2019) 8321–8344.
- [319] R. Ragg, A.M. Schilman, K. Korschelt, C. Wiesotte, M. Klunker, M. Viel, L. Voelker, S. Preiss, J. Herzberger, H. Frey, K. Heinze, P. Bluemler, M.N. Tahir, F. Natalio, W. Tremel, *J. Mater. Chem. B* 4 (2016) 7423–7428.
- [320] D. Zhu, X.H. Zhu, S.Z. Ren, Y.D. Lu, H.L. Zhu, *J. Drug Target.* 29 (2021) 911–924.
- [321] X.L. Zhang, G.L. Li, D. Wu, X.L. Li, N. Hu, J. Chen, G. Chen, Y.N. Wu, *Biosens. Bioelectron.* 137 (2019) 178–198.
- [322] Z.R. Lu, *Current Opinion in Biomedical Engineering* 3 (2017) 67–73.
- [323] H. Wu, F. Xia, L. Zhang, C. Fang, J. Lee, L. Gong, J. Gao, D. Ling, F. Li, *Adv. Mater.* 34 (2022) 2108348.

- [324] H. Ding, Y. Cai, L. Gao, M. Liang, B. Miao, H. Wu, Y. Liu, N. Xie, A. Tang, K. Fan, X. Yan, G. Nie, *Nano Lett.* 19 (2019) 203–209.
- [325] S. Jiang, J. Lin, P. Huang, *Adv. Healthc. Mater.* 12 (2022) 2202208.
- [326] T. Yan, M. Su, Z. Wang, J. Zhang, *Small* 19 (2023) 2300539.
- [327] D. Ni, E.B. Ehlerding, W. Cai, *Angewandte Chemie-International Edition* 58 (2019) 2570–2579.
- [328] P.J. Gawne, F. Man, P.J. Blower, R.T.M. de Sales, *Chem. Rev.* 122 (2022) 10266–10318.
- [329] D. Chen, D. Yang, C.A. Dougherty, W. Lu, H. Wu, X. He, T. Cai, M.E. Van Dort, B. D. Ross, H. Hong, *ACS Nano* 11 (2017) 4315–4327.
- [330] S.M. Ametamey, *Chem. Rev.* 108 (2008) 4036.
- [331] B. Li, M. Zhao, J. Lin, P. Huang, X. Chen, *Chem. Soc. Rev.* 51 (2022) 7692–7714.
- [332] L. Wu, H. Zou, H. Wang, S. Zhang, S. Liu, Y. Jiang, J. Chen, Y. Li, M. Shao, R. Zhang, X. Li, J. Dong, L. Yang, K. Wang, X. Zhu, X. Sun, *Wiley Interdisciplinary Reviews-Nanomedicine and Nanobiotechnology* 13 (2021) 533–544.
- [333] J. Son, G. Yi, J. Yoo, C. Park, H. Koo, H.S. Choi, *Adv. Drug Deliv. Rev.* 138 (2019) 133–147.
- [334] A.M. Zhang, S.J. Pan, Y.H. Zhang, J. Chang, J. Cheng, Z.C. Huang, T.L. Li, C. L. Zhang, J.M. de la Fuentea, Q. Zhang, D.X. Cui, *Theranostics* 9 (2019) 3443–3458.
- [335] Q. Dan, Z. Yuan, S. Zheng, H.R. Ma, W.X. Luo, L. Zhang, N. Su, D.H. Hu, Z. H. Sheng, Y.J. Li, *Pharmaceutics* 14 (2022) 1645.
- [336] F. Paladini, M. Pollini, A. Sannino, L. Ambrosio, *Biomacromolecules* 16 (2015) 1873–1885.
- [337] A.R. Cocco, W.L. de Oliveira, A.F. da Rosa, R.G. da Silva, E.P. Lund, *Dent. Mater.* 31 (2015) 1345–1362.
- [338] S.B. Levy, B. Marshall, *Nat. Med.* 10 (2004) S122–S129.
- [339] Y. Zhong, T. Wang, Z. Lao, M. Lu, S. Liang, X. Cui, Q. Li, S. Zhao, *ACS Appl. Mater. Interfaces* 13 (2021) 21680–21692.
- [340] M. Wang, X. Zhou, Y. Li, Y. Dong, J. Meng, S. Zhang, L. Xia, Z. He, L. Ren, Z. Chen, X. Zhang, *Bioact. Mater.* 17 (2022) 289–299.
- [341] J. Shan, X. Li, K. Yang, W. Xiu, Q. Wen, Y. Zhang, L. Yuwen, L. Weng, Z. Teng, L. Wang, *ACS Nano* 13 (2019) 13797–13808.
- [342] W. Yan, L. Yang, H. Wang, J. Zhang, W. Shen, *Nanoscale* 10 (2018) 15661–15668.
- [343] Y. Wu, L. Zhang, Y. Zhou, L. Zhang, Y. Li, Q. Liu, J. Hu, J. Yang, *Chin. J. Catal.* 40 (2019) 691–702.
- [344] N. Yu, T. Cai, Y. Sun, C. Jiang, H. Xiong, Y. Li, H. Peng, *Int. J. Pharm.* 552 (2018) 277–287.
- [345] B. Huang, X. Liu, Z. Li, Y. Zheng, K.W.K. Yeung, Z. Cui, Y. Liang, S. Zhu, S. Wu, *Chem. Eng. J.* 414 (2021) 128805.
- [346] W. Zhang, X. Ren, S. Shi, M. Li, L. Liu, X. Han, W. Zhu, T. Yue, J. Sun, J. Wang, *Nanoscale* 12 (2020) 16330–16338.
- [347] Z.H. Du, L.J. Zhu, P.F. Wang, X.Y. Lan, S.H. Lin, W.T. Xu, *Small* (2023) 1–12.
- [348] C. Liu, M. Zhang, H. Geng, P. Zhang, Z. Zheng, Y. Zhou, W. He, *Appl. Catal. B-Environ.* 295 (2021) 120317.
- [349] X. Wang, Q. Shi, Z. Zha, D. Zhu, L. Zheng, L. Shi, X. Wei, L. Lian, K. Wu, L. Cheng, *Bioact. Mater.* 6 (2021) 4389–4401.
- [350] S. Zhang, Q. Lu, F. Wang, Z. Xiao, L. He, D. He, L. Deng, *ACS Appl. Mater. Interfaces* 13 (2021) 37535–37544.
- [351] C.X. Sun, W.Q. Wang, X.L. Sun, W.H. Chu, J. Yang, J.J. Dai, Y.M. Ju, *Biomater. Sci.* 9 (2021) 8323–8334.
- [352] J. Cao, Q. Sun, A.G. Shen, B. Fan, J.M. Hu, *Chem. Eng. J.* 422 (2021) 130090.
- [353] Q. Xu, Y. Hua, Y. Zhang, M. Lv, H. Wang, Y. Pi, J. Xie, C. Wang, Y. Yong, *Adv. Healthc. Mater.* 10 (2021) 2101374.
- [354] S. He, Y. Feng, Q. Sun, Z. Xu, W. Zhang, *ACS Appl. Mater. Interfaces* 14 (2022) 25042–25049.
- [355] A. Cui, Y. Bao, H. Xu, X. Mu, X. Zhong, W. Wee, F. Wu, G. Shan, *Biomater. Sci.* 11 (2023) 2243–2252.
- [356] M. Dryden, J. Cooke, R. Salib, R. Holding, S.L.F. Pender, J. Brooks, *Journal of Global Antimicrobial Resistance* 8 (2017) 194–198.
- [357] G. Yim, C.Y. Kim, S. Kang, D.H. Min, K. Kang, H. Jang, *ACS Appl. Mater. Interfaces* 12 (2020) 41062–41070.
- [358] Y. Tao, E. Ju, J. Ren, X. Qu, *Adv. Mater.* 27 (2015) 1097–1104.
- [359] Z. Du, L. Zhu, P. Wang, X. Lan, S. Lin, W. Xu, *Small* (2023) 2301048.
- [360] L. Gao, K.M. Giglio, J.L. Nelson, H. Sondermann, A.J. Travis, *Nanoscale* 6 (2014) 2588–2593.
- [361] T. Wang, Q. Bai, Z. Zhu, H. Xiao, F. Jiang, F. Du, W.W. Yu, M. Liu, N. Sui, *Chem. Eng. J.* 413 (2021) 127537.
- [362] K. Wu, D. Zhu, X. Dai, W. Wang, X. Zhong, Z. Fang, C. Peng, X. Wei, H. Qian, X. Chen, X. Wang, Z. Zha, L. Cheng, *Nano Today* 43 (2022) 101380.
- [363] J. Xiao, L. Hai, Y. Li, H. Li, M. Gong, Z. Wang, Z. Tang, L. Deng, D. He, *Small* 18 (2022) 2105465.
- [364] Q. Liu, A. Zhang, R. Wang, Q. Zhang, D. Cui, *Nano-Micro Letters* 13 (2021) 154.
- [365] S. Li, E. Pang, C. Gao, Q. Chang, S. Hu, N. Li, *Chem. Eng. J.* 397 (2020) 125471.
- [366] S. Cai, X. Jia, Q. Han, X. Yan, R. Yang, C. Wang, *Nano Res.* 10 (2017) 2056–2069.
- [367] Q. Mu, Y. Sun, A. Guo, X. Xu, B. Qin, A. Cai, J. Hazard. Mater. 402 (2021) 123939.
- [368] S. Bhattacharyya, S.R. Ali, M. Venkateswarulu, P. Howlader, E. Zangrando, M. De, P.S. Mukherjee, *J. Am. Chem. Soc.* 142 (2020) 18981–18989.
- [369] N. Chakraborty, S. Gandhi, R. Verma, I. Roy, *Biomedicines* 10 (2022) 1378.
- [370] G. Saleem, X. Chen, R. Gu, M. Qasim, M. Usama, N. Rajput, *Nanotechnol. Rev.* 11 (2022) 2575–2583.
- [371] Z. Qin, Y. Zheng, Y. Wang, T. Du, C. Li, X. Wang, H. Jiang, *Coord. Chem. Rev.* 449 (2021) 214218.
- [372] Z. Liu, F. Wang, J. Ren, X. Qu, *Biomaterials* 208 (2019) 21–31.
- [373] S. Wang, X. Yu, F. Xu, Q. Liu, Y. Zhao, C. Liu, X. Lan, Y. Wang, Y. Liu, C. Liu, *Mater. Lett.* 343 (2023) 134381.
- [374] Z. Liu, F. Wang, J. Ren, X. Qu, *Biomaterials* 233 (2020) 21–31.
- [375] F. Xu, Q. Lu, P.J.J. Huang, J. Liu, *Chem. Commun.* 55 (2019) 13215–13218.
- [376] Z. Chen, H. Ji, C. Liu, W. Bing, Z. Wang, X. Qu, *Angewandte Chemie-International Edition* 55 (2016) 10732–10736.
- [377] N. Wang, X. Zhai, F. Guan, R. Zhang, B. Hou, J. Duan, *Int. J. Mol. Sci.* 24 (2023) 2445.
- [378] Z. Zhou, S. Li, G. Wei, W. Liu, Y. Zhang, C. Zhu, S. Liu, T. Li, H. Wei, *Adv. Funct. Mater.* 32 (2022) 2206294.
- [379] H. Xiong, X. He, T. Lou, X. Bai, *Biochem. Eng. J.* 195 (2023) 108931.
- [380] X. He, F. Tian, J. Chang, X. Bai, C. Yuan, C. Wang, A. Neville, *ACS Sustain. Chem. Eng.* 8 (2020) 6744–6752.
- [381] J. Huo, Q. Jia, H. Huang, J. Zhang, P. Li, X. Dong, W. Huang, *Chem. Soc. Rev.* 50 (2021) 8762–8789.
- [382] J.W. Xu, K. Yao, Z.K. Xu, *Nanoscale* 11 (2019) 8680–8691.
- [383] Y. Zou, Y. Zhang, Q. Yu, H. Chen, *Biomater. Sci.* 9 (2021) 10–22.
- [384] Y. Tang, Z.Y. Qiu, Z.B. Xu, L.Z. Gao, *Prog. Biochem. Biophys.* 45 (2018) 118–128.
- [385] M. Shen, F. Forghani, X. Kong, D. Liu, X. Ye, S. Chen, T. Ding, *Compr. Rev. Food Sci. Food Saf.* 19 (2020) 1397–1419.
- [386] X. Fan, F. Yang, C. Nie, L. Ma, C. Cheng, R. Haag, *Adv. Mater.* 33 (2021) 1–21.
- [387] X. Fan, Y. Gao, F. Yang, J.L. Low, L. Wang, B. Paulus, Y. Wang, A. Trampuz, C. Cheng, R. Haag, *Adv. Funct. Mater.* 33 (2023) 2301986.
- [388] D. Ma, P. Li, X. Duan, J. Li, P. Shao, Z. Lang, L. Bao, Y. Zhang, Z. Lin, B. Wang, *Angewandte Chemie-International Edition* 59 (2020) 3905–3909.
- [389] B. Li, L. Tan, X. Liu, Z. Li, Z. Cui, Y. Liang, S. Zhu, X. Yang, K.W.K. Yeung, S. Wu, *J. Hazard. Mater.* 380 (2019) 120818.
- [390] V. Vedarethinam, L. Huang, W. Xu, R. Zhang, D.D. Gurav, X. Sun, J. Yang, R. Chen, K. Qian, *Small* 15 (2019) 1803051.